QATAR UNIVERSITY

COLLEGE OF PHARMACY

SYNTHESIS, CHARACTERIZATION AND CYTOCOMPATIBILITY OF HIGHLY POROUS, THREE DIMENSIONAL POLY (1, 10 DECANEDIOL CO-TRICARBALLYLATE) BASED SCAFFOLDS FOR CARDIAC & OTHER TISSUE ENGINEERING APPLICATIONS

BY

HESHAM MAMDOUH AHMED ISMAIL

A Thesis Submitted to the Faculty of

Pharmacy

in Partial Fulfillment

of the Requirements

for the Degree of

Master of Science in Pharmacy

June 2016

The members of the Committee approve the thesis of Hesham Mamdouh Ahmed Ismail defended on 24th of April, 2016

_____

Dr. Husam Younes

Thesis Supervisor

_____

Dr. Feras Qasem Alali

Committee Member

_____

Dr. Wael Kafienah

Committee Member

_____

Dr. Mohamed Elrayess

Committee Member

_____

Dr. Abdelbary Elhissi

Committee Member

Approved:

_____

Ayman El-Kadi, Dean of College Of Pharmacy

Abstract

Electrospinning is one of the recently developed methods that produces scaffolds resembling the natural extracellular matrix. It can utilize a wide array of natural and synthetic polymer materials to produce three dimensional, porous, biocompatible, biodegradable scaffolds by the aid of different variations of the machine setup. Reactive electrospinning is one type that produces *in-situ* cross-linked scaffolds. It has the advantages of being fast and efficient with tunable scaffold mechanical, morphological and thermal characteristics.

In this work, we aim to synthesize, characterize and investigate the *in vitro* cytocompatibility of electrospun scaffolds of acrylated Poly (1, 10 decanediol-co-tricarballylate) (APDT) copolymer using photo-reactive electrospinning process with UV radiation for crosslinking, to be used for cardiac tissue engineering applications.

The pre-polymer was synthesized via a poly condensation reaction between tricarballylic acid and decanediol. This was followed by an acrylation reaction to render the polymer UV photocrosslinkable. The effect of adding polyvinyl pyrrolidone (PVP) to act as chain entanglement enhancer on the porous structure formation was also investigated. An optimized solution with concentrations of 20% (w/v) APDT and 8% (w/v) PVP in ethanol was successfully electrospun. Effect of PVP molecular weight was also assessed. Porous scaffolds produced by solvent free particulate leaching method using sodium chloride and trehalose as porogens were also prepared for comparison purposes.

Characterization of the produced scaffolds was performed using chemical, thermal, and morphological techniques followed by *in-vitro* cell viability testing using H9C2 cardiomyoblasts and adipose tissue derived mesenchymal stem cells.

Chemical and thermal characterization confirmed the successful synthesis of the polymer. Morphological analysis revealed successful production of the porous scaffolds with porosity of more than 70% and a higher fiber diameter and smaller pore size in case of higher molecular weight PVP. In addition, mechanical testing confirmed the elastomeric nature of the scaffolds that is required to withstand cardiac contraction and relaxation.

Finally, cell viability assay showed no significant indirect cytotoxic effect on the cardiomyoblasts. Moreover, cell scaffolds interaction study showed noticeable cell attachment and growth on the electrospun scaffolds more than the references. This rendered our scaffolds a very promising candidate for cardiac tissue engineering applications.

Table of Contents

List of tables

List of figures

Abbreviations

TE, Tissue engineering

ES, Electrospinning

ESS, Electrospun scaffolds

TCA, Tricarballylic acid

PDT, Poly (1, 10 decane diol) co- tricarballylate prepolymer

APDT, Acrylated poly (1, 10 decane diol) co tricarballylate

PVP, polyvinyl pyrrolidone

PCL, Polycaprolactone

GTA, Glutaraldehyde

UTS, Ultimate tensile Testing

NA, Porous scaffold produced by solvent free particulate leaching using sodium chloride as a porogen

TRE, Porous scaffold produced by solvent free particulate leaching using trehalose dihydrate as a porogen

Acknowledgments

I would like to thank my supervisor and mentor Dr. Husam Younes for his continuous guidance, assistance and unconditional support and motivation. Dr. Husam has done a tremendous effort in providing me with the needed knowledge; research skills and skepticism that made this dissertation come to light. He also provided me with maximum reinforcement personally and financially while being patient and supportive to the highest levels. Dr. Husam, you were a teacher that affected my eternity and no one can tell when your influence will stop - as Henry Adams once said.

I would also like to acknowledge the members of my supervisory committee; Dr. Mohamed Al Rayess, Dr. Wael Kafienah, Dr. Abdelbary Al-hissi and the committee chair, Dr. Feras Alali, for their efforts, critical appraisal of this thesis work, constructive feedback to make it better and their acts of motivation along the way. You were all great teachers that not only educated, but also inspired.

My deepest gratitude for Dr. Mohammad Al-Rayess for his close supervision during my internship at the ADLQ. Dr. Mohammad fully guided me through the cell viability studies. Dr. Mohammad also availed all the resources and facilities as well as the adipose tissue derived mesenchymal stem cells used in this study. Dr. Mohammad, I am much obliged to your positive and encouraging actions and words. I believe you are a perfect fit for the Japanese proverb “better than a thousand days of diligent study, is one day with a great teacher”.

I also want to thank Dr. Wael Kafienah for opening the doors of his lab to me during my internship at the University of Bristol and supporting us with human mesenchymal stem cells. I would like to thank Ms. Michelle Somerville for her help with the practical fundamentals of cell culture as well as the qualitative cytocompatibility studies and flow cytometric analysis.

I would like to appreciate the support of Dr. Fatima Mraiche for the cardiomyoblasts used in this study as well as availing all the facilities in her lab when needed. I would like to thank Mr. Nabeel Abdulrahman for his help with the fluorescent microscope imaging, Dr. Saeed Al Meer and his team at the central lab unit for their support with chemical and morphological analysis and Jordan University for science and Technology for the proton NMR analysis.

I would like to thank Qatar University and College of Pharmacy for all their support. They helped me through the funding I got as a graduate teaching assistant and through funding my internship at the University of Bristol, UK. I would like to acknowledge QNRF for the support through the NPRP grant that funded this work and through the student salary.

I would like to express my warm gratitude to my Colleagues at the Pharmaceutics and Polymeric Drug Delivery Research Lab. I would like to thank Ms. Soumayeh Zamani for sharing her knowledge of Polymer chemistry and her support in the literature review. I would also thank Ms. Shijimol Arakkal, the hard worker and the big sister, for her support in every step along this project. I would like to thank both Mrs. Jensa

Joseph and Mrs. Taqdees Mahroof for their continuous support to keep the lab facilities and materials in a pristine condition. Many thanks to Ms. Youmna Hassouna for sharing her experience. A big thank you to our lab members: Mrs. Bayan Alemrayat, Ms. Nada Khudair and Mr. Loay Saifan for their support. Finally, I would like to thank Mr. Khaled Al Zahabi my colleague and brother in arms for his support and for making every moment in the lab as joyous as it gets.

My deepest gratitude for Dr. Ahmed Nader who was always a guiding mentor, a wise brother and a trustworthy friend throughout the entire work, both personally and professionally. He was always leading me to defy the borderlands of my mind, pushing me to be a better scientist. Dr. Ahmed, I am and I will be forever in debt to your priceless advice. In addition, a big shout out to all my friends, the catalysts that showed all forms of support, love and motivation to the levels of infinity. You people showed up in times I was on the verge of quitting, telling me to dig deeper and reach my maximum effort. Thank you for being who you are.

Finally, yet importantly, I would like to express my greatest gratitude to my supportive, heartwarming, accountable, honest and delightful parents, brothers and Family for their unconditional emotional and mental support. I would have never done this without you.

Dedication

To my Exquisite Family

Mrs. Zainab Zidan

Ahmed, Khaled, Bassant, Aya, Mohamed ElKhadem.

And

My loving Father

Mr. Mamdouh A. El-Khadem (1944-2014)

Chapter 1: Introduction and Literature review

1.1 Introduction

Myocardial Infarction (MI) is one of the primary causes of death globally. It affects almost million patients yearly with a development rate to heart failure of more than 30% of the cases. Many treatment strategies are being used currently that can be classified into two main categories: 1) conventional therapy and 2) Regenerative therapy. Conventional strategies such as coronary angioplasty and cardiac transplantation require complex surgical operations for both as well as finding an appropriate donor for the later. In addition, the use of thrombolytic drugs to restore the perfusion in the infract causing artery and restore cardiac perfusion is also used. However, it showed low flow restoration in almost half of the participants in a previous large clinical trial (1). In addition, most of the agents used are known to cause side effects. Regenerative strategies such as indirect mobilization of stem cells using colony stimulating factors were studied. However, it was reported to have no effect on the enhancement of the ventricular function over the placebo group after MI (2). In addition, catheter based direct endomyocardial injection of stem cells have variable results with questionable efficiency and the optimum route of delivery of stem cells to specific site remains undetermined (3).

Tissue engineering (TE) is a rapidly growing field for the treatment of organ failure that has gained a lot of interest in the past two decades. It is defined as the process of

repair and/ or substitution of damaged cells or tissues using a mixture of cells, biomaterial scaffolds and the appropriate bioactive molecules (4). It was proven to possess many advantages over the current conventional treatment approaches (5). Several methods were studied to successfully deliver cells to their specific sites. However, those methods such as synthetic implants showed several disadvantages reported earlier (6).

Biomaterial scaffolds have become potential carriers in both drug delivery and TE applications. They provide cells with the favorable environment for proper growth and proliferation in a function resembling that of the extra cellular matrix (ECM) (4). In order to serve this purpose, the ideal scaffold should be hydrophilic with a three dimensional (3D) highly porous structure to facilitates the growth and proliferation of cells within the porous structure in a way similar to their original ECM habitat. In addition, it should allow the proper suction of cell culture media during cell seeding (7). It should also be biocompatible and biodegradable to prevent any immune reaction and avoid the need for their removal via surgery (8). Moreover, it has to possess a suitable mechanical strength to physically support cell growth and allow response to different signaling pathways (9). Most importantly, it should be able to carry, deliver and release biomolecules essential for cell growth (10). All of the aforementioned characteristics serve in mimicking the natural cellular niche and therefore enable the successful growth and proliferation of the seeded cells.

Several approaches have been reported to produce porosity in a typical biomaterial scaffolds to make it suitable for TE applications such as: particulate leaching (11),

lyophilization (12), membrane lamination (13), colloidal technique (14)gas foaming (15) and electrospinning (16).

1.2 Particulate leaching and tissue engineering applications

Other methods were reported to be used to produce structures with high structural resemblance to the ECM for TE purposes (17). Particulate leaching is a conventional process widely used to produce scaffolds of three dimensional highly porous morphology (18,19). It constitutes the use of a porogen or combination of porogens with a certain particle size and concentration embedded within the polymer scaffold. The scaffold is then placed in a suitable solvent that can selectively remove porogen particles leaving a porous scaffold. The process results in a structure with more than 90% porosity with interconnected pores with sizes up to 500 micrometers (20).

1.2.1 Advantages of particulate leaching

The advantages of particulate leaching includes the ability to control the porosity and pore size easily by manipulating the particle size and concentration of the porogen. Moreover, it is a simple process that does not require many steps or complicated instrumentation. Having said that, the porogen removal can take up to several days, which is a time consuming process. It is also very hard to remove all the porogen particles especially with thick scaffolds. This constituted the reason why the thickness of most of the reported scaffolds did not exceed 2mm (21).

1.2.2 Types of particulate leaching

1.2.2.1 Single Porogen

1.2.2.1.1 Controlled pore size

Several porogens have been reported to be used for this process. Sodium chloride (NaCl) was used in the fabrication of a silk fibroin/ collagen/ hydroxyapatite composite scaffold (22). Variation of particle size and weight ratio of NaCl to scaffold components took place to examine several properties, such as pore size, pore density, swelling ratio and crystalline structure. In addition, the osteoblast cell proliferation was examined after seeding on the scaffold for a maximum period of 14 days. They reported an optimum weight ratio of polymer: porogen of 0.04:1 and an optimum NaCl particle size of 180-250 micrometers. When the weight ratio was higher, damage and changes in the shape of the scaffold took place. Finally, they reported confocal laser scanning microscope photos showing the proliferation of MG63 cells into the scaffold 3D structure. The successful fabrication of a patient specific vascular scaffold from poly (l-lactide-co-ε-caprolactone) by the aid of salt leaching played a crucial role to produce the porous flexible scaffold that resembles the blood vessels (23). They examined the properties of the scaffold in terms of porosity and mechanical strength. A 3.3% wt. of Sodium Chloride with the polymer and also varied the ratios of porogen to polymer Reach the optimum tensile strength that resembled human blood vessels.

Particulate leaching can be combined with other processes to produce scaffolds with customized characteristics. In a study conducted by Ko *et al*. particulate leaching was

combined with melt ES to produce poly (ε-caprolactone) (PCL) ES fibers with porous structure (24). In this report, they used table sugar as a porogen that was molten, mixed with molten PCL then electrospun and the resulted fibers were analyzed. Different concentrations of sugar were used and the effect on porosity was examined. They demonstrated the increase in porosity with increasing sugar concentration. However, further studies need to be done to fully characterize the electrospun scaffolds (ESS) and test them for different applications.

Particulate leaching can be used to produce multi pore size per scaffold. For instance, gelatin solutions of various concentrations were used to produce biphasic macro/micro porous scaffolds for soft tissue engineering. The porous structure was achieved using cross-linked alginate particles, which were leached out using tri-sodium citrate solution. The most appropriate elasticity was achieved at 7% w/v concentration, which also resulted in acceptable porosity and pore size. The gelatin walls had a microporous structure which facilitated the transport of small nutrients when cells were seeded. In addition, the leaching out of the alginate beads lead to a macro porous inner structure that is advantageous for cell growth. Cell growth using adipose derived stem cells was tested using hematoxylin-eosin staining and cell surface markers were analyzed using flow cytometry. To simulate conditions of extra cellular matrix, fibrin hydrogels were added while seeding the cells. Scaffolds demonstrated uniform cell growth through the interconnected pores and cell differentiation was successful when stimulated (25).

1.2.2.1.2 Shape control

Another advantage of particulate leaching is the ability to manipulate the shape of the produced scaffold as needed using different techniques. Poly (lactic-co-glycolic) acid (PLGA) was utilized to produce scaffolds of porosity up to 83%. PLGA and NaCl particles of variable mixing ratios and particle sizes were placed in a creatively designed setup. That was followed by three stages of liquid washing: a) A PLGA solvent that solubilizes the polymer particles, b) A PLGA precipitating agent that precipitates the polymer particles around the NaCl particles and c) Water to leach out NaCl leaving a porous polymer structure. They reported that different mold shapes could be used to produce different shapes (i.e. ear and bone) which if used for cell seeding, can produce organs with these shapes. However, further studies were needed to test the practical aspect of such a concept (26). It was also reported that magnetic sugar particles (MSPs) combined with NaCl were used to produce porous poly (l-lactide-co-ε caprolactone) (PLCL) scaffolds for soft tissue engineering applications. Magnetic field strength was used to control the aggregation of MSPs and hence controlling the orientation of porogen thickness and pore distribution. Results showed that less particle size and more weight faction of salt lead to higher porosity of the scaffold. In addition, they reported non-harmful toxicity levels when cytotoxicity testing was performed (27).

1.2.2.1.3 Porous composite polymers production

Particulate leaching technique was used with composite polymers as well. In the work done by Niu *et al*. they used NaCl with bioglass/ poly(l-lactide) composite to create a

porous scaffold for TE applications (28). The report showed improved water absorption, degradability and cell growth and proliferation that was due to the bioglass content. When animal studies were performed, improved osteogenesis and bioactivity were reported. This indicated how promising this scaffold was for bone TE applications. Similarly, porous scaffolds were produced using polycaprolactone/ polyethylene glycol/ hydroxyapatite composite using NaCl as a porogen (29).

1.2.2.1.4 Solvent free particulate leaching

Particulate leaching can be also performed without the incorporation of solvents. This is advantageous in terms of time since the final solvent evaporation step is skipped. Moreover, it is safer for biomedical applications due to the absence of any solvent traces, especially organic solvents. For example, PCL/ Hydroxyapatite scaffolds were produced using this technique with polyethylene oxide (PEO) as a porogen (30). In this case, PEO was used because it has a melting point close to that of PCL. Particle size of all constituents was controlled before mixing followed by melting all the components in an environmental chamber at an elevated temperature. This was followed by leaching out of PEO by immersion in water. For comparative purposes, they produced similar scaffolds but with the incorporation of NaCl. This lead to improved porosity but it gave unexpected results in the stress strain curve. This was attributed to the fact that NaCl particles are hard to be completely leached out (30,31). Generally, results showed that the incorporation of Hydroxyapatite (HA) particles lead to suitable mechanical properties for bone TE applications, enhanced cell attachment to the scaffold without any effect on porosity or pore sizes (30). In another report, a technique called “salt

leaching using powder" was utilized to produce porous PCL scaffolds. In this technique, powdered PCL and salt of a certain particle size were mixed together and put in a mold. The mold was placed in an oven at 80 ^{o}C to melt the PCL polymer particles, which was then allowed to cool down and solidify producing PCL scaffold with embedded salt particles. Afterwards, salt was leached out by immersion in water forming a porous scaffold. Porosity of the scaffold was 80% and SEM results confirmed the porous structure. Advantages of using such a method lied in the absence of solvents or pressure that might affect the cytotoxicity of the scaffold or the porous structure of the scaffold respectively. However, cytocompatibility testing was performed qualitatively, which rendered the scaffolds promising for TE applications but needed quantitative data to confirm the findings (32).

1.2.2.2 Combination of several porogens

Salt particles were also reported to improve porosity of scaffolds when used in combination with other porogens In another report, Reignier & Huneault, combined both particulate and selective polymer leaching to successfully produce a highly porous PCL scaffold (33). They used different concentrations of both PEO and NaCl (porogens) and they obtained 3D scaffold with a porosity level reaching 88%. In another study, poly ethylene glycol (PEG) was combined with NaCl to create PCL porous scaffolds for bone TE applications (34). They reported that the use of a combination of porogens lead to higher porosity, pore interconnectivity and better cell growth and proliferation for mouse Calvaria-derived pre-osteoblastic cells (MC3T3-E1).

Combination of PEG and NaCl porogens was also used to obtain porous PCL/Polyurethane scaffolds modified by aniline pentamer to be utilized for cardiac TE applications. They used N-methyl pyrrollidone to dissolve all ingredients and then placed them in an over at 80 ^{o}C to remove the solvent. Afterwards, the product was milled then compressed into a disc that was placed in water to leach out PEG and NaCl leaving a porous scaffold. Morphological analysis showed highly porous structure with interconnected pores and porosity of 75-80%. Cardiomyocytes were successfully seeded and they showed growth after 3 days throughout the scaffold which rendered this scaffold as a qualified candidate for *in vivo* studies (35).

Apart from what is reported here, a variety of other porogens have been reported less frequently ranging from, ice (17), paraffin microspheres (18) and organic material such as saccharide (36).

1.3 Electrospinning

1.3.1 Introduction and History of Electrospinning

Nanofibers production have been reported in the literature using several methods including drawing, template synthesis, phase separation, and self-assembly. Each of those method's advantages and disadvantages have been reported elsewhere (37). Electrospinning (ES) on the other hand, is another very promising fiber production method that is capable of producing fibers of diameter ranging from several micrometers down to 50 nanometers. This makes it the only known method to produce continuous fibrous structures with these dimensions (16). ES can be used with various

types of blends, fluids and polymers. It is also used in a wide array of applications ranging from filtration membranes, protective clothing, biosensors, catalysis, fuel cells to drug delivery and tissue-engineering applications (38,39). Synthetic and natural polymers can be electrospun under specific material, process and environmental factors that can be easily controlled and manipulated. ES can be also utilized to produce fibers loaded with drugs or proteins of various particle sizes and properties. The diversity of its uses, simplicity of the instrument, easy manipulation of the produced fibers according to the intended application, and the scalability of the process are the main criteria that made ES one of the most promising methods to produce biomaterial scaffolds, specifically used for TE purposes.

Historically, the first ES attempt was carried out in 1934 when Formhals and coworkers used a basic form of ES machine to produce synthetic filaments (40). Due to its flaws, evolution of this basic setup occurred via several modifications in the apparatus leading to two other patents (41,42). It was not until 1960s when attempts to understand the mechanism of ES process started. Tylor *et al.* explored the mechanism of ES process by describing the behavior of the polymer droplet at the tip of the needle to reveal what's referred to today as Tylor cone (43). This was followed in the 1970s by continuous efforts to characterize the ES fibers by different techniques (44). Finally, in 1978, Polyurethane matts were used for vascular prosthesis which was followed in 1985 by the study of the *in vivo* behavior of arterial prosthesis using ES fibrous scaffolds (45,46). These later events marked the very first efforts to use ES fibrous mats for TE purposes that were followed by numerous research work in this new field.

1.3.2 Conventional Electrospinning Machine

One of the main characters that make electrospinning process very promising is the simplicity of the machine setup. It is composed of: a) a syringe with a capillary needle that act as a polymer solution reservoir. b) A syringe pump that controls the flow rate of the polymer solution. c) A metal collector for the collection of fibers and d) A high voltage power supply with positive and negative terminals. A schematic illustration of the typical ES machine is shown in Figure 1.

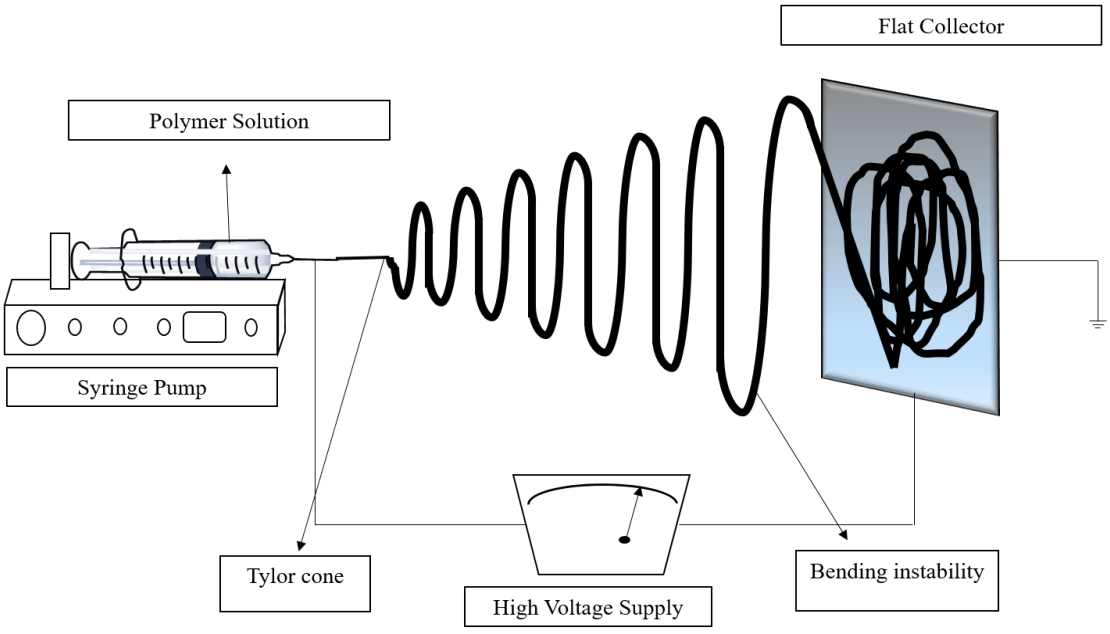

Figure 1**.** Illustrative diagram of the conventional electrospinning machine

The ES process starts with setting the pump to a proper flow rate to extrude the polymer solution out of the capillary needle. The power supply terminals are connected to both the metal needle and collector to induce voltage difference between the two poles. This creates two types of electrostatic forces, which are an attraction between the needle and the collector and a repulsion between the polymer particles of similar charge flowing through the needle. As the applied voltage elevates, the electrostatic forces increases until they overcome the surface tension of the polymer solution leading to a cone shaped liquid deformation at the tip of the needle named Tylor cone. Afterwards, a jet of the polymer solution flows towards the collector and evaporation of the solvent occurs in the meantime. The later, together with the electrostatic repulsion of polymer jet leads to a bending instability before they deposit on the collector forming the electrospun fibers (47). The machine has typically two types of setup, horizontal and vertical. In both setups, it is reported that gravitational forces do not affect the process as the jet flows at very high acceleration of $600 m/s^2$ which is double the acceleration caused by gravitational force (48).

Several parameters must be adjusted in the electrospinning process with which the produced fibers morphology and characteristics can be controlled. These factors are all interconnected and can be classified as follows: A) Material parameters, which include the type of polymer, used, solution concentration, molecular weight of the polymer used, viscosity, conductivity and solvent used. B) Process parameters, which cover pump flow rate, voltage difference, applied, needle to collector distance, and type of

collector C) Environmental parameters, which include relative humidity, airflow and temperature.

1.3.3 Factors affecting Electrospinning process

1.3.3.1 Material Parameters

1.3.3.1.1 Concentration

Concentration is one of the crucial factors affecting ES process. At low concentration, droplets come out of the needle and electrospraying takes place instead of ES (49,50,51). Upon elevating the concentration, beaded fibrous structure starts to form till those beads disappear at the ideal concentration forming bead-less uniform fibrous structure (16) (49,50,51) . For example, Gudkova *et al.* reported that at low concentration, styrene acrylonitrile co-polymer produced beaded fibers due to the high surface tension. Those beads disappeared upon elevating the polymer concentration in solution while fixing the other operational parameters (52). Moreover, increasing the concentration results in increasing fiber diameter. This is due to the increase in the number of charged particles that leads to a higher opposing force to the applied electric field (52,53). It is worth mentioning that changing the concentration manipulates the viscosity, which is the primary factor that governs fiber formation.

1.3.3.1.2 Chain entanglement and molecular weight

Sufficient degree of chain entanglement is an essential requirement for obtaining bead-less electrospun fibers (ESF). At low molecular weight, the insufficient molecular chain entanglement, low chain relaxation time, applied strain rate and the chain extension

between the entanglement junctions leads to the breakdown of the polymer stream before reaching the collector(54,55). This disruption of the polymer stream leads to the formation of beads or small droplets instead of uniform fibers and can even convert the process to electro-spraying. On the contrary, with higher molecular weight polymers, sufficient chain entanglement stabilizes the stream, allowing more electrostatic stretching and hence eliminates the beads formation. Shenoy *et al*. reported a calculation method based on entanglement analysis to calculate the entanglement molecular weight (Me) which is the average molecular weight among the entanglement junctions. In addition, a critical molecular weight was reported at which sufficient chain entanglements are achieved in a good polymer solvent mixture and hence, fibers are obtained (56). Moreover, higher molecular weight leads to higher viscosity of the polymer solution, which in turn help in the formation of bead-less, uniform ESF. Nonetheless, polymers of molecular weight lower than this critical value cannot be rendered as non-electrospinnable. Studies showed that the addition of high molecular weight polymers - even at low concentrations - to those of low molecular weight acted as chain entanglement enhancers, which leads to fiber formation and bead elimination. The main characteristics of the ideal entanglement enhancers are: relatively very high molecular weight, readily electrospinnable, has a wide range of solubility in different organic and inorganic solvents and relatively inert to the main polymer material. For example, Chen *et al.* have attempted the sole ES of chitosan in acetic acid, which formed beads only. However, upon the addition of polyethylene oxide (PEO) (Mw= 5000KDa), chitosan ESF were obtained (50). PEO was used as chain entanglement

enhancer in other reports where it lead to fiber formation by ES with a non spinnable material (57,58,59). Polyvinylpyrrolidone (PVP) on the other hand, was also used as chain entanglement enhancers in electrospinning (60).

1.3.3.1.3 Viscosity

Viscosity is a key parameter that has influence on fiber formation, fiber geometry and structure during ES. Generally, very high viscosity polymer solutions are hard to be ejected from the needle, while low viscosities tend to form droplets, converting the process to electrospraying. In between the aforementioned extremes, lies a gradient change from beads to beaded fibers and up to the critical viscosity where ESF are formed. This critical viscosity is followed by a range of optimum viscosities at which fibers are formed but vary in diameter with varying the viscosity within this range. Critical viscosity varies from one polymer material to another depending on several factors. For example, Chen *et al.* have determined the critical viscosity for poly (D,L lactide) in chloroform to be above 400cp and below 1600cp. Outside this range, either beads or beaded fibers are formed or ES is not possible (50). In addition, they referred the change in viscosity to the change in the concentration as being one of the major factors that controls viscosity. Moreover, ES of poly acrylonitrile in dimethylformamide was attempted and the viscosity was controlled by varying the concentration (61). It was reported that the low concentration solution (4%w/v) was not spinnable due to the very low viscosity. Upon increasing the concentration and hence the viscosity, a mixture of beads and fibers was formed followed by beads disappearance and uniform fibers formation at concentrations above 10 %w/v. The

polymer solution was non-spinnable at 20 % w/v onwards due to the very high viscosity that hindered its flow from the needle. In addition, the type of solvent used where the same material might have different viscosities in different solvents impacts viscosity. PVP solutions, for example, show remarkably different viscosities when different solvents were used which affected their electrospinnability indicating the importance of choosing the suitable solvent system for ES (62). It is also worth mentioning that an increase in the solution viscosity corresponds to an increase in the fiber diameter and vice versa (61,62).

1.3.3.1.4 Surface tension

Electrospinning process takes place when the applied electrical force exceeds the surface tension of the polymer solution. Therefore, the lower the surface tension, the easier the ES process. High surface tension is associated with low polymer solution concentration and low viscosity (63). It also prevents fiber formation in electrospinning under a certain concentration leading to the formation of droplets, rendering the polymer solution as non-spinnable (16). In one study, it was reported that with low gelatin solution concentration (7%), no fibers were formed due to the high surface tension and low degree of entanglements (49). This has been overcome by increasing the concentration of the solution to 20%, which resulted in higher viscosity and lower surface tension which eventually lead to nanofibers formation (49). In addition, the solvent system used caused changes in surface tension and consequently to the ES fibers produced. This was represented by the variation of surface tension and hence

fiber properties when using ethanol only versus ethanol and water as solvents for PVP prior to ES (64).

1.3.3.1.5 Conductivity

ESF are mainly formed under the domination of electrical force. Thus, the surface charge of the polymer particles, presence of ions and hence the conductivity plays a major role in the final structure of the fibers. Since different materials have different conductivities, controlling conductivity is essential for ES in some cases. Generally, increasing the conductivity leads to smaller fiber diameter and aids in bead elimination. It was found that as the conductivity and surface charge of the polymer increases, more repulsion between polymer particles occurred resulting in the decrease of the fiber diameter (65,66). However, very high conductive solutions were reported to be unable to form Tylor cone (67). On the other hand, very low conductivity will prevent the electric force from forming Tylor cone and hence a continuous stream from needle to collector will not be established (67). Either using solvent mixtures or salt additions can control solution conductivity. The same polymer material can have different conductivities in different solvent/solvent mixture. For example, PVP has variable conductivities when dissolved in ethanol only versus ethanol/ water mixture (64). Also, the increase in the water content lead to an increase in the electrical conductivity. (64). In addition, when ES was attempted on polystyrene, different conductivities were reported when using the same solvents from different suppliers like dimethyl formamide, tetrahydrofuran and chloroform (65). The second factor that can manipulate conductivity is the addition of ionic salts. Those ionic charged salts, even

in the lowest concentration, can affect the fiber morphology, diameter and the formation of beads. For instance, magnesium chloride, lithium chloride and sodium chloride produced a variation in conductivities of PVP in ethanol during ES. The overall result was a decrease in the bead formation associated with a decrease in the fiber diameter for the same reason mentioned earlier (65). Similarly, when PEO/water mixture was electrospun, addition of NaCl caused an increase in the conductivity and a decrease in the fiber diameter, following a power law relation (67). Chen *et al.* have also reported that conductivity can be used as guidance signals for cell growth and proliferation. Upon the addition of polyaniline in low concentration to ε-polycaprolactone, conductivity was significantly increased. In addition, presence of polyaniline salt improved myoblast differentiation compared to polycaprolactone alone (68).

1.3.3.2 Process Parameters

1.3.3.2.1 Flow rate

Low flow rate could result in the inability of the polymer to be ejected from the needle while high flow rate could result in beaded fibers. This is due to a malformed Tylor cone and incomplete drying of the solvent before reaching the collector. Generally, a low flow rate that is high enough to eject the solution is favorable to allow solvent evaporation and prevent bead formation. This was clear when a low and a high flow rate was used to electrospin poly acrylic acid in ethanol. Ribbon structure was formed on high flow rate indicating the presence of unevaporated solvent while the Tylor cone could not be preserved on low flow rate (69). In addition, it was reported that increasing

flow rate lead to a significant increase in fiber diameter. This was due to the increased amount of polymer solution expelled from the needle, which lead to larger fibers depositing on the collector. This also led to thicker scaffolds, higher porosity and larger pore size at higher flow rate. However, more uniform diameter distribution was established at lower flow rates (70). In addition, an increase in the average pore size was the result of elevating the flow rate (71).

1.3.3.2.2 Applied Voltage

The applied voltage is another characteristic parameter for the ES process. It is responsible for charging the polymer solution and therefore pushing the polymer jet to the grounded collector. At a low applied voltage, the electric force is insufficient to counteract the surface tension of the polymer drop on the needle and the jet fails to flow to the collector. A critical voltage has to be applied to enable the electric potential to overcome the surface tension and the jet starts flowing to the collector. The variation in voltage affects both the fiber diameter and the diameter distribution. Generally, increasing the applied voltage leads to a decrease in the fiber diameter (53,72). This is referred to the increase in the repulsion forces between the polymer particles leading to more extension and hence a decrease in the fiber diameter (73). When the voltage is increased to a very high level, an increase in the fiber diameter takes place due to the forced increase in the polymer solution expelled from the needle which might form beads (72,73). In addition, increasing the voltage was found to resolve the problem of beaded fibers as in the previously reported electrospinning of gelatin solutions (53,73).

1.3.3.2.3 Needle to collector distance and collector type

The distance between the needle tip and the collector needs to be optimum to allow enough time for solvent evaporation and hence, fiber formation. A very short distance will form a straight jet only due to the inadequate length to form the bending instability (47). Moreover, a short distance leads to bead formation in a way similar to that with a very high applied voltage. This is due to an increase in the field strength which causes stream instability (72). Longer or shorter distances than the optimum, will cause fiber diameter differences. In general, an increase in the distance leads to a decrease in the fiber diameter. This is attributed to the increased elongating of the stream before hitting the collector (72). In addition, different collector types yield different fiber geometry and alignment. Generally, in TE applications, flat plate or rotating mandrel collectors are typically used to obtain uniform, random or aligned fibers for different uses. Flat collector can be used to produce randomly aligned ES scaffolds. Rotating collector produces more aligned fibers which mostly aim for aligned cell growth on the scaffolds (50). Vaquette *et al.* have used different collector morphologies of variable patterns to examine the effect on scaffold porosity and cell proliferation compared to conventional ES scaffolds. They reported that produced ESF take the shape of the collector and there was an overall enhancement of porosity, pore size, cell penetration and growth. However, mechanical properties were lower than conventional scaffolds because of the higher porosity attained (74).

1.3.3.3 Environmental Parameters

It is important to perform ES under controlled environment since the surrounding environment plays a critical role in shaping the final fibers formed by ES. However, there are not too many reports discussing that role. When ES was conducted under various humidity levels, beads formation was noticed under low level while the beads disappeared under high humidity level (75). It was also reported that when the humidity level was elevated above 30%, the fiber surface became porous due to evaporative cooling of the solvent under high humidity (76). Temperature alone had no significant effect on the process but with high humidity, its effect was well presented by bead disappearance. Moreover, fiber diameter was found to decrease with the elevation of temperature due to the decreased viscosity of the solution (77). In addition, if there was an air flow around the flowing jet, this might affect the interaction of the polymer particles together leading to a non-expected change in the pattern of the fibers (78). In summary, as seen in the above overview on the other factors affecting ES process, all parameters are cross-correlated and affect one another. For instance, concentration of the solution and the dispersed polymers' molecular weight affects viscosity and chain entanglement, which influences the fiber diameter. The distance between needle and collector and applied flow rate influence the morphology of fibers with variable applied voltages. Surface tension variation will lead to the variation of the applied voltage. Material conductivity influences the used applied voltage, which in turn changes the fiber diameter. Thus, the ES process and the produced Nano fibrous

scaffolds can be controlled by finding out the optimum combination of all the aforementioned factors.

1.3.4 Types of Electrospinning

Changes in the basic setup of the ES machine can be done to accommodate the different materials used, the intended structure, and application to be achieved. For example, poly-ε-caprolactone and gelatin based ESF were investigated as a potential sustained-release drug delivery system which appeared not to be very promising at the beginning, as immediate drug release was the dominating mechanism (79). Addressing this issue lead to the discovery of the two-phase electrospinning techniques such as co-axial and emulsion electrospinning, that produced fibers with core shell properties capable of forming ESF for use as sustained-release drug delivery systems (80,81). Some other applications required loading of different materials on the produced scaffold as in case of blend or composite ES that were used widely for bone TE. This concept of ES involved blending all the needed components into the polymer solution, forming a suspension, which was then electrospun to form loaded fibers (82,83). In some other cases, the elimination of the use of organic solvents was a necessity. In that case, solid material or combination of materials were melted within the syringe of the ES machine and then directly electrospun in a process called melt electrospinning (84,85). Moreover, some materials that can be used in TE applications are non-electrospinnable. Collagens for example, were considered non-electrospinnable although they are natural components of ECM with relatively high cell adhesive properties and biocompatibility

compared to synthetic materials. However, these materials were successfully electrospun upon mixing with other electrospinnable polymeric materials in a multi-source multi-power electrospinning design (86).

1.3.4.1 Reactive Electrospinning

In this type, the ES process is combined with a crosslinking method applied *in-situ* to the jet flowing from the needle to the collector (87). The crosslinking mechanism of the nanofibers was further used to classify the process into two main subtypes. If the jet was exposed to a chemical crosslinking agent, it was called chemical reactive ES (CRES). Similarly, upon exposing the flowing jet to different types of radiations (e.g. visible light, ultraviolet light or gamma radiation), the process was named as photo-reactive ES (PRES). The mode and location of exposure of the polymer to the crosslinker was also used to classify the process into several types reported elsewhere (87)

1.3.4.1.1 Chemical Reactive Electrospinning (CRES)

In CRES, the chemical crosslinking reaction takes place *in situ* during the ES. It can take place within the syringe just before expulsion of the solution to the collector or while the jet is flowing towards the collector. Several approaches have been applied to utilize CRES to yield products suitable for the intended applications.

1.3.4.1.1.1 Environmental crosslinking

It can take advantage of environmental conditions to establish a fast crosslinking. In a report by Molnar *et al.,* Polyamide based gel scaffolds were prepared using CRES by

utilizing the oxygen in the atmosphere. In their report, polysuccinimide grafted with cysteamine moieties dissolved in dimethylformamide for ES was used. When the polymer solution was ejected from the needle, the oxygen in the air caused a rapid crosslinking reaction at the sulfide moieties, which lead to the *in situ* crosslinking of the jet to form the intended ESF. The authors conducted a thorough job in explaining the chemistry and the mechanism of both the reaction and fiber formation. Although their main aim was to hydrolyze the produced fibers to form gel fibers, investigating the effect of crosslinking was not explored beyond the effect on the viscosity of the ES solution and the diameter of the produced fibers. In addition, a control scaffold was produced using the linear non-grafted, non-crosslinked polysuccinimide. SEM analysis showed the formation of ESF which was not compared with an SEM of its crosslinked replica. However, the approach of producing gel fibers by these investigators was a new approach to enhance the diffusion of molecules into the mesh microstructure. Unfortunately, as per atomic force microscopy conducted, fibrous structure produced was lost upon wetting due to the inflation of the fibers, which upon drying stuck together due to the high hydrophilicity(88). The advantage of such a process could be discovered in a future study.

Dong *et al.* used an innovative approach to minimize the toxicity of Cyanoacrylates used for wound closures. An airflow assisted ES process was used with the FDA approved n-octyl-2-Cyanoacrylate medical glue for what was called "*in-situ* precision ES". This process can be referred to as *in-situ* crosslinking where cyanoacrylate crosslinked upon exposure to anionic initiators once electrospun on wound surfaces. In

that study, water molecules in the atmospheric air acted as an *in situ* crosslinker to form the thin fibrous membrane on wound surface. In addition, the ESF were crosslinked more via the amino groups abundantly found in the liver tissues. This aided in the complete wound closure and hence stopping further blood loss. They were able to decrease the dose by approximately 80% compared to that used with conventional spraying. Consequently, this decreased the toxic effects of cyanoacrylates like inflammation and necrosis to moderate and low ranges as confirmed by the histological examinations after seven days with hepatocytes. In addition, fast restoration of homeostasis occurred represented by the liver enzyme levels at three and five days compared to spraying. Also upon attempting to close the wound and amputating the suture, the operation was easily performed in case of ESF due to the accurate controllable range of the ES process. On the contrary, three rats died upon performing the same operation due to the wide range of deposition in case of spraying. This innovative approach is very promising for civilian and military applications. However, further elaboration on the ES process parameters, machine setup, chemical and morphological characterization would have been be a good addition to their work. In addition, the researchers reported the use of n-octyl-2-CA on liver cells although it was FDA approved for external use only instead of using n-butyl-2-CA, which was approved for internal use already. Moreover, the sample size varied in their experiments and only rat liver was used as an example of the application (89).

1.3.4.1.1.2 Direct mixing

A modified variation of hyaluronic acid (HA) with low molecular weight was reported to utilize dual syringe setup with concurrent chemical crosslinking. In their report, Ji *et al.* used 2 %w/v of 3, 3′-dithiobis (propanoic dihydrazide) modified HA as the main component with PEO as viscosity modifier in one syringe. The chemical crosslinker, polyethylene glycol diacrylate, was used in the second syringe with concentration of 9 % w/v. Upon initiating ES, the two solutions were mixed and crosslinking occurred *in situ as* the jet flows to the collector. The formed scaffolds were soaked in water to undergo PEO removal, which was confirmed by FTIR and DSC analysis. Afterwards, to enhance cell attachment the scaffolds were covered with human fibronectin and examined cell growth of 3T3 fibroblasts. Confocal microscopy showed that cells grew into the scaffold forming a 3D dendritic structure. This approach had the advantage of controlling the crosslinking degree and hence the physical properties of the scaffolds by controlling the ratios of crosslinker to polymer in the ES process. However, further testing of the mechanical properties of the scaffolds might be needed to determine the exact TE purpose of use (90).

CRES was also applied to produce fibers with pores embedded on the fiber surface. Mentonite particles were formed *in-situ* from its precursors during the ES process. This reaction produced water as a side product, which induced pore formation on the surface of the fibers. This porous structure was reported to have its advantages for future biomedical uses (91).

1.3.4.1.1.3 PH change

Another strategy is to use the ES process itself in favor of fiber formation. The pH change that occurred due to solvent evaporation facilitated the polyelectrolyte complexation (PEC) of lignin/chitosan/PEO based solutions in acetic acid/water solvent system to produce ES fibers (92). In that report, the authors soaked the formed fibrous mats in water to eliminate the PEO. Soaking in water gave the advantage of enhancing the PEC bond strength and hence rendered them thermally more stable. However, ES was not attempted without PEO for comparison reasons. In addition, the SEM images of the fibrous structure contained some branching and some fusion points where several fibers merged to one thick fiber. Yet, the advantage of using green solvents paved the road for many applications that can be pursued in future studies.

1.3.4.1.1.4 Combining with other crosslinking strategies

Co-axial setup together with thermal crosslinking was utilized in a report by Niu *et al.* Polydimethylsiloxane (PDMS) was used as a core polymer cured thermally by collection on a hot plate at 100 ^{o}C during electrospinning with a PVP shell in a Co-axial ES setup. This was followed by leaching out the PVP coat, leaving the formed crosslinked PDMS fibers. The main characteristic of the produced scaffolds was the high elasticity and tensile strength. Both sole fibers and fibrous mats showed an exceptionally high elongation ratio of 212% and 403% respectively. The study included comparisons between conventional film and fibrous mats. Despite the lack of comparison with other polymers designed for the same intended use, this study utilized

the high elasticity of silicone polymers to be used in different applications, including biomedical ones (93).

1.3.4.1.1.5 CRES and post-crosslinking

The advantages of CRES versus post crosslinking of the fibrous mats have also been investigated (94,95). In these studies, post-crosslinking process caused a non-uniform crosslinking between the surface and the interior part of the scaffold. This lead to the loss of porous morphology of the fibrous mats. In addition, it might have produced fibrous mats with traces of toxic crosslinking agents, which would affect their use for biomedical applications (94,95). In an attempt to prove the superiority of CRES, Meng *et al*. compared both the *in situ* and the post crosslinking processes for electrospun collagen only scaffolds using a mixture 1-ethyl-3-(3-dimethyl-aminopropyl)-1-carbodiimide hydrochloride and N-hydroxysuccinimide crosslinkers (96). In their work, collagen was mixed with the crosslinking agents and the mixture was transferred to a syringe after which ES was performed. The work demonstrated that *in situ* crosslinking prevented the drop in the size of the scaffold that resulted from using post crosslinking strategies when placed in water. Moreover, a preserved porous structure was still seen even after immersion in water suggesting sufficient water resistance. Mechanical testing showed reasonable results between dry and hydrated *in situ* crosslinked scaffolds. However, a comparison between the mechanical properties of *in-situ* crosslinked versus post cross-linked scaffolds would have added more advantages to the CRES. Although it is a one-step process, it is very delicate that is affected by other factors as humidity and the ratio of cross linkers. In addition, no *in-*

vitro study for cell or drug release was performed to assess the extent of using that scaffold in biomedical applications.

CRES with post-crosslinking strategies was also discussed in several reports using synthetic materials for TE applications. In a report by Yuan *et al.*, the pure, glutaraldehyde (GTA) *in situ* crosslinked and GTA post crosslinked PVA electrospun fibers were compared (97). In this report, a 12% pure PVA was used as a reference to get ideal material parameters for ES. Afterwards, GTA post-crosslinked electrospun fibers were used as a control and compared to the *in situ* thermal/ GTA crosslinked fibers in terms of fiber morphology, water resistance, mechanical properties and thermal stability (97,98). Results showed that the *in situ* crosslinked PVA scaffolds had higher elastic modulus with reserved fibrous structure after water immersion for 24hours. Moreover, the *in situ* crosslinked fibers were thermally more stable than the control. However, weight loss upon water immersion for more than 24 hours was not assessed which could limit the use of these scaffolds in case of sustained-release delivery. In addition, enhanced mechanical properties of the fibers in case of *in situ* crosslinked fibers was reported which was represented by an increase in young's modulus compared to control. This requires a comparison to a reference value of young's modulus depending on the intended use. SEM results showed beaded fibers for concentrations less than 12%. However, 10% PVA was reported to produce non-beaded fibers (99). Finally, the use of these scaffolds in TE applications need further testing, especially with the use of GTA, which has cytotoxic effects, and with the use

of heat, which might hinder the application of these scaffolds for bioactive molecules and protein incorporation and delivery.

1.3.4.1.2 Photo- Reactive Electrospinning (PRES)

Photocrosslinking was proven to overcome many limitations present in chemical crosslinking processes. For instance, removal of residues of some cytotoxic cross linkers such as glutaraldehyde was always a challenge. Therefore, achieving photocrosslinked fibers without these issues is a trending interest. Moreover, for *in situ* crosslinking, the crosslinking is usually more evenly dispersed throughout the fibers, while the post crosslinking method can lead to an un-even crosslinking on the surface and interior of the fibers, which in turn has an impact on the mechanical characteristics of the produced ES mats. Several approaches have been followed to maximize the benefits of PRES according to the purpose of use. These can be listed as follows:

1.3.4.1.2.1 PRES with Ultraviolet (UV) irradiation

For PRES to work, sufficient energy source should be used to achieve efficient crosslinking in the short period of time when the jet is flowing to the collector. On the other hand, it should be relatively safe. Visible light was not used with PRES due to its low energy, requiring longer periods to achieve the needed degree of crosslinking. Consequently, most of the reports published, used UV light the crosslinking source as it satisfies the above criteria. Few reports utilized Gamma radiation due to safety concerns.

1.3.4.1.2.1.1 Polymeric materials with photo reactive double bonds

Photocrosslinking was reported to offer control over few properties such as elasticity. While electrospinnable polymers are mostly thermoplastics, few of them are elastomeric. In an attempt to have viscoelastic fibers, Tian *et al*. reported the fabrication of polybutadiene rubber (BR) electrospun, photo cross-linked fibers (100). These fibers have the potential to be used in innovative composites with improved mechanical properties compared to the conventional composites. To achieve their goal, entanglement concentration was calculated of BR in THF solution using equations based on viscosity then the optimum concentration for ES was chosen accordingly. The optical microscope images confirmed that any concentration below or equal to the entanglement concentration, beads and beaded fibers were obtained respectively. Further increase in concentration resulted in the formation of uniform bead-less fibers that started to lose their morphology after 8 hours of storage under ambient temperature. To overcome the change in morphology, *in situ* photo-crosslinking using a halogen lamp was introduced during electrospinning in the presence of camphorquinone initiator. The obtained fibers preserved their morphology under ambient temperature for 20 hours. Although the results were interesting and promising for new composites, further studies are required regarding the mechanical, thermal properties of the fibers and morphological analysis using SEM. Commercial medical polyurethane was modified chemically with acyl chlorides, electrospun and crosslinked during electrospinning using UV light to manufacture vascular grafts with suitable characteristics. SEM images showed the successful ES of Polyurethane, which showed

an enhancement in the solvent resistance to both H_2O_2 and $AGNO_3$ due to UV crosslinking. The produced grafts possessed suitable burst pressure and a decrease in the compliance after crosslinking due to the relatively low porosity in the wall of the graft, which was yet within the physiological range. The modified polyurethane also showed a reduction in hysteresis and creep. There is no doubt that a cytotoxicity study using the modified polyurethane was needed to confirm its cytocompatibility and hence its validity for vascular grafts production. Moreover, a comparison in the mechanical properties of both crosslinked and un-crosslinked ES grafts taking into consideration the degree of modification would have been of considerable value. Having said that, the ease of controlling the degree of crosslinking with chemical modification and the utilization of *in situ* low toxicity and efficient UV crosslinking have rendered it a promising technique for broadening the area of application of the medical polyurethane (101). In another context, photo reactive methacrylate groups were added chemically to PVA, which was further UV crosslinked in a PRES process. The crosslinking process rendered the fibers resistant to different solvents and sarcoma cells were grown successfully on the scaffolds. Although UV crosslinking has its advantages, this report contained only qualitative data without showing the quantitative aspect in terms of the fibers physical, mechanical, degradation properties and in relevance to cytotoxicity assays (102). Another example for chemical modification of a material rendering it suitable for PRES was reported. Wu *et al*. reported the synthesis of Poly (2, 3-dihydroxycarbonate) followed by the addition of UV responsive methacrylate group. This was followed by ES with an *in situ* UV crosslinking using a variety of

methacrylation degrees, UV intensities and ratios of PEO as an entanglement enhancer. The variation in the methacrylation degree affected the degree of crosslinking and hence several aspects of the characterization. FT-NIR analysis showed the successful reaction completion with variation in methacrylation peaks. Morphological analysis showed the successful production of fibers with and without UV crosslinking. However, upon immersing the fibers in chloroform for 24 hours, the un-crosslinked fibers completely dissolved while the crosslinked fibers preserved their physical structure. In addition, fiber diameter increased with increasing the crosslinking degree and ESF showed amorphous behavior after crosslinking indicating higher thermal stability compared to the non-UV crosslinked. Moreover, an enhancement in elastic modulus and tensile strength corresponding to increasing degree of crosslinking occurred while biodegradation rate showed a decrease with increasing the crosslinking degree. This was an indication of the ability to control the fiber properties with controlling the initial synthesis reaction. The produced ESF also demonstrated efficient cytocompatibility compared to both the film and the control tissue culture treated plastic. The cells were able to attach and grow on the surface of the scaffolds more efficiently than the control indicating its promising future for tissue engineering applications (103). The methacrylation approach was also utilized in another study used poly (2-hydroxyethyl methacrylate). The produced fibers after UV crosslinking showed an enhancement in the elasticity upon immersion in water as shown by atomic force microscopy. The fibers were not produced without UV exposure indicating the importance of PRES for fiber production. However, more analysis in terms of

morphological, thermal, mechanical testing and cytotoxicity assessment is needed to render the polymer material as a promising candidate for TE application (104).

1.3.4.1.2.1.2 Addition of photo reactive groups

This is the most common approach used when it comes to PRES. One of the earliest PRES attempts was performed through the addition of a cinnamoyl group to poly (methyl methacrylate- co-2-hydroxyethyl acrylate) to render the polymer UV cross-linkable. Different percentages of cinnamoyl groups were incorporated and the successful reaction was confirmed by absorbance FT-IR. In addition, UV absorbance was measured for both UV crosslinked and non-crosslinked ES fibers indicating the successful addition of cinnamoyl groups. However, SEM results showed no major differences between UV crosslinked and non-crosslinked ES fibers. In addition, the effect of UV on mechanical properties was not explored. Yet, this work opened the door for other attempts to utilize UV crosslinking in the ES machine setup (105).

In another study report by Xu *et al*., PRES was attempted using methacrylated L-poly ethylene imine (PEI) to produce scaffolds for TE purposes. They attempted to electrospin different concentrations of methacrylated PEI in ethanol with *in situ* crosslinking using UV light. It was found that porous ESF could not be produced with concentrations varying from 10% and up to 30% w/v and using different methacrylation degrees ranging from 3% and up to 59.2 %. The reason behind the collapse of the fibrous structure was attributed to the hydrophilic nature of the polymer material. The other reason was the low molecular weight of the PEI used in preparation

of ESF which lead to a degree of chain entanglement below the critical level needed for fiber formation. Those reasons made the research team use 2% w/v of high molecular weight PVP to act as an entanglement booster. The SEM results showed successful formation of porous fibrous structure of PEI concentrations of 10, 20 and 30%. Fiber diameters showed an increase with increasing the UV intensity. On the other hand, a mean fiber diameter of 419 ± 256 nm for non-UV crosslinked fibers was reported, which contradicted the SEM results that showed no fiber formation. Moreover, the UV crosslinking process rendered the scaffold resistant to ethanol, water and culture medium preserving the porous structure. Also the effect of different UV intensities (140 and191 mW/cm^2 at 14.8% acrylation degree and 140 mW/cm^2 for 59.2 % acrylation) on the morphology was examined. However, ESF prepared under UV intensity of 85mW/cm^2 were subjected to mechanical testing in which they reported an increase in the apparent tensile strength with increasing the crosslinking degree. It is worth mentioning that the acrylation degrees used for tensile testing were only up to 14.8% without testing the other acrylation degrees reported in other tests. In addition, further future testing of the scaffold porosity, pore size and in vitro cytocompatibility could make those scaffolds a promising candidate for TE applications (60).

A study reported by Lin and Tsai was another example of *in situ* photocrosslinking of gelatin fibers (106). Unlike the majority of work on PRES, where the polymer usually constitute a double bond activated by a photo initiator for crosslinking, their work was based on azido (AZ) group that was activated to an active nitrene group upon exposure to UV. This short-lived group readily reacted with any CH or NH available group

rendering chemical bond. The azido group was incorporated to polyacrylic acid chains (PAA) and PAA-AZ was mixed with gelatin prior to ES. A comparison from mechanical and cell attachment/cytotoxicity point of view was done between the azido cross-linked gelatin and conventional glutaraldehyde (GTA) cross-linked gelatin. DSC results revealed that unlike PAA-AZ cross-linked fibers; crosslinking by GTA was uneven throughout the fibers. That was due to creation of a cross-linked layer on the surface preventing the diffusion of GTA vapor into interior of the fibers. Cell culture on gelatin fibers cross-linked by GTA showed some cytotoxicity while PAA-AZ cross-linked fibers had superior cellular compatibility. Finally, to improve bioactivity of gelatin ESF, the authors incorporated hydroxyl apatite nanoparticles into the fibers and observed better mineralization of the cells that confirmed the suitability of these fibers for tissue engineering applications.

1.3.4.1.2.1.3 Using pre-crosslinked material

Another PRES approach was implemented on PVA. First, it was chemically cross-linked with tetraethyl ortho-silicate and 3-trimethoxysilylpropylmethacrylate to render it water insoluble. Afterwards, it was mixed with 4-vinylbenzene boronic acid/ hydroxyl appetite/ keratin prior to ES. The nanofibrous scaffold was *in situ* crosslinked using UV light and it was subjected to cytotoxicity testing using MTT assay. The results were satisfactory especially for the formulations containing keratin. However, the benefit of reactive ES with UV crosslinking was not thoroughly investigated. Further studies are needed to investigate the effect of UV on the fibrous morphology using a non-cured scaffold as a control. In addition, mechanical properties of the scaffold needs

to be further explored as it might have an effect on cell proliferation and development (107).

1.3.4.1.2.1.4 Addition of a Photo Reactive Polymer material

The PRES was reported to also enhance the mechanical properties of the ESF when implied. For instance, polyurethane based scaffold demonstrated enhanced tensile strength when mixed with variable ratios of polyethylene glycol methacrylate and *in situ* UV cross-linked during ES. It was found that the higher the percentage of the methacrylate moiety, the higher the tensile strength of the scaffold compared to other scaffolds with less methacrylate and more polyurethane. Moreover, hydrophilicity showed an enhancement as represented by water uptake and contact angle measurements. Cytotoxicity testing was done on human umbilical cord vein cells and the scaffolds were rendered cytocompatible (108,109).

1.3.4.1.2.2 PRES and Gamma radiation

Fibrous structures can sometimes be hard to be established using UV light. The polymer stream in some cases needed higher energy to achieve the required degree of crosslinking for maintaining the fibrous structure. Dargaville *et al*. studied the ES of low Mwt poly (trimethylene carbonate- l-lactide) by acrylation of the end groups of the polymer (110). Their attempts to *in situ* or post crosslink the fibers using UV light were not successful due to the low glass transition of the polymer and slow crosslinking kinetics compared to fiber fusion. The heat produced by UV lamp was another parameter increasing the fiber fusion speed. It was believed that to have fibers produced

from a polymer solution, the concentration of the solution should exceed that of critical entanglement concentration in order to resist the stretching caused by the voltage without breaking into droplets. With the low Mwt copolymer used, this was not possible. Therefore, Gamma irradiation was utilized to achieve a stable morphology of fibers. Although there was a possibility of induced degradation, Gamma irradiation had many advantages to offer including high efficiency, sterilization effects and elimination of the need for photo-initiators with possible toxicity. The obtained fibers showed good resilience and elasticity in cyclic mechanical testing and fatigue testing, which was too important for applications in mechanically dynamic environments such as the vascular system. In addition, the moduli that was in the range of human arteries and enhancement of the growth and proliferation of human mesenchymal stem cells (hMSCs), gave the researchers a good reason to conclude that these scaffolds are an appropriate candidate for vascular tissue engineering.

The chain degradation induced by gamma rays can affect mechanical properties of the polymer. For instance, plastics are usually gamma irradiated to induce crosslinking and therefore improve their mechanical properties. However, this effect may sometimes be negative on the properties as is the case with Polyamide 66 (PA66) fibers. In one study, this drawback was resolved by adding the crosslinking agent triallyl cyanurate (TAC) at a low concentration. The mechanical properties of PA66-TAC were improved by irradiation induced crosslinking (111). The effect of irradiation on cell response is especially important in biomedical applications where gamma irradiation is one of the approved techniques for sterilization. A study on polycaprolactone (PCL) fibers

showed that gamma irradiation affects many properties of the fibers. Decreased molecular weight, increased crystallinity and decreased mechanical properties, which were expected due to the lower molecular weights, were some examples. However, a comparison of sterilization using gamma irradiation and by submerging in ethanol revealed that there is no significant difference between the two methods and both supported the cell proliferation (112).

Table 1 represent a summary list of the most recent studies utilizing reactive electrospinning with details pertaining to the utilized polymer, the chemical crosslinker used in case of CRES, source of radiation and initiator used in case of PRES.

Table 1. A list summary of the most recent studies utilizing reactive ES

Polymer	Type of reactive ES	Crosslinker or Radiation Source	Initiator	References
Polyvinylalchol	Chemical	Glutaraldehyde	N/A	(113) (97)
Hyaloronic Acid	Chemical	Thiolated HA derivative, 3,3′-dithiobis(propanoic dihydrazide)/ poly(ethylene glycol) diacrylate	N/A	(90)
poly(2-hydroxyethyl methacrylate)/ 2-ethoxyethyl methacrylate	Chemical	ethylene dimethacrylate	N/A	(114)
Poly(2-hydroxyethyl methacrylate)	Photo	Ultra Violet light	2,2′-azobis (isobutyronitrile) and Darucur 1173	(104)
Chitosan	Chemical	Glutaraldehyde	N/A	(115)
Poly(methyl methacrylate-co-2-hydroxyethyl acrylate)	Photo	Ultra Violet light	2,2′-azobis (isobutyronitrile) / no photoinitiator	(105)
Poly (aspartic acid)	Chemical	Atmospheric oxygen	N/A	(88)
Lignin/ Chitosan	Chemical	PH change due to solvent evaporation	N/A	(92)
Poly lactic acid/Mentonite	Chemical	Orthophosphoric acid/ Calcium hydroxide	N/A	(91)

Collagen	Chemical	1-ethyl-3-(3-dimethyl-aminopropyl)-1-carbodiimide hydrochloride/ N-hydroxysuccinimide	N/A	(96)
Bis maleimide terminated Poly-L-Lactide/ bis furan terminatedPoly-D lactide	Chemical	Spnotaneous Diel alder's coupling	N/A	(116)
Methacrylated polyvinyl alchol	Chemical/ Photo	3-mercaptopropyl trimethoxysilane/ UV	Camphorquinone and Darocur 173	(102,117)
Methacrylated cellulose acetate butyrate/ collagen	Photo	UV light	Irgacure 184	(118)
Poly butadiene	Photo	UV	Camphorquinone	(100)
Gelatin/ phenylazide-conjugated poly(acrylic acids)	Photo	UV	N/A	(119)
Poly vinyl alchol/ 4-vinylbenzene boronic acid/ hydroxyl appetite/ keratin	Chemical/ Photo	Tetraethyl ortho silicate and 3-trimethoxysilylpropylmethacrylate/ UV light	Darocur 1170	(120)
Polyurethane/ Poly ethylene glycol methacrylate	Photo	UV light	Benzophenone	(108,109)
poly (trimethylene carbonate- l-lactide)	Photo	Gamma radiation	Camphorquinone	(110)
Polyamide 66	Photo	Gamma radiation	N/A	(111)
Polycaprolactone	Photo	Gamma radiation	N/A	(112)
n-octyl cyanoacrylate	Chemical	Atmospheric water molecules/ amine groups in the liver	N/A	(89)

Poly (2,3 L-hydroxy carbonate)	Photo	UV	Bis (2,4,6trimethylbenzoyl) phenyl-phosphine oxide	(103)
Medical poly urethane	Photo	UV	Cumene hydroperoxide (CHP), dicumyl peroxide (DCP) 2,2′Azobisisobutyronitrile (AIBN) (thermal) ω,ω-dimethoxy-ω-Phenylacetophenone (DMPA) (Photo)	(101)
L-Polyethylene imine	Photo	UV	phenyl-bis(2,4,6-trimethylbenzoyl)-phosphine oxide	(60)
polydimethylsiloxane (PDMS)	Thermo-Chemical	100^{o}C heated collector	N/A	(93)
3,3′-dithiobis(propanoic dihydrazide)-modified HA (DTPH-HA)	Chemical	Polyethylene glycol diacrylate	N/A	(90)

1.3.5 Types of Polymers used for Electrospinning

1.3.5.1 Introduction

Several natural and synthetic materials have been used generally to produce ESS for TE applications and they were reported previously (121,122,123). Each of those materials has its advantages, disadvantages and methods to improve the electrospun product for the intended application.

1.3.5.2 Natural materials for electrospinning

Since they readily exist in the human body as in ECM, natural materials are the most biocompatible with the least immunogenic reaction. They allow cell adhesion, growth and proliferation of cells remarkably. Several natural polymers were successfully electrospun, yet few of them have been solely electrospun. For example, Gelatin was solely electrospun successfully by optimizing the solvent composition of acetic acid and water together with the other ES parameters (124). A concentration of 16% gelatin in acetic acid/water (70%:30%) solvent produced fibrous mats that supported the attachment, growth and proliferation of keratinocytes for skin regeneration. Further histological analysis performed on mice revealed successful collagen growth and reduced inflammation within 7 days.

On the other hand, there are several challenges facing the ES of natural materials. One of the challenges is there limited solubility in water; this is the reason why strong organic solvents such as 1, 1, 1, 3, 3, 3-hexafluoro-2-propanol and trifluoroacetic acid are used to dissolve them. Collagen was reported to be electrospun without additives

in several occasions using strong organic solvent systems (125,126,127). However, Punnoose *et al*. have reported electrospinning of collagen using a relatively mild acetic acid/ dimethyl sulfoxide solvent system (DMSO) (93%:7% ratios). Fabricated collagen fibrous mats were of reasonable porosity and mechanical properties. In addition, in vitro MTT testing using rat skeletal L6 myoblasts and proliferation study with primary cell lines of neonatal rats cardiomyocytes demonstrated acceptable biocompatibility and proliferation suggesting a potential use in cardiac TE applications (128). In addition, some natural materials are very challenging to be electrospun as Chitosan. This is due to its low viscosity, restricted solubility in organic solvents and its inflexible crystalline morphology. In such cases, other strategies should be implied to produce the ES fibrous scaffolds as chemical modification. Nada *et al*. used a nitro benzaldehyde derivative of chitosan to render it electrospinnable. They used different degrees of substitutions to obtain the optimal scaffolds for regenerative TE applications. The 12% degree of substitution lead to an enhanced viscosity that made it easier for electrospinning to produce bead free fibers. In addition, Human skin fibroblast were used for cytotoxicity testing which proved the scaffold biocompatible. Moreover, the scaffolds demonstrated antimicrobial activity against different types of microorganism as E-coli and bacillus subtilis (129).

Other challenges with the natural materials are poor mechanical properties, which are hard to be controlled, and the faster degradation rate compared to synthetic materials. Lower mechanical properties will not allow cellular response to different signaling pathways and will not withstand high continuous stress as in joints or skeletal muscles.

These disadvantages limited the spectrum of use of these natural materials and therefore researchers sought other alternatives to eliminate those disadvantages.

1.3.5.3 Combination of materials for Electrospinning

One of the alternatives is composite ES that was reported before with different variations. The first was by combining the natural polymer with a synthetic electrospinnable one. In a recent study, PCL fibers were combined with gelatin fibers to enhance its mechanical properties for bone TE applications. This was done by collecting fibers of both materials on the same collector. The combination was reported to overcome the hydrophobicity of PCL and hence enhanced cell adhesion and growth. In addition, PCL enhanced the mechanical properties of gelatin rendering the combination suitable for TE applications. Moreover, they added calcium phosphate to facilitate the mineralization for bone TE applications. In this study, they reported an improvement in the mechanical properties by 43% compared to the gelatin/ calcium phosphate scaffold. PCL showed the highest elongation, gelatin alone was the lowest and the mixture was second to PCL with overall superior porosity (130). Similar strategy was achieved with hydroxyl ethyl cellulose and mineralization was successfully achieved (131). In another variation of the same approach, several natural biopolymers were combined with synthetic ones to mutually benefit the final scaffold. Polyurethane (PU) with its controllable mechanical properties was electrospun with zein/ cellulose natural polymers. This combination improved the hydrophilic character of the final scaffold and hence improved the cell proliferation. In this report, the authors demonstrated the successful electrospinning of fibrous mats loaded with streptomycin

sulfate. They also demonstrated the successful blood clotting and platelet activation to the scaffold upon the addition of blood while preserving the porous fibrous structure. Upon anti-microbial testing, the final Zein/ cellulose/PU/ drug scaffolds showed a remarkable zone of inhibition against several gram positive and gram-negative microorganisms compared to absence of inhibition of the control scaffolds. Moreover, the MTT assay showed an increasing fibroblast cell viability in the drug loaded scaffolds as well as the control ones for up to six days. It demonstrated the role of the natural polymers in the promotion of cell growth. Morphological analysis via SEM showed a normal cellular morphology for fibroblasts. Those findings qualified this scaffold to be used as wound dressing to prevent infections, induce blood clotting and enhance the cell growth and proliferation for wound healing (132). A combination of more than two components was also implemented previously where each component had a role for the intended application. PCL/ Poly methyl methacrylate (PMMA)/ Gelatin were used as a combination to produce ESS for drug loading and biomedical applications (133). PCL was used for its mechanical properties, its good flexibility, PMMA was added to prolong the degradation rate, and Gelatin played the compatibility-inducing agent that rendered the scaffold cytocompatible for cells and facilitated drug release. The mechanical properties of the three blends were superior for all compared to the control scaffolds made of the sole components. High PCL -content scaffolds showed better elongation than the other two. However, scaffolds with higher PMMA and those with higher gelatin content showed remarkable enhancement in their elongation and their young modulus compared to their controls. Similar results

for the ultimate strength were obtained. On the other hand, scaffolds with the high PCL content preserved their fibrous porous structure upon immersion in ethanol- a common solvent used for drug loading. When scaffolds were tested for their release capacities using rhodamine B dye, scaffolds with the highest PCL content showed the longest degradation rate with the highest structural integrity in the release medium. Scaffolds with the highest gelatin content rapidly released the dye due to their rapid degradation. Interestingly, scaffolds with higher PMMA content showed high stress relaxation (as per SEM results) which influenced the porosity causing slower release and hindered diffusion of the dye in the release medium. This renders PMMA-high scaffolds as a potential candidate for prolonged transdermal release. Diffusion coefficient was calculated for all three combinations under different conditions confirming these findings. The findings of this study made this combination a good candidate for a wide array of applications just by varying the content of each polymer. In addition, more in depth studies for the release profiles of different drugs and cell proliferation needs to be done. Similarly, a blend of three polymers using 3 to 1 syringe needle was used to formulate ES multilayered vascular grafts. Scaffolds of different polymer compositions were tested and proven a successful candidate for synthesizing vascular grafts (134,135).

1.3.5.4 Synthetic materials for Electrospinning

The second alternative to natural biopolymers is to use synthetic polymers. Those polymers might be inferior in certain aspects as cytocompatibility, non-uniform biodegradability and difficult optimization of their synthesis for successful cell growth

and proliferation compared to natural materials. However, they are superior in their mechanical properties that can be also controlled based on the intended application by controlling the synthesis process or the ES process parameters. Several synthetic materials have been reported to be electrospun before and were utilized for a wide array of TE applications. Hydrophilic Polymers such as polyvinyl alcohol (PVA) (136), poly urethane (PU) (137) and (138), poly ethylene oxide (PEO) (139), Hydrophobic polyesters such as PCL (140), poly glycolic acid (PGA) (141), poly lactic acid (PLA) (142,143) and Co-polymers as poly (lactic -co-glycolic acid) (PLGA) (144) have been electrospun before and studied thoroughly in the last 2 decades. However, most of the recent studies involving synthetic polymers constituted composite ES by mixing synthetic with natural or a couple of synthetic polymers. For example, PCL was reported to have good mechanical properties but its hydrophobic nature made its degradation time high and also prevents efficient cell attachment, growth and proliferation. To overcome this, it was mixed with PGA rendering the composite more biocompatible with better mechanical properties than each polymer alone (145). In addition, PCL fibers were used to encapsulate PCL/ PGA fibers making good use of its long degradation time to prolong that of PGA fibers (146). It was also found that composite fibers had higher yield strength, significantly higher young's modulus and lower elongation at break than the fibers of the individual components. In another creative approach, a sandwich designed scaffold was fabricated with two layers: a base layer to inherit the scaffold mechanical strength composed of PCL/ PLLA, and a surface layer containing PCL/ Gelatin to overcome the cell attachment deficient

properties of PCL (147). In the middle, gelatin microspheres loaded with fibroblast growth factor 2 (FGF-2) were added for sustained release of growth factors. The base layer improved the mechanical strength of the scaffold and allowed easier handling, while the upper layer improved the cell attachment properties of the scaffold due to the gelatin content. Bioactivity testing using 3-(4, 5-dimethylthiazol-2-yl)−5-(3-carboxymethoxyphenyl)−2-(4-sulfophenyl)−2H-tetrazolium (MTS) assay on human osteoblast cells showed higher levels on the first and the seventh day compared to the unloaded microspheres with no effect on the microspheres during preparation. Moreover, cell attachment was performed on the sandwich scaffold and compared to PCL/PLLA and PCL/Gelatin controls. MTS assay showed lower cell attachment for the former control while the later showed deformations during the fabrication steps. This rendered this preparation method and this scaffold suitable for soft to hard tissues as bone to cartilage.

Study Objectives

As stated in the above literature review, the optimum treatment strategy for MI with simplest procedures, highest recovery rate and lowest side effects remains a challenge. TE have proven to be a promising approach compared to conventional methods with studies currently investigating the optimum delivery technique. A lot of research work was conducted to develop the ideal scaffold with the highest resemblance for the natural ECM that can be used safely and effectively for cell delivery in TE applications. Natural materials had high biocompatibility but were of poor mechanical properties

while synthetic ones had superior tunable mechanical properties. In addition, most of the studies reported were using chemical crosslinking strategies. Moreover, few studies compared porous scaffolds produced by different techniques in terms of cytocompatibility and cell scaffold interaction. Consequently, the challenge remains to produce the porous structure with tunable mechanical properties, without using toxic crosslinking agents, while being cytocompatible, biodegradable with a promising cell attachment, growth, and proliferation and differentiation capacity.

We have previously reported on the successful production of our novel, patented elastomer of the moiety poly (diol-co-tricarballylate) to be used for TE and drug delivery applications (148). This molecule based on tricarballylic acid- a natural product of the Krebs cycle- and alcohols was produced via a condensation reaction followed by an acrylation reaction to render the polymer photocrosslinkable. This later characteristic feature of our polymer allowed the easy manipulation of mechanical properties by controlling the degree of acrylation to suit the purpose of use. Different characterization methods showed the amorphous nature of the produced elastomer. In addition, the elastomer was biodegradable and biocompatible, showing a bulk hydrolysis behavior by esterases in the human body with structural integrity for over 12 weeks (149). Moreover, its high photocrosslinking efficiency and the ability to disperse drugs without a solvent was of special importance for different controlled drug delivery applications. In a following study, interleukin 2 (IL-2) was found to be fully stable during a release study with bioactivity studies of more than 94% compared to its conventional activity over 28 days (150). Moreover, an osmotic driven release study

demonstrated linear and manageable release profile (151). However, most of the work done before was to exploit and utilize all those characteristics for controlled drug delivery applications with minimal work related to TE applications.

In this dissertation, we claim that the acrylated poly (1,10 decanediol-co-tricarballylate) (APDT) synthetic copolymer, photocrosslinked mesh scaffolds that act as a cellular niche suitable for cell loading to repair the diseased myocardium could be designed. We aimed to synthesize and characterize both the PDT prepolymer and the acrylated polymer. Afterwards, we proposed two methods to design a 3D scaffold for TE which are: 1) Conventional solvent free particulate leaching using the most commonly used porogen, sodium chloride, and the novel trehalose dihydrate which was to the best of our knowledge, have never been used before as a porogen. 2) Novel photo-reactive electrospinning to produce an electrospun elastomeric mesh scaffolds via optimized ES parameters. Scaffolds produced from both processes were compared via different characterization techniques. Finally, this study was concluded with *in vitro* investigation of the cytocompatibility and cell scaffold interaction assessment using H9C2 cardiomyoblasts and adipose derived mesenchymal stem cells.

As stated in the above literature review, the optimum treatment strategy for MI with simplest procedures, highest recovery rate and lowest side effects remains a challenge. TE have proven to be a promising approach compared to conventional methods with studies currently investigating the optimum delivery technique. A lot of research work was conducted to develop the ideal scaffold with the highest resemblance for the natural

ECM that can be used safely and effectively for cell delivery in TE applications. Natural materials had high biocompatibility but were of poor mechanical properties while synthetic ones had superior tunable mechanical properties. In addition, most of the studies reported were using chemical crosslinking strategies. Moreover, few studies compared porous scaffolds produced by different techniques in terms of cytocompatibility and cell scaffold interaction. Consequently, the challenge remains to produce the porous structure with tunable mechanical properties, without using toxic crosslinking agents, while being cytocompatible, biodegradable with a promising cell attachment, growth, and proliferation and differentiation capacity.

We have previously reported on the successful production of our novel, patented elastomer of the moiety poly (diol-co-tricarballylate) to be used for TE and drug delivery applications (148). This molecule based on tricarballylic acid- a natural product of the Krebs cycle- and alcohols was produced via a condensation reaction followed by an acrylation reaction to render the polymer photocrosslinkable. This later characteristic feature of our polymer allowed the easy manipulation of mechanical properties by controlling the degree of acrylation to suit the purpose of use. Different characterization methods showed the amorphous nature of the produced elastomer. In addition, the elastomer was biodegradable and biocompatible, showing a bulk hydrolysis behavior by esterases in the human body with structural integrity for over 12 weeks (149). Moreover, its high photocrosslinking efficiency and the ability to disperse drugs without a solvent was of special importance for different controlled drug delivery applications. In a following study, interleukin 2 (IL-2) was found to be fully

stable during a release study with bioactivity studies of more than 94% compared to its conventional activity over 28 days (150). Moreover, an osmotic driven release study demonstrated linear and manageable release profile (151). However, most of the work done before was to exploit and utilize all those characteristics for controlled drug delivery applications with minimal work related to TE applications.

In this dissertation, we claim that the acrylated poly (1,10 decanediol-co-tricarballylate) (APDT) synthetic copolymer, photocrosslinked mesh scaffolds that act as a cellular niche suitable for cell loading to repair of the diseased myocardium could be designed. We aimed to synthesize and characterize both the PDT prepolymer and the acrylated polymer. Afterwards, we proposed two methods to design a 3D scaffold for TE which are: 1) Conventional solvent free particulate leaching using the most commonly used porogen, sodium chloride, and the novel trehalose dihydrate which was to the best of our knowledge, have never been used before as a porogen. 2) Novel photo-reactive electrospinning to produce an electrospun elastomeric mesh scaffolds via optimized ES parameters. Scaffolds produced from both processes were compared via different characterization techniques. Finally, this study was concluded with *in vitro* investigation of the cytocompatibility and cell scaffold interaction assessment using H9C2 cardiomyoblasts and adipose derived mesenchymal stem cells.

Chapter 2: Materials and Methods

2.1 Materials

2.1.1 Materials used for chemical synthesis and characterization

Tricarballylic acid (TCA), 1, 10-decanediol, stannous 2-ethylhexanoate, Triethyl amine (TEA), 2,2-dimethoxy-2-phenylacetophenone and Polyvinylpyrrolidone (PVP), absolute Ethanol, 4-dimethylamino pyridine (DMAP) and phenolphthalein were all purchased from Sigma-Aldrich Chemie GmbH, Germany. Acryloyl chloride Lichrosolv® Acetone, Acetic anhydride, Pyridine, Hydrochloric acid (37%) and Chloroform were purchased from Merck, USA. All chemicals were used as received without any further purification.

2.1.2 Materials used for in vitro cytocompatibility studies

Gibco® RPMI (1640) Fetal bovine serum, L-Glutamine 200mM (100X), 2-Mercaptoethanol (50mM) and Live/Dead® Viability/Cytotoxicity assay kit for mammalian cells, Dulbecco modified eagle's medium (DMEM) and Gibco® F-12 Nutrient Mixture were purchased from Life Technologies Co., Invitrogen, UK. Penicillin- streptomycin and Dulbecco's phosphate buffered saline (DPBS) were purchased from Sigma-Aldrich Chemie GmbH, Germany; DAPI (4′, 6-diamidino-2-phenylindole) for nucleic acid staining was purchased from Thermo-Fisher scientific, USA. Lonza Trypsin/ EDTA (10X) was purchased from SLS life sciences Co. UK. All were used without further purification.

2.2 Poly (Diol co-tricarballylate) co polymer synthesis

2.2.1 Prepolymer synthesis

Synthesis of the pre-polymer is illustrated in Figure 2 and a diagrammatic illustration of the equipment setup is shown in Figure 3. Poly (diol co-tricarballylate) pre-polymer (PDT) was prepared by adding 7.05 gm (0.04 mol) of Tricarballylic acid (TCA) and 11.3 gm (0.065 mol) of 1, 10 Decanediol in a three necked 100 ml round bottom flask supplied with argon inlet, condenser and a magnetic stirrer. The flask was placed in an oil bath and heated at 140-150 ^{o}C. In the meantime, Stannous-2-ethylhexanoate (1 x 10^{-4} mol) was added as a catalyst and the reaction was allowed to proceed for 45minutes. Afterwards, the reaction was continued under vacuum for 35 minutes to remove the water formed by the condensation reaction. The flask was removed and left to cool down over night. After that, the pre polymer was dissolved in chloroform, which was then filtered. Finally, the polymer was left to dry under the hood until the chloroform was removed. Another preparation of higher molecular weight was prepared by the same procedure with slight modifications in the reaction time and temperature.

2.2.2 End group Analysis

Catalyzed acetylation was used to determine the millimoles of hydroxyl end groups per one gram of the prepolymer (152). This was done to calculate the required amount for the acrylation reaction. In two separate volumetric flasks, a 2% w/v 4-dimethylamino

pyridine solution in pyridine and a 25% v/v of acetic anhydride in pyridine was prepared.

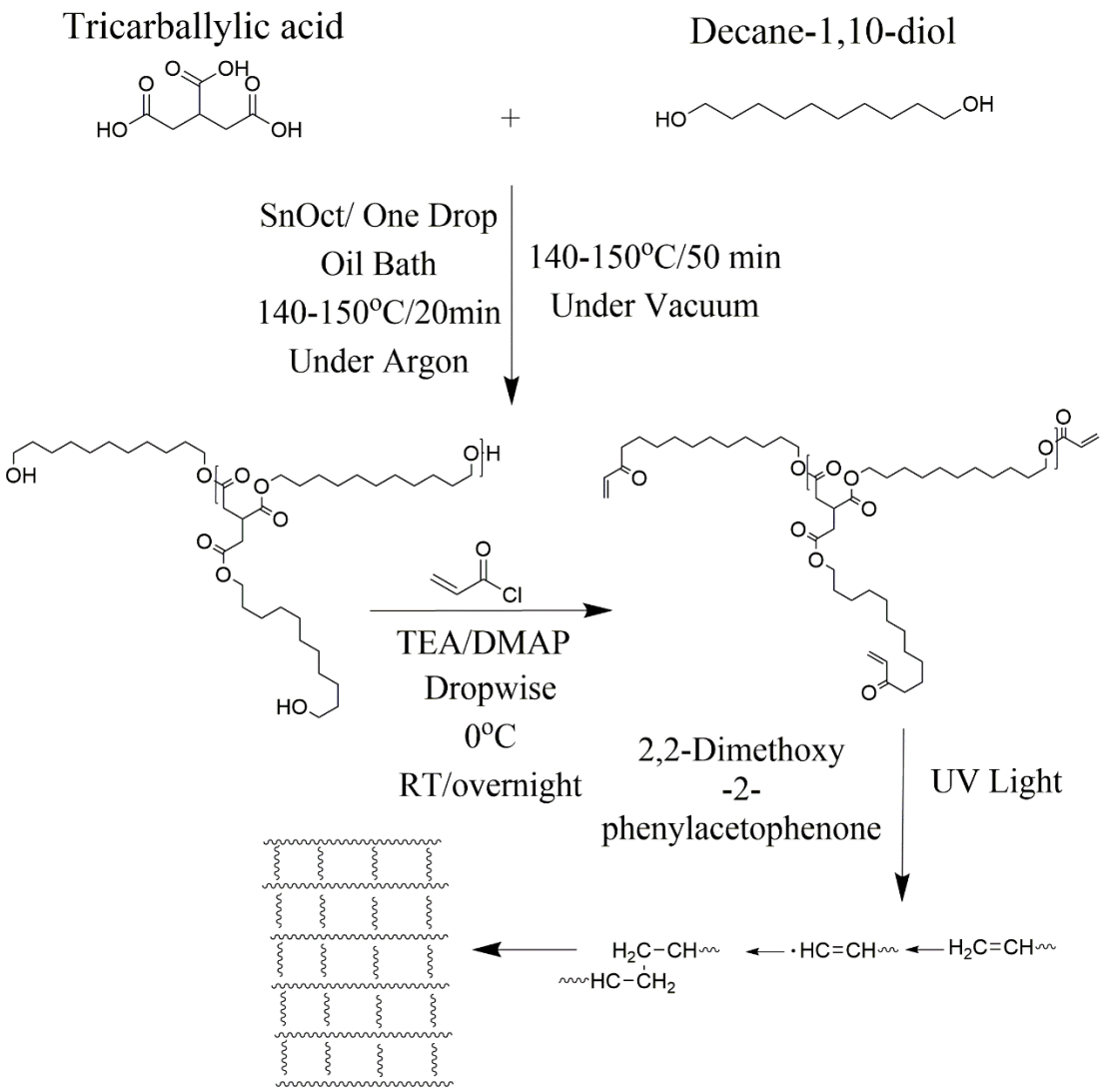

Figure 2. Schematic representation of the synthesis, acrylation and UV curing of the acrylated PDT polymer

Afterwards, in a 250 ml conical flask 1 gm of the prepolymer was dissolved in 1 ml of pyridine. This was followed by the addition of 2 ml of the prepared acetic anhydride solution and 5 ml of the 4-dimethylamino pyridine (DMAP) catalyst solution.

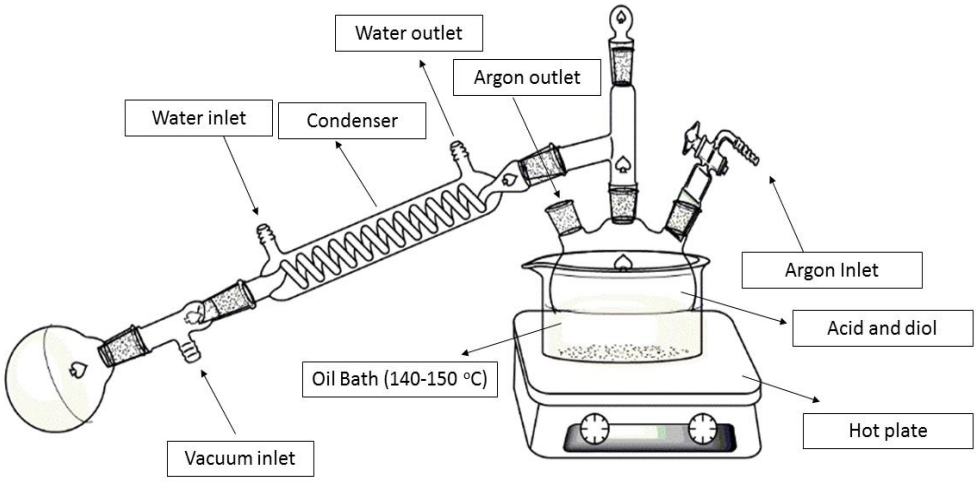

Figure 3**.** Schematic diagram of pre-polymer synthesis

The flask was covered and placed in a water bath at 50 ^{o}C for 20 minutes. Then 25 ml of distilled water was added to the mixture where a white color was observed. To complete the experiment, two blanks were prepared; the normal blank which contained the same constituents of the analyte flask without the prepolymer and the acid blank flask, which contained 1 gm of the prepolymer dissolved in pyridine and 25 ml of distilled water to exclude the interference of the unreacted tricarballylic acid. Then two drops of 1% phenolphthalein as indicator (1% w/v of phenolphthalein in 70% ethanol)

were added. The analyte flask, blank flask and acid blank flask were titrated against 0.5 M sodium hydroxide solution till the first persistent faint pink color was formed, representing the end point. The equation used for the calculation was as follows:

$$\text{Milli moles of OH/ gm of pre-polymer} = N\,[(Vb+Va)-Vs)$$

Where N is the solution used, V_b is the volume of titrant consumed by the blank, V_a is the titrant volume consumed by the acid blank and V_s is titrant volume consumed by the sample.

2.2.3 Acrylation of the pre-polymer

Acrylation was performed using Acryloyl Chloride (ACRL) to react with OH terminal of the prepolymer in presence of DMAP as a catalyst and Triethylamine as a scavenger for the resultant hydrochloric acid. Figure 1 shows the synthesis and acrylation scheme used that was reported previously (149). In a 100 ml three-necked, round bottom flask supplied with an argon inlet, a magnetic stirrer and placed in an ice bath at 0 ^{o}C, PDT pre-polymer was dissolved in 20 ml of acetone. This was followed by the addition of equimolar amounts of TEA and the catalyst DMAP. Afterwards, dropwise addition of ACRL (2 mol) was performed then the reaction was left at room temperature overnight under argon. Next, the mixture was filtered and left under the hood to allow acetone evaporation. The acrylated polymer was then purified by dissolving in chloroform and washing 3 times with 10 mM HCL solution to remove excess TEA, TEA-HCL and ACRL from the acrylation reaction. The purified polymer in the chloroformic layer was then mixed with 0.2 gm of magnesium sulfate to remove excess water and then it was

filtered and left to dry under the hood. Table 2 lists the amounts used from each of the reaction constituents.

Table 2. Different reaction compositions of the APDT polymer

Formulation	PDT (gm)	TEA (ml)	DMAP (mg)	Acryl (ml)
Low molecular weight	6	1.3	6	1.6
High molecular weight	6	0.9	6	1.1

2.3 Scaffold production by conventional solvent-free particulate leaching process

Trehalose dihydrate was sieved into a defined particle size as reported in Table 3 using Retsch AS200 (Retsch, Germany) Sieve. As shown in Figure 4, APDT was added in an Eppendorf tube with 1µL of photo initiator (2, 2-dimethoxy-2-phenylacetophenone in acetone, 20% w/v) and mixed by a spatula followed by the addition of trehalose. Ingredients were mixed again until a paste is formed. The whole mixture was transferred into the middle of a petri dish. Afterwards, the cover of the petri dish was placed upside down to spread the paste into a disc. The petri dish containing the disc paste was placed under UV light of 100 watts and 365nm wavelength (Blak-Ray, UVP-Canada) for 10 minutes for each side of the dish for homogenous crosslinking.

Afterwards, the upper cover was removed slowly, followed by filling the Petri dish with deionized water for 5 min and the disc was removed slowly by a spatula. A blank 2D scaffold was prepared using the same procedure but without the addition of TH particles to be used as a control. Scaffolds were immersed into 1500 ml of deionized water (Milli-Q Direct, Millipore, USA) for 4 days with mild stirring. The scaffolds were then allowed to dry under the hood for 24 hours to remove any traces of water.

Table 3**.** Different porogens used with their pore size and concentration.

Porogen	Particle size	Concentration
NaCl	250<X<500 µm	70% w/w
Trehalose	250<X<500 µm	70% w/w

2.4 Scaffold production by electrospinning of the acrylated polymer

The electrospinning solution was prepared by dissolving APDT in ethanol in a sealed glass vial using a magnetic stirrer until a clear solution was obtained. This was followed by the addition of PVP with continuous stirring until the solution became clear again. The ideal preparation composition was: 20% (w/v) APDT, 8% (w/v) PVP 1300 kDa in ethanol. The solution was vortexed and stirred till homogeneity is achieved. Afterwards, 0.1 gm of the photo initiator, 2, 2-dimethoxy-2-phenylacetophenone was

added and allowed to dissolve. The solution was transferred into a syringe supplied with an electrospinning needle of size 23 G. As shown in Figures 5 and 6, the syringe was placed in a syringe pump (Nabond-China). The needle was then connected to one of the electrodes of a power supply that generated the voltage difference between the needle and the grounded collector. ES fibers were collected on a flat-grounded collector using the shadow collection method.

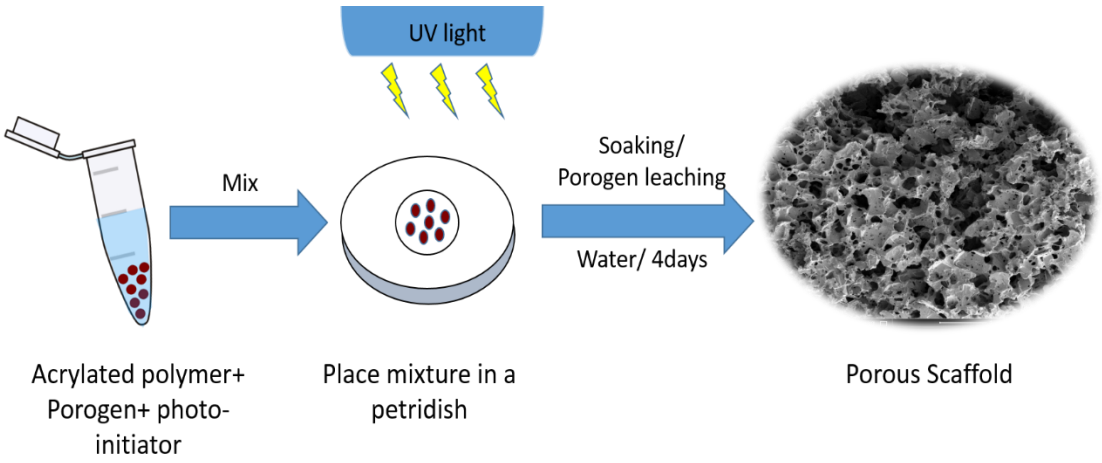

Figure 4. Schematic diagram for scaffold production via salt leaching

Where the top of the aluminum foil is bent forward so that the fibers are hung between the bent part and the body of the aluminum foil. Finally, since this is a photo-reactive electrospinning process, *in situ* crosslinking was performed by placing a UV lamp of 200 watts (Neo pro, Nabond- China) at a distance 20 cm from the collector. The parameters of the ES process using the Neo Pro ES machine (NaBond-China) were as

follows: Voltage difference of 17-22KV, tip to collector distance (TCD) of 18cm, UV lamp was placed 10 cm away from the polymer jet, flow rate was 10ml/hr for 30 minutes. The ESS was left under UV for 20 minutes after ES to guarantee full crosslinking of the polymer. ES was also attempted on APDT polymer without a solvent. This was performed as follows: The APDT polymer was placed directly in a syringe with 20 µl of 2, 2-dimethoxy-2-phenylacetophenone (20% w/v in acetone). ES parameters were: 8G needle, flow rate of 3ml/hr, 22-25KV voltage, TCD of 15cm, 2 UV lamps each of 500 watts (NaBond-china). Flat collector was used for this process as well. Finally, a control scaffold made of ES polycaprolactone in a 3:1 ratio of methanol to chloroform solvent system was produced and used for mechanical properties comparisons. ES parameters were: Voltage of 10-12 KV, Flow rate of 2 ml/hr, TCD 25 cm, a 23 G needle and a flat collector for 20 minutes.

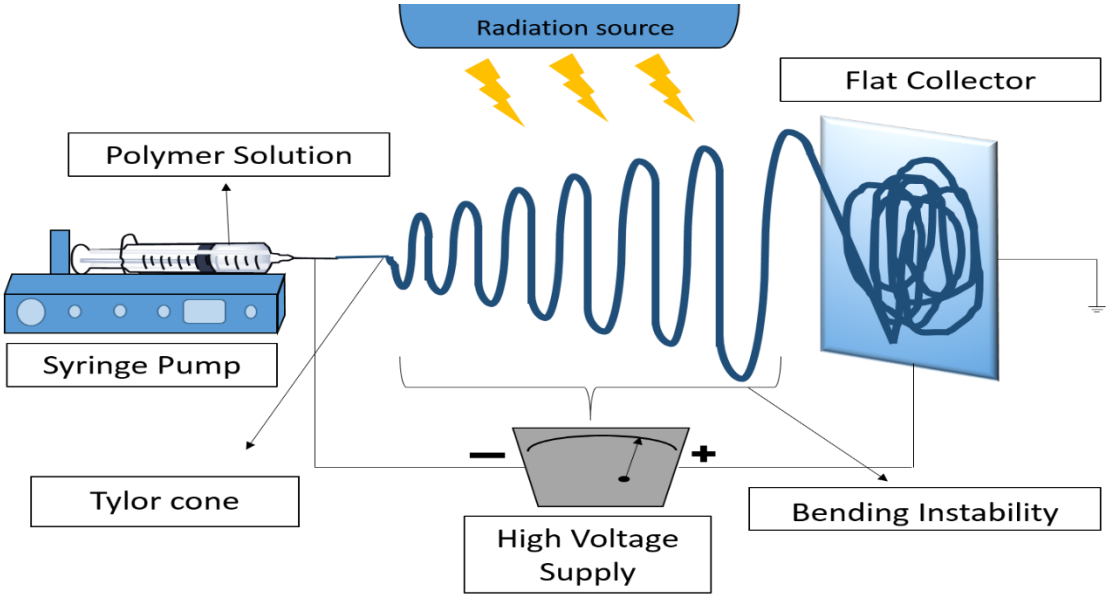

Figure 5. Illustrative diagram of photo-reactive electrospinning device

2.5 Characterization

2.5.1 Chemical and thermal characterization

2.5.1.1 Fourier Transform Infrared

Fourier transform infrared (FTIR) was performed on prepolymer, acrylated polymers PVP and ES meshes at room temperature using Jasco FT/IR 4200 (Jasco Inc., Japan) equipped with attenuated total reflection unit (ATR pro 470-H). The spectra were collected with a resolution of (16cm^{-1}) over the range of wavelengths from 4000-400cm^{-1} on a scan number 32 using DLA-TGS detector.

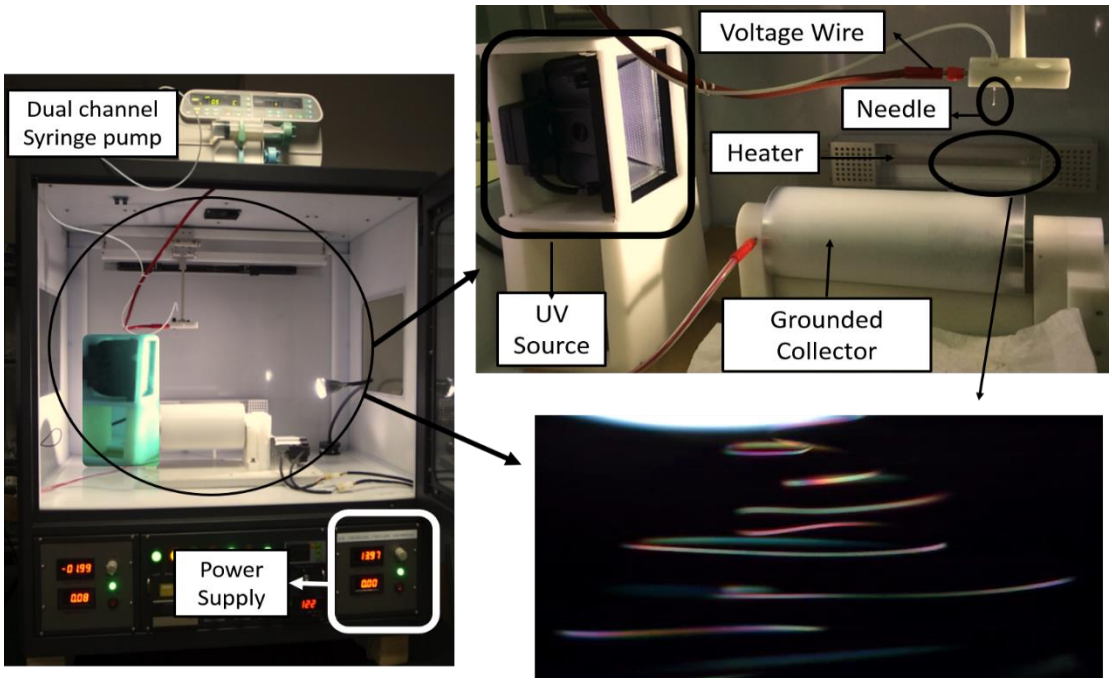

Figure 6**.** Basic setup of the reactive electrospinning machine. (Left side) the machine, (upper right) the electrospinning chamber and (bottom right) the magnified image of the electrospun fibers flowing from the needle to the collector.

2.5.1.2Proton Nuclear Magnetic Resonance

Proton nuclear magnetic resonance (^{1}H-NMR) analysis was done on the PDT prepolymer and the APDT acrylated polymer on a Bruker Ascend 600 MHz NMR spectrometer (Bruker Co., Germany). Sample was dissolved in chloroform-d ($(CD_3)_2CO$) with 0.1% v/v trimethylsilane (TMS) in 5 mm NMR tubes. Chemical shifts for the spectra were compared to TMS (0.00 ppm) as the internal reference. The degree of acrylation was calculated using the peak integration of the methylene group protons and those of the terminal carbons next to the OH group of the prepolymer and vinyl group in the acrylated ones.

2.5.1.3 Gel permeation chromatography/ Size Exclusion chromatography

Molecular weight and molecular weight distribution of the synthesized pre-polymer were determined using Viscotek GPC max VE2001 gel permeation chromatography (GPC)/ size exclusion chromatography (SEC) system (Viscotek, Malvern instruments, UK). The GPC max was equipped with triple detector array TDA 305 multiple detection composed of a refractive index (RI) detector, right angle and low angle light scattering detectors (RALS/LALS) a viscometer and UV detector. The column setup composed of general purpose aqueous column set of a single pore size column (T6000, org GPC/SEC col, 300x 8 mm, exclusion limit 20,000 kDa), two single pore size columns (T1000, Org GPC/SEC col, 300 X8mm, exclusion limit 1500Da) and one flow injection polymer analysis (FIPA) non-polar organic column (H100-3078, 100X 7.8mm). As for the mobile phase, the polymer sample was dissolved in analytical grade acetone at a concentration of 20mg/ml the flow rate was 1ml/min and the injection

volume was 100 microliters at 35^{o}C. Molecular weight determination was performed using dn/dc of 0.954ml/g and the data was collected and analyzed using OmniSEC 5.02 software package.

2.5.1.4 Differential Scanning Calorimetry

Thermal properties of the prepolymer, PVP powder, PVP ES fibers and PVP/ APDT ES fibers were analyzed using Differential Scanning Calorimetry (DSC-8000) analysis with liquid nitrogen intracooling system (Intracooler II). The heating rate was 10 ^{o}C/min. The samples were cooled down to -70 ^{o}C and then heated up to 300 ^{o}C to record the DSC. This was done to provide the same thermal history.

2.5.2 Morphological analysis

2.5.2.1 Scanning Electron Microscopy, fiber diameter and pore size analysis

Scanning Electron Microscope (SEM) (Bruker-USA) and Nikon eclipse (LV100NPOL) polarizing microscope (Nikon, Japan) were used to examine the structure and surface morphology of both the ES fibers and the discs produced by particulate leaching. SEM was performed on gold sputter coated samples to improve the sample conductivity. Polarizing microscope was also used especially during the in process monitoring of ES. A glass slide was placed on the collector and left for one minute to allow the fibers to deposit on the slide. The slide was then placed under the microscope and a series of magnifications was used to obtain the results. Average fiber diameter and pore size were calculated using the NIH approved ImageJ software for

image analysis. The calculation was performed by measuring 25 fibers and pores respectively. Results were reported as mean ± SEM (n=3).

2.5.2.2 Solvent resistance

The ESS were placed in different solvents to make sure that the fibrous structure is maintained and hence testing their suitability for different biomedical applications. ESS were placed in water and ethanol for 24 hours then left to dry for 24 hours. Morphological analysis using SEM was performed to check the structure after immersion.

2.5.2.3 Porosity calculation

The porosity of the produced scaffold was calculated using the liquid intrusion method. The weight of the dry scaffold is measured then it was placed in ethanol for 24 hours. Afterwards, the scaffold surface was wiped gently to remove excess ethanol and then it was weighed. Porosity was calculated using the following equation:

$$\varepsilon = V_{ETH} / (V_{ETH} + V_{APDT})$$

Where: V_{ETH} is the volume of ethanol absorbed by the scaffold into the pores. It was calculated by dividing the change in scaffold mass after immersion in ethanol and the density of ethanol (0.789 g/cm3). V_{APDT} is the volume of the dry scaffold fibers and it was calculated as the ratio between the weight of the dry scaffold and the density of TCA.

2.5.3 Tensile testing

Tensile testing was done using Instron 3343 single column table frame (Instron Co., USA) equipped with 1 N load cell as in Figure 7. The ES meshes were cut into rectangular shape and placed between the grips of the machine at room temperature. The samples were pulled at a rate of 1 mm/second until break. Mean ± standard deviation, percent elongation and young's modulus were calculated using Bluehill management software at n=5. Young's modulus was calculated from the initial slope of the stress strain curve. The crosslinking density was calculated according to the theory of rubber elasticity using the equation: $\rho_x = E/ 3RT$. Where ρ_x is the number of active network chain segments per unit volume (mol/m^3), E is the young modulus in Pascal and R is the universal gas constant (R=8.314 J/mol K) and T is the absolute temperature in kelvin.

Figure 7**.** Tensile tester machine setup

2.5.4 Contact Angle measurement

The Contact angle for the ES meshes was measured using DSA25 goniometer (Krüss GmbH, Germany) provided with a microsyringe with a PTEF needle with diameter of 0.5mm. The drop shape was analyzed using sessile drop method on a drop of purified water, 10 microliters in volume dispensed from the PTEF needle. After the drop and the mesh surface came in contact, a digital camera captured the drop shape in 5sec., and the drop contour was mathematically represented by Young Laplace equation. Contact angle was calculated as the slope of contour line at the three-phase contact point. Five measurements were taken for different sites and the data was represented as mean ± SEM.

2.6 In Vitro cytocompatibility Studies

2.6.1 Cell Isolation

Collagenase digestion (153) was used to isolate human adult subcutaneous adipose tissue-derived stromal vascular fraction (SVF, n=3, passage 2-5). The SVF pellet was cultured in T25 culture flask (BD falcon) in stromal medium composed of high glucose DMEM-F12 (1:1), 10% FBS, 1% Pen/Strep, and maintained in at 37 °C with 5% CO2 until confluence. The cells were passaged, as necessary Immunophenotyping of preadipocytes was performed using anti-human antibodies: CD31-FITC, NG2-PE, CD166-PerCP-efluor, CD105-APC, CD45-Alexa flour 700, .CD11b- Brilliant Violet 421, CD73- Brilliant Violet 605 (all from R&D Systems). Sample processing was performed using FACSCanto II flow cytometer (BD Bioscience) and analyzed with

FlowJo Software (Treestar). H9C2 myoblasts - a clonal cell line obtained from the embryonic heart tissue of rats- were obtained from the European Collections of Cell Cultures (ECACC) and were cultured using the same media and conditions.

2.6.2 Cell seeding

H9C2 myoblasts were seeded in 48 well plates (BD Falcon) with seeding density of 30,000 cells/well in 300 μl of media. MSCs from three different patients were seeded in tissue culture treated 48 well plates with seeding densities in Table 4. Cells were incubated and allowed to attach for 24 hours before scaffold addition.

Scaffolds were cut as discs using biopsy punches with unified diameter and were sterilized by the immersion of the scaffolds in 70% ethanol for 10 minutes. This was followed by washing the scaffolds three times with PBS solution to remove any traces of ethanol. Scaffolds were added in three technical replicates and incubated for 24 and 48.

Table 4**.** Seeding density of mesenchymal stem cells from each replicate

Patient (n)	Cell density (Cells/well)
1	1800
2	6300
3	3300

2.6.3 In-vitro quantitative cell viability assay:

Cells were fixed by adding 30 µl of 38% formaldehyde to the media in each well and leaving it for 15 minutes. The media was then discarded and replaced by 150 µl of 0.2% DAPI in DPBS staining solution for 10 minutes. Afterwards, the staining solution was removed and replaced by 300 µl DPBS. The plates were scanned using ArrayScan™ XTI live high content platform (ThermoFisher Scientific, USA) equipped with Zeiss™ Axio Z1 Observer microscope and Zeiss Definite Focus Hardware Laser-Autofocus. Cell number was assessed by automated quantitation of DAPI positive nuclei using target activation module. Images were taken for 20 fields per well and the Image analysis and cell counting was performed by HCS Studio™ Cell Analysis Software. A sample of image analysis with and without selection of DAPI positive nuclei is shown in Appendix 4.

2.6.4 Cell/ scaffold interaction

Sterile scaffolds were placed in two plates; one is an ultra-low attachment (non-tissue culture treated) (Thermoscientific, USA) and the other is tissue culture treated (BD Falcon) plates. Cells were added directly to the scaffolds at a seeding density of $1X10^4$ cells/scaffold and were allowed to attach for 2 hours under 5% CO_2/ air atmosphere at 37 ^oC. Afterwards, proper volume of culture media was added to the wells and was changed every other day for a total of 14 days. At the end of the incubation period, cells were stained using Calcien-AM from the LIVE/DEAD® viability/ cytotoxicity assay kit to stain living cells attached to the scaffold. Fluorescent images were taken using an inverted microscope with a monochrome digital camera using 5x magnification (Carl

Zeiss Micro-Imaging, New York, USA) Cell viability was assessed visually and compared to control.

2.7 Statistical analysis:

All values were reported as mean ± SEM. Statistical analysis was done using independent t-test for fiber diameter and pore size analysis and ANOVA for cell viability using SPSS software. Results were considered statistically significant at $P<0.05$.

Chapter 3: Results and Discussion

Our main aim was to design scaffolds from APDT prepolymer utilizing UV light through PRES. First, the pre-polymer was synthesized from tricarballylic acid and excess decane diol via condensation reaction. The reaction was carried out under argon followed by vacuum to remove the produced water. To synthesize the low and high molecular weight variations of the pre-polymer, we diversified the reaction temperature (130- 160 ^{o}C), the argon interval (10-45 minutes) and the vacuum interval (35-75 minutes). The optimized reaction with the best viscous yet flowing pre-polymer was achieved at a temperature range of 140-150 ^{o}C, argon interval of 20 minutes and vacuum interval of 50 minutes. When the temperature, argon or vacuum intervals were increased slightly above these conditions, the polymer changed into its rubbery state due to extensive thermal crosslinking. The produced pre-polymer was of slight yellow color. The pre-polymer was then dissolved in chloroform followed by filtration to remove any excess unreacted residues.

The second step involved the acrylation of the pre-polymer where the terminal hydroxyl groups were converted into vinyl groups to prepare it for further crosslinking. Both the acrylated and the non-acrylated preparations were soluble in most organic solvents as ethanol, chloroform, acetone, and methanol but formed a colloidal dispersion with water that was white in color.

3.1 Chemical and thermal characterization

3.1.1 Molecular weight Measurement

The molecular weight (MWt) and molecular weight distributions of the pre-polymer using GPC are reported in Table 5. Variations of MWt have been prepared by varying the conditions of the pre-polymer condensation reaction to vary the thermal crosslinking degree. As expected, the measurements showed that the variation in the reaction conditions changed the MWt of the pre-polymer. This is because the increase in time and temperature of the reaction supplied the monomers with the needed energy and time to allow more thermal crosslinking reaction between the carboxylic and alcoholic groups forming longer chains. The highest MWt the prepolymers reached while still flowing freely was 5190 Da. At that MWt, the viscous portion was still exceeding the elastic portion and hence, it was still in a liquid state. When the MWt reached a higher value, the prepolymer crosslinked to a rubbery state in which the elastic portion exceeded the viscous portion. Moreover, the extensive reaction lead to the consumption of most of the hydroxyl groups, which made the pre-polymer flow poorly and further acrylation could not be performed easily. In addition, end group analysis of both the high and low MWt variations of the prepolymer was conducted and was reported in Table 4. This was necessary to determine the amount of terminal hydroxyl groups, which corresponded to the optimum amount of acryloyl chloride, needed for successful acrylation. It was also important to adjust the degree of acrylation and hence to ensure successful crosslinking through the added vinyl groups.

Table 5**.** Molecular weights, molecular weight distribution and the determined hydroxyl end groups of different pre-polymer variations determined via GPC.

Formula	Mw	Mn	Mw/Mn	OH (mmol/gm)
Very high molecular weight	6542	6104	1.072	--
High molecular weight	5190	3657	1.419	1.1
Low molecular weight	3538	1031	3.4	1.6
Very low molecular weight*	1366	1090	1.25	2.7

* Data were reported by our group (149)

3.1.2 Fourier Transform Infrared Spectroscopy (FT-IR)

Figure 8 shows the FT-IR spectra of the PDT prepolymer and the crosslinked APDT. As shown, a broad band appeared at 3600-3400 cm^{-1} that was indicative of the hydroxyl stretching vibrations. In addition, C-H stretching bands at around 2900-2800 cm^{-1}. The sharp absorption band at 1730 cm^{-1} was attributed to the ester carbonyl group. The bands between 1000-1300 cm^{-1} represents the vibrations of C-O stretching. After crosslinking, The broad at 3600-3400 cm^{-1} corresponding to the hydroxyl group almost disappeared and two new bands at 1630 and 815 cm^{-1} appeared corresponding to CH_2=CH_2. Those two small bands are indicative of the successful incorporation of the acryloyl terminal moieties. However, the band areas were very small due to the consumption of most of the acryloyl moieties during the free radical polymerization reaction when crosslinking occurred. To primarily analyze the change in the amount of the hydroxyl groups with changing the MWt of the pre-polymer, the ratio between the

areas under the bands of hydroxyl group to that of the carbonyl group was determined. Table 6 reports the ratios between both band areas (OH group band area/ CO band area).

Table 6**.** Band ratio of hydroxyl group and carbonyl group for high and low molecular weight variations of the pre-polymer

Molecular weight	**band ratio(A(OH)/A(CO))**
High Molecular Weight (5190 KDa)	0.2
Low Molecular Weight (3538KDa)	0.42

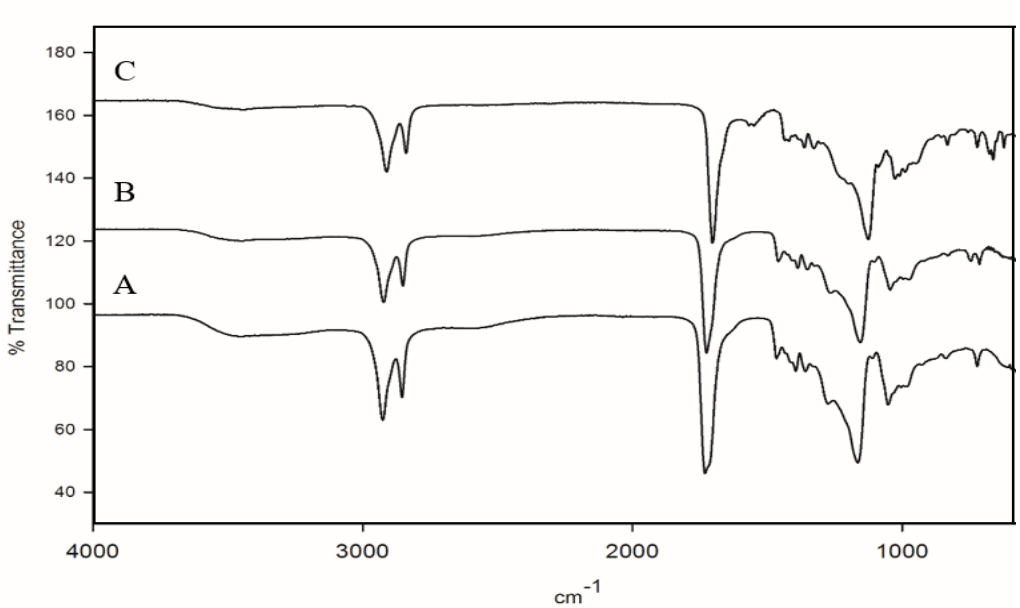

Figure 8**.** FT-IR Spectra of PDT. (A) Low molecular weight (3538 KDa) prepolymer, (B) High molecular weight prepolymer (5190 KDa) and (C) crosslinked elastomer.

3.1.3 Differential scanning calorimetry (DSC)

DSC analysis was performed to analyze the thermal characteristics of PDT before and after crosslinking as well as after reactive electrospinning. This was done to detect the effects of UV crosslinking as well as electrospinning on the polymer. As shown in Figure 9, PDT prepolymer showed a crystalline structure arrangement with a melting point of -3 ^{o}C and a glass transition temperature (Tg) of -36 ^{o}C. After acrylation, the vinyl group introduction at the terminals of the prepolymer caused a restriction in the chains movement preventing them from rearrangement and resulting in an increase in Tg to -26 ^{o}C. This restriction was intensified after UV crosslinking due to increased structural stiffness upon the change from liquid state to elastomeric state. PVP was reported to have a melting point larger than 130 ^{o}C. It showed no melting endotherm for up to 180 ^{o}C indicating its amorphous structure as shown in Figure 10. Consequently, after PRES the ESS preserved their amorphous structure with no effect resulting from PVP addition. We also electrospun PVP in ethaol and subjected the PVP ESS to heating up to 180 ^{o}C as reported Appendix 2. Results showed amorphous behavior as well, which confirmed that PVP was incorporated in the scaffold after ES and had no effect on the molecular arrangements.

3.1.4 Proton Nuclear Magnetic Resonance (^{1}H-NMR)

Figure 11 shows the ^{1}H-NMR spectra for the pre-polymer and the acrylated pre-polymer. As shown in the Figure 11A, peak (a) represents protons of the methylene groups of the 1, 10 decanediol that appeared at 1.35 ppm. The protons of the pre

terminal carbon of the diol were represented by peaks (b) and (c) at 1.5 ppm and 1.6 ppm respectively.

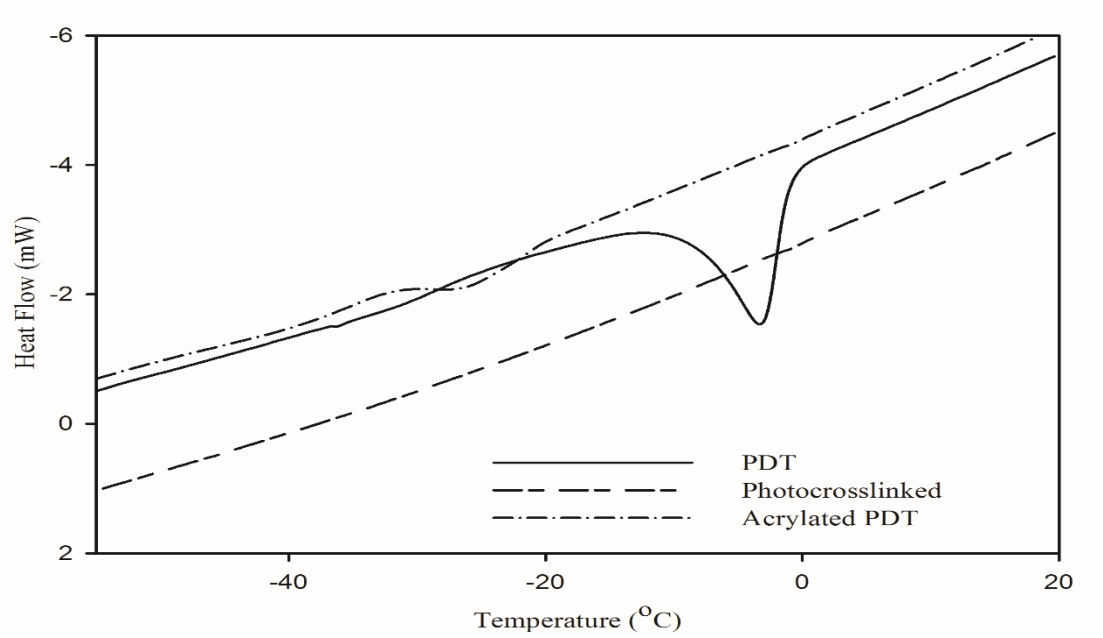

Figure 9. DSC Thermograms of PDT before and after acrylation and crosslinking

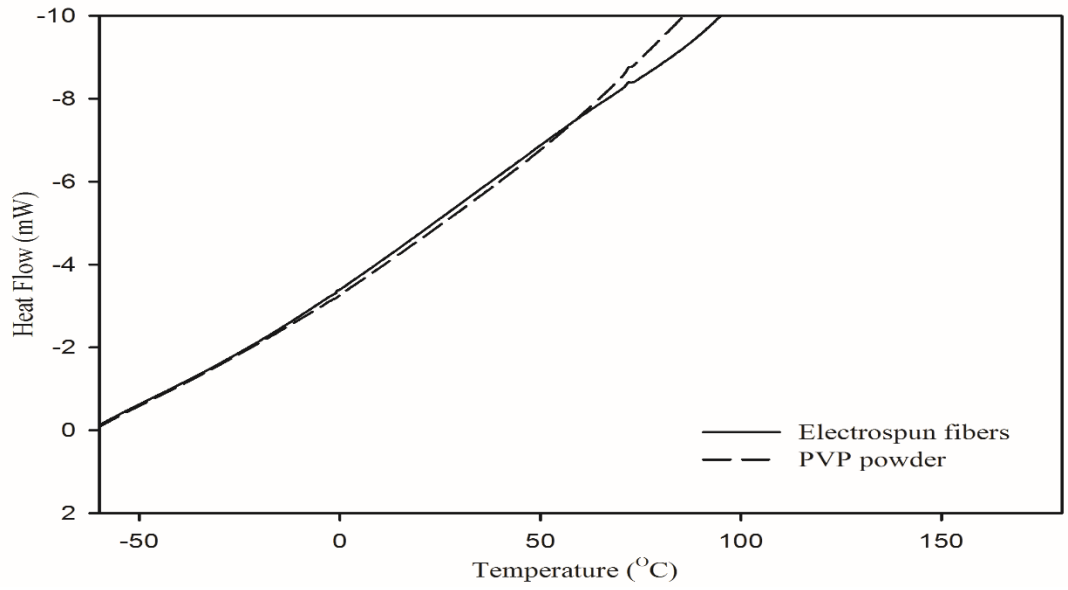

Figure 10. DSC Thermograms of electrospun ADPT and PVP powder

Protons next to the pro-chiral center of TCA were embodied by peaks (d) and (e) at 2.65 ppm and 2.75 ppm respectively, while the peak (f) at 3.2 ppm signified the protons of the pro-chiral center of TCA. As for protons of the diol's terminal carbon (adjacent to the hydroxyl group) and protons of the carbon attached to the ester bond, they were seen as peaks at 3.5 ppm (g) and 4.05 ppm (h) respectively. The acrylation process was proven successful upon the appearance of the three peaks at 5.8 (j), 6.1 (k) and 6.4 ppm (m) representing the newly introduced vinyl group in figure 12B. It is worth mentioning that for more accurate and exact peak assignment; two-dimensional NMR analysis would be advantageous but not very essential to ensure the successful acrylation of the prepolymer and for the determination of the degree of acrylation.

3.2 Morphological Analysis

The main objective of this current work was to synthesize 3D porous scaffolds to be as potential candidates for tissue engineering applications. Three types of scaffolds were synthesized: The first two were using solvent free particulate leaching using trehalose dihydrate as a porogen that was never used before, while the second was using sodium chloride as a conventional reference scaffold. The third type was using the PRES process to utilize its unique advantages to produce a highly porous scaffold for the same purpose.

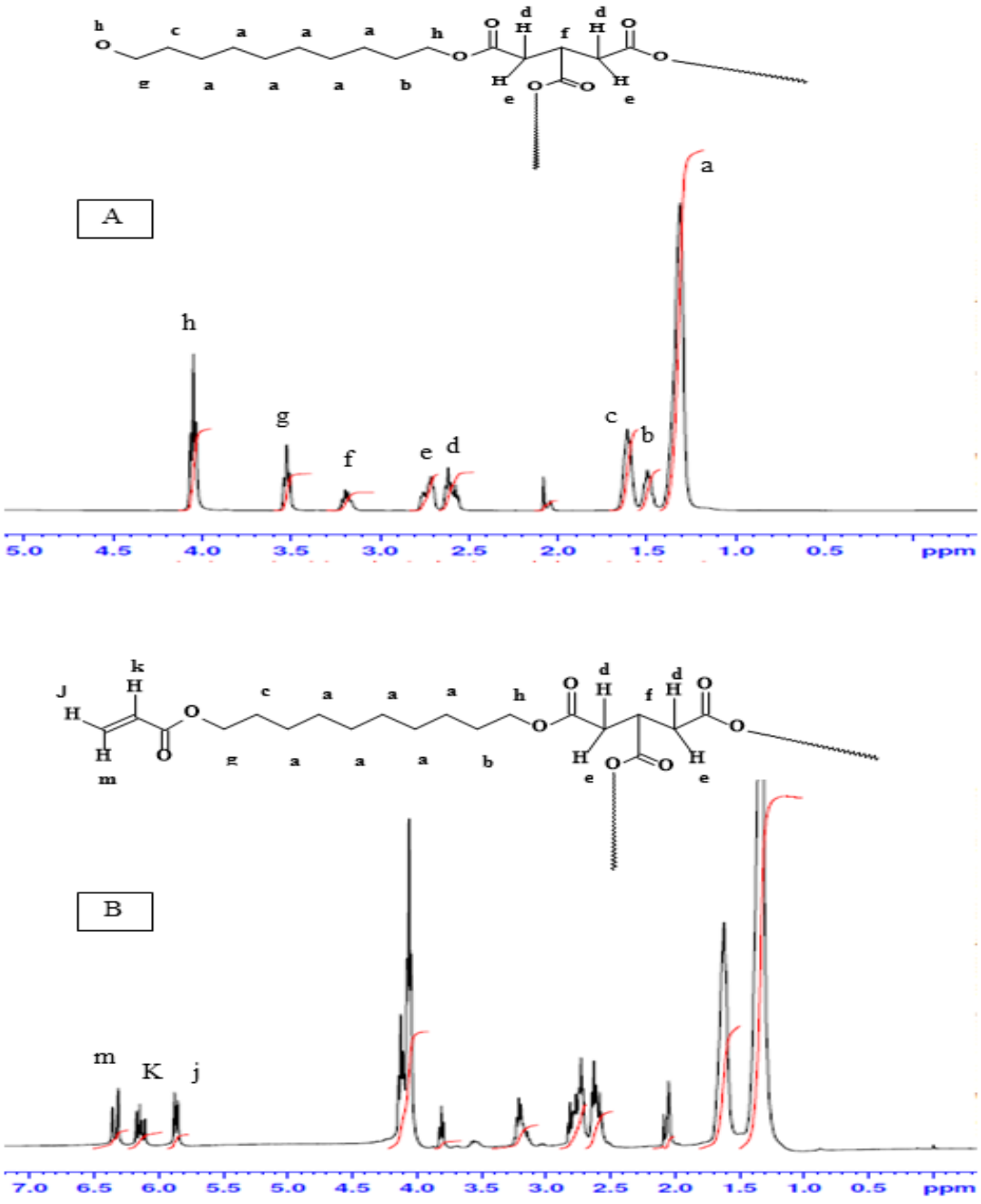

Figure 11. H-NMR spectra of (A) PDT and (B) APDT

3.2.1 Solvent-free particulate leaching

Figure 12 shows SEM images of ESS produced by particulate leaching. As shown in the figure, scaffolds produced using NaCl as a porogen were of very low porosity compared to the ones using TH. This was because it was difficult to leach out all NaCl particles and residual crystals existed within the matrix even after the leaching out period as shown in Figure 12 G, H. The inner part of the scaffolds and the surface of all scaffolds were porous compared to the blank film. In addition, the scaffolds where TH was used as a porogen, showed a relatively higher porosity without any TH visible traces after leaching out. This is advantageous in TE applications as it creates higher surface area with suitable controlled sizes for cell seeding, growth and nutrient exchange between the surrounding media and the seeded cells. However, one of the disadvantages of particulate leaching is that the size of the interconnected pores is hard to control no matter how the size of the porogen particles was the same.

3.2.2 Solvent free Electrospinning

At the beginning, we attempted direct electrospinning of APDT polymer using solvent free reactive ES. The attempt with the low molecular weight variation (3538KDa) was not successful and only liquid drops were obtained. However, upon using the high molecular weight variation, different outcome was obtained. Figure 13 represents optical microscope images of that attempt with and without UV crosslinking during the ES process.

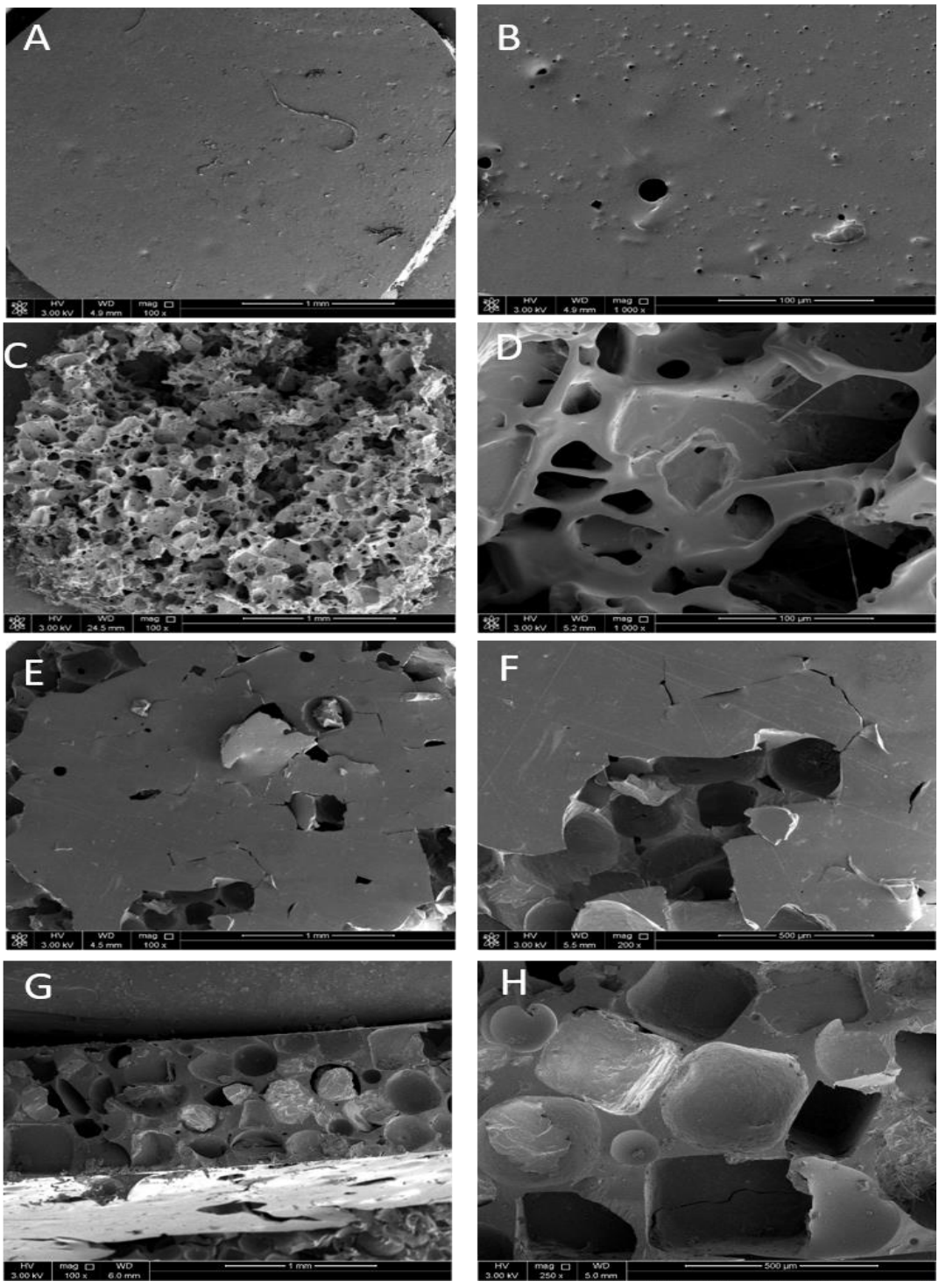

Figure 12**.** SEM micrographs of porous APDT scaffolds produced by particulate leaching using different porogens with low and high magnification. (A, B) Blank film, (C, D) Trehalose, (E, F) NaCl, top view, (G, H) NaCl, side view

As seen, UV crosslinking lead to certain degree of structural preservation of the formed fibers than those of the non-UV crosslinked, which were more of viscous liquid splatters, rather than elastomeric fibers. However, the fibrous structure was lost with time as the ES process progressed. This was attributed to the very low molecular weight of our polymer relative to other electrospinnable materials, which corresponded to very low viscosity and a low degree of chain entanglement. In addition, the hydrophilic nature of our polymer lead to more humidity absorption from the atmosphere, all are factors that lead to the fusion of any formed fibers soon after hitting the collector. This was in agreement to what was reported before by Xu *et al.* who concluded the importance and advantages of using high molecular weight polymer such as PVP 1300 kDa to act as a chain entanglement enhancer to preserve the fibrous morphology of the ESS sufficient for successful crosslinking and fiber fusion prevention. (60)

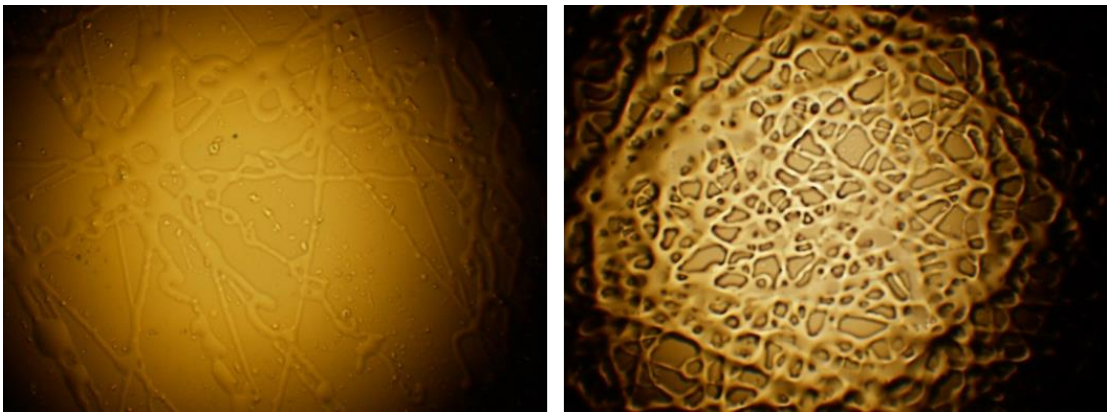

Figure 13**.** Optical microscope images for solvent free electrospun APDT. (A) Without UV crosslinking and (B) After UV crosslinking

3.2.3 ADPT Electrospinning with PVP as Chain Entanglement Enhancer

Two PVP molecular weights were used: PVP 90 kDa (PVP90) and PVP1300 kDa (PVP1300) mixed with different concentrations of ADPT polymer in ethanol. Ethanol was used because it was a suitable solvent to all solution components, PVP showed acceptable solubility with it, it gave the best bead-less fibrous structure during ES of PVP with a narrow fiber distribution compared to other organic solvents and it had a high dielectric constant that will aid in the ES process (62,154). In addition, it did not evaporate rapidly causing the breakdown of the polymer jet during ES and hence suppressing the fiber formation process.

3.2.4 Effect of UV crosslinking and collection method

At first, we used PVP 90K as an entanglement enhancer. Figure 14 shows the difference between UV and non-UV exposed meshes. This was done to make sure that our polymer and not PVP was influencing the formation of ES fibers. As expected, no fibers or scaffolds were formed without UV exposure. This was because our polymer will not convert into elastomer and will stay as viscous liquid without UV crosslinking. On the other hand, exposure to UV eventually formed a scaffold and started to slightly define the structure of the fibers with minimal amount of pores. However, optimization of the concentration of both the ADPT and PVP was required to obtain the porous fibrous mesh structure. At that stage, we made several attempts to collect the ES fibers. The flat and rotating metallic collector caused the fibers to fuse shortly after contacting the collector. This occurred due to the non uniform exposure of the deposited fibers to

UV light. Hence, the shadow collection method was used to expose the fibers to UV for longer period of time, increasing the degree of crosslinking and lowering the tendency of the fibers to collapse and fuse. As shown in Figure 15, the aluminum foil was bent at its top so that fibers hung and were forced to be straight in between the bent side and the body of the collector. This shadow technique forced the formed fibers to stay separated from each other which sustained the porous structure long enough to increase the degree of crosslinking and prevent fiber fusion.

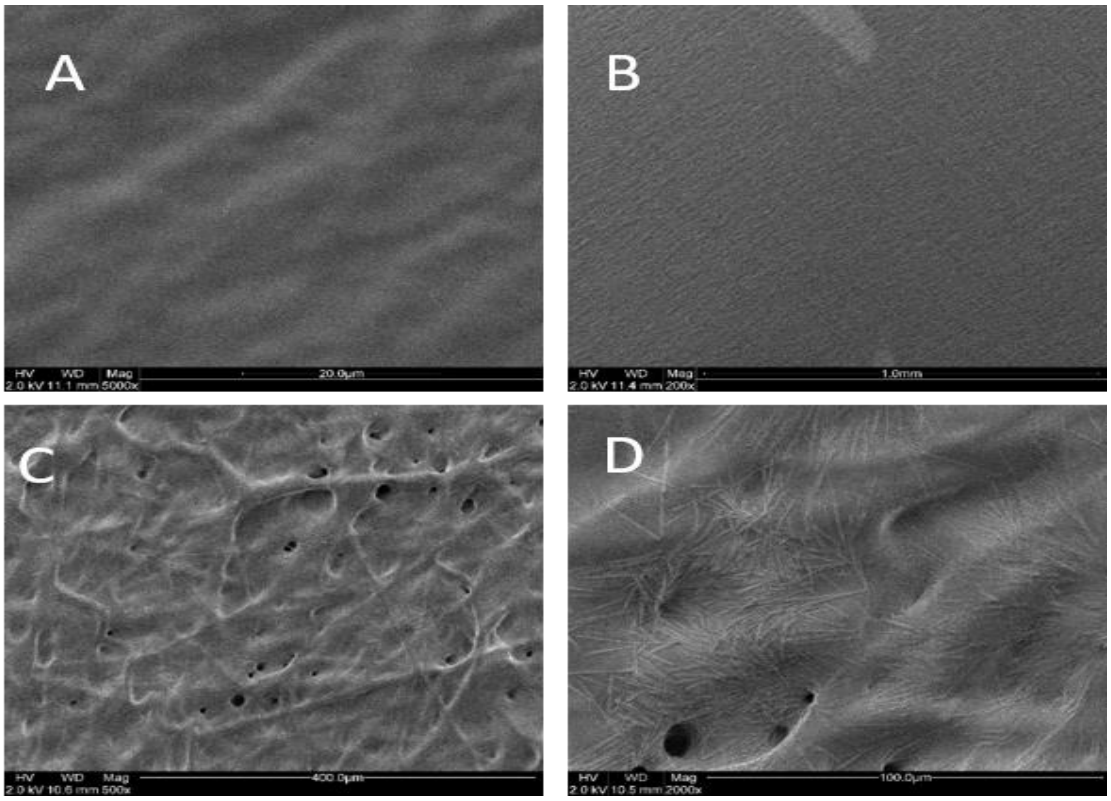

Figure 14. SEM micrographs of APDT/PVP (A, B) without UV crosslinking, (C,D) with UV crosslinking

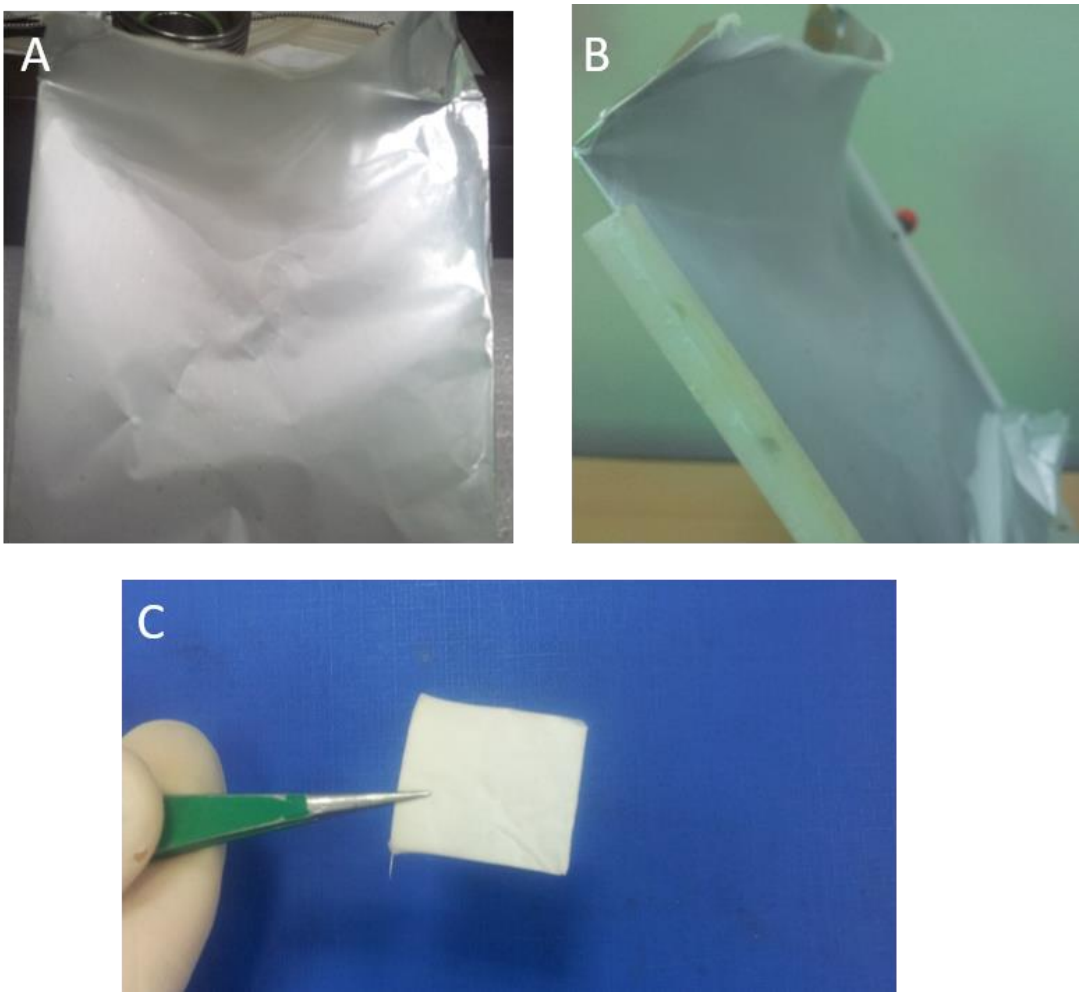

Figure 15**.** Macroscopic images after collection and crosslinking of APDT scaffold. (A, B) front and side view of the meshes on the collector. (C) Final scaffold.

The collection method was efficient considering the available resources but it had its disadvantages. One was the low yield as the part of the scaffold that could be separated was only the hung part. We believe this could be overcome upon the use of the open cage collector that will utilize all the electrospun solution, ensure full exposure of the fibers to UV and would produce aligned fibers (155).

Another limitation was the probability for non-uniform exposure to UV along the duration of ES process. This was overcome by exposing the scaffolds to UV for 20 minutes after the end of ES process.

3.2.5 Effect of polymer concentration on fiber formation

To optimize the fiber formation process, ideal combination of concentration of ADPT/PVP in the solution had to be concluded. Theoretical entanglement concentration for PVP was calculated previously to be 7.5% W/V of PVP in ethanol. However, their experiments showed an ideal concentration that formed bead-less fibers at 7-9%w/v (154). In our case, 8% PVP concentration gave the optimum viscosity and lead to bead-less fiber formation.

Several trials were conducted to optimize the ADPT concentration, which was found to be 20 % (w/v) . As shown in Figure 16 below this concentration, fiber fusion tookplace. This may be due to insufficient ADPT for a proper degree of crosslinking enough to prevent fusion.

Above 30%, very fast crosslinking took place for the polymer droplet on the tip of the needle, which lead to needle clogging. The 20% (w/v) APDT concentration was the optimum that produced porous mesh without blocking the needle.

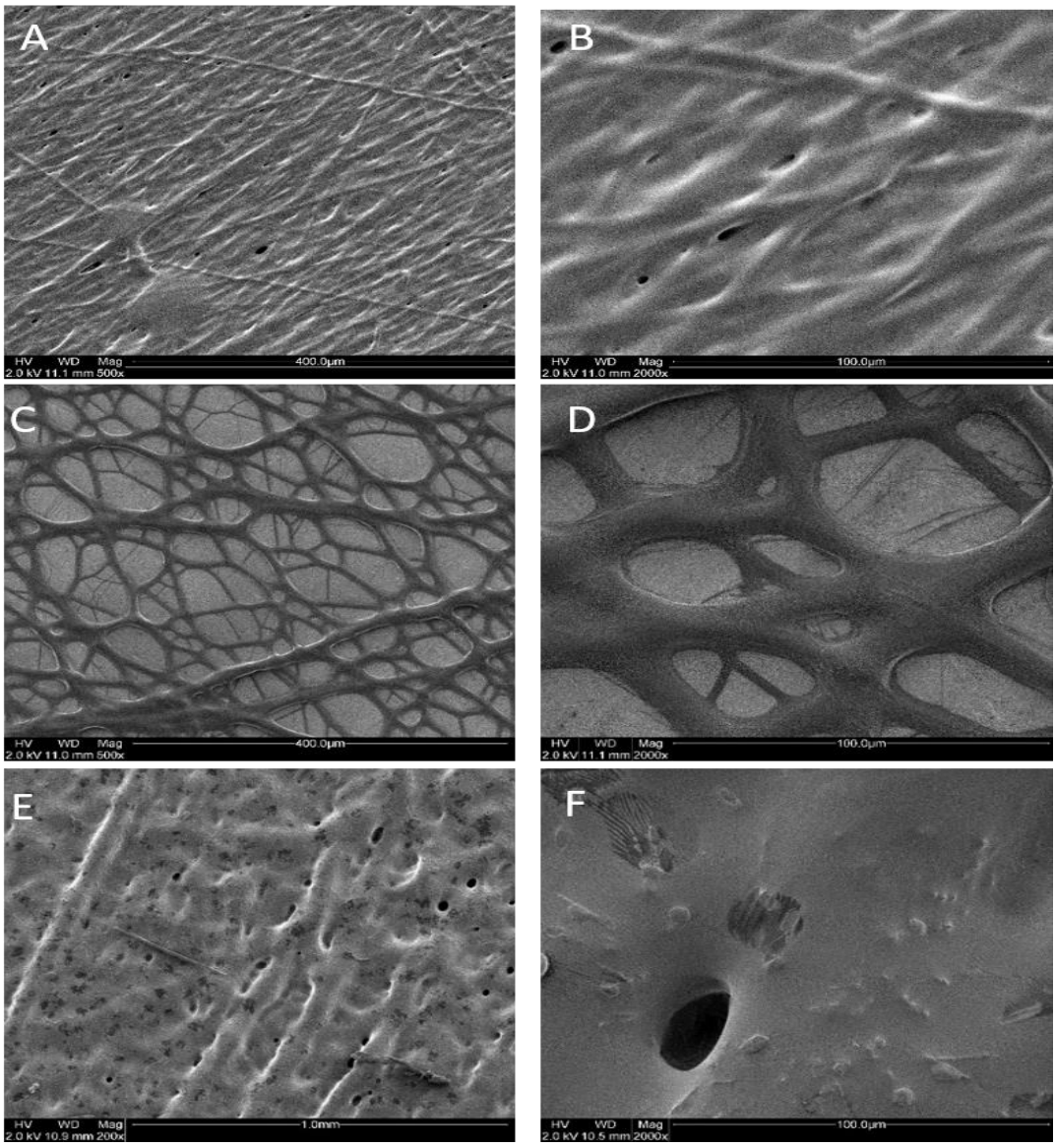

Figure 16. SEM micrographs of electrospun APDT with 8% PVP (w/v) PVP90kDa at different APDT concentrations with UV crosslinking. (A, B) 10%, (C, D) 20% (E, F) 30%.

A possible solution to this problem would be wrapping the needle with a UV blocking material to only expose the polymer stream to UV and not the tip of the needle or the liquid drop at the tip.

3.2.6 Effect of PVP molecular weight and acrylation degree on fibrous structure

All previous experiments were conducted using a 1.5x degree of acrylation. In order to examine the effect of increasing the degree of acrylation on the fibrous structure, acrylation degree was increased to twice the amount of terminal hydroxyl groups. When ES was attempted using PVP 90, a porous fibrous mesh was produced as shown in Figure 17. This was due to the higher acrylation degree, which increased the number of terminal double bonds that elevated the crosslinking degree and hence guaranteed faster, more efficient crosslinking, less fiber fusion and more structural integrity. Other studies have reported the use PVP1300 as an entanglement enhancer which aided in the successful formation of fibers (60). We attempted using PVP1300 in our experiments as in Figure 17 (C, D). Porous mesh structure was formed but with significantly larger fiber diameter and smaller pore size than when PVP90 was used (Figure 17). This resulted from the increased viscosity of the solution as the molecular weight of the used PVP increased (58,59,156). The mesh fibers produced using PVP 1300 kDa was further used for *in vitro* studies since it was the one used to calculate the critical entanglement concentration reported before (157).

All of the produced porous mesh scaffolds showed secondary fiber branching as demonstrated by the SEM micrographs that rendered our scaffolds resembling the spider net nanofibers reported earlier (158). This is due to the branching of the primary polymer stream into several secondary jets due to further instabilities within the straight jet or after Tylor cone (159). These secondary jets might give rise to beads or fibers depending on their stability upon responding the applied voltage. If those streams were

broken into droplets, beads were formed. On the contrary, to that, in our case, the unbroken secondary polymer jets formed fibers and were deposited on the collector causing the appearance of those branches of smaller diameter that stemmed from the main fibers (160,161). Further assessment of the structure using PVP of higher molecular weight (i.e. PVP 360 kDa) might prove useful to resolve this issue. However, polyethylene oxide (PEO) 5000,000 Da molecular weight was utilized in our experiments with a concentration down to 0.1% (w/v) but the viscosity of the solution was too high to be ejected from the needle. Another cause for the mesh structure might be the partial crosslinking of the droplet on the tip of the needle. This might have caused partial clogging of the needle tip leading to primary jet splitting. This might also explain the reason behind using high flow rate of 10 ml/hr below which the needle clogging occurred. This could be prevented in future studies by covering the needle and its tip with UV blocking film to only expose the jet in an attempt to study effect of variation of ES parameters on the fiber morphology.

3.2.7 Porosity analysis

The porosity and pore sizes of the scaffolds produced by ES and particulate leaching method were compared and reported in Table 7. As seen, all scaffolds were highly porous with porosities exceeding 70%. It was reported in previous studies that porous scaffolds produced via different methods with porosities of down to less than 30% porosities and more than 90% were used for various bone tissue engineering applications (162).

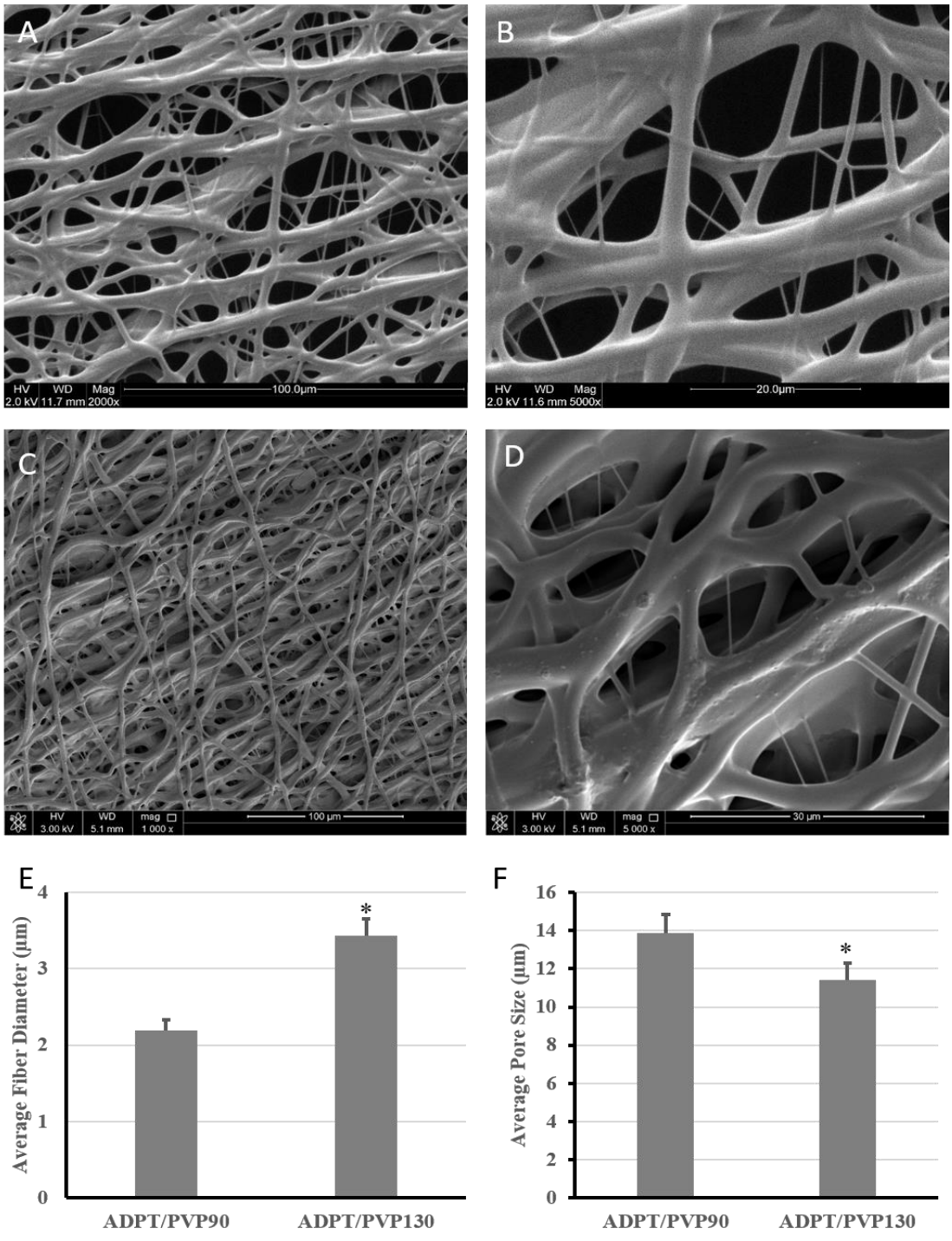

Figure 17**.** Scaffold morphological structure and analysis of APDT/PVP meshes with 2x acrylation degree at different PVP molecular weights. (Upper) SEM micrographs with PVP (A, B) 90KDa, (C, D) 1300KDa. (Lower) Average pore size (E) and Fiber diameter. Data were represented as mean ±SEM (n=5), * P<0.05 independent T-test.

However, pore size analysis revealed a difference between the three scaffolds. First, scaffolds produced by particulate leaching using NaCl as porogen showed the highest pore size (304.8 ±13.2µm) compared to the ones using TH (80.4 ± 6.4µm) although the former had less surface pores compared to the later as shown in Figure 13. Electrospun scaffolds showed the least pore size among all. The importance of the pore size, porosity together with fiber diameter appeared upon the assessment of cells interactions with the scaffold where an optimum combination of all factors should facilitate the cell attachment and growth in the 3D scaffolds. This is discussed later under the *in vitro* studies section.

Table 7**.** Pore size and porosity analysis of different porous scaffolds.

Scaffold	**Pore Diameter (µm)**	**Porosity**
TRE	127.97± 13.34	78%
Na	314.47± 10.38	72%
ESS	11.43± 0.78	78%

Data reported as mean ± SEM

3.2.8 Solvent resistance

Un-crosslinked ADPT is soluble in most organic solvents and it forms a colloidal dispersion in water. Upon UV crosslinking, it was converted into an amorphous structure that was hydrophilic, yet insoluble in most solvents. This is advantageous for

TE applications where the structural integrity of the scaffold is needed long enough for cell attachment, proliferation and differentiation.

As shown in Figure 18, minimal changes occurred to the porous structure of the ES meshes upon immersion in ethanol and water for 24hours. This simulates and eliminates the effect of the sterilization conditions on the porous structure of the mesh scaffolds prior to *in vitro* testing. This was not necessary to be done for the other two scaffolds because during porogen leaching step, the scaffolds were immersed in water for several days to remove porogen particles. Therefore no major deviations in the porous structure were expected than from Figure 12 by default.

3.3 Tensile testing

Table 8 summarizes the results of the tensile testing performed on the electrospun scaffolds using PCL scaffolds as control in a dry state. PCL was chosen because it was widely used for the same area of application and was known to be the material of choice for tunable mechanical properties, alone or in combination with other materials (163).

It was reported previously that mechanical stress enhanced bioengineered cardiomyocyte proliferation, intercellular organization and cardiomyocyte hypertrophy. The bioengineered human cardiomyocytes could contract autonomously with proper response to contraction. Moreover, when bioengineered cardiomyocytes were transferred into hearts of nude rats, they survived, engrafted onto the heart and were perfused by blood vessels of the host (164).

Table 8**.** Mechanical properties of different scaffolds

Sample/ Parameter	**UTS (Mpa)**	**Elongation (%)**	**Modulus (Mpa)**	**Crosslinking density (mol/m^3)**
PCL control	1.63 ± 0.32	175.43 ± 22.74	2.4 ± 0.79	N/A
ESS	0.54 ± 0.24	46.93 ± 11.93	1.35 ± 0.34	168.85± 29.43
PDET (149)	0.14 ± 0.02	61.23 ± 5.83	0.33 ± 0.02	44.39 ±3.09
Adult rat myocardium (167)		Right ventricle	0.02 ± 0.004	
		Left ventricle	0.084 ± 0.008	

UTS: Ultimate tensile strength

Values are reported as mean ±Standard deviation (n= 5). Young's modulus of rat myocardium is reported for comparative reasons (167).

Consequently, the mechanical properties of the scaffolds should be suitable for physical support of the cells. It should also be lenient and flexible, possessing suitable tensile strength and young's modulus to withstand and allow the conduction of impulses to the loaded cells through the myocardium. If both of these properties were high, this would cause resistance to the cardiac contraction and might constrain the heart relaxation. In Table 8, the ESS showed low young's modulus compared to the PCL scaffold.

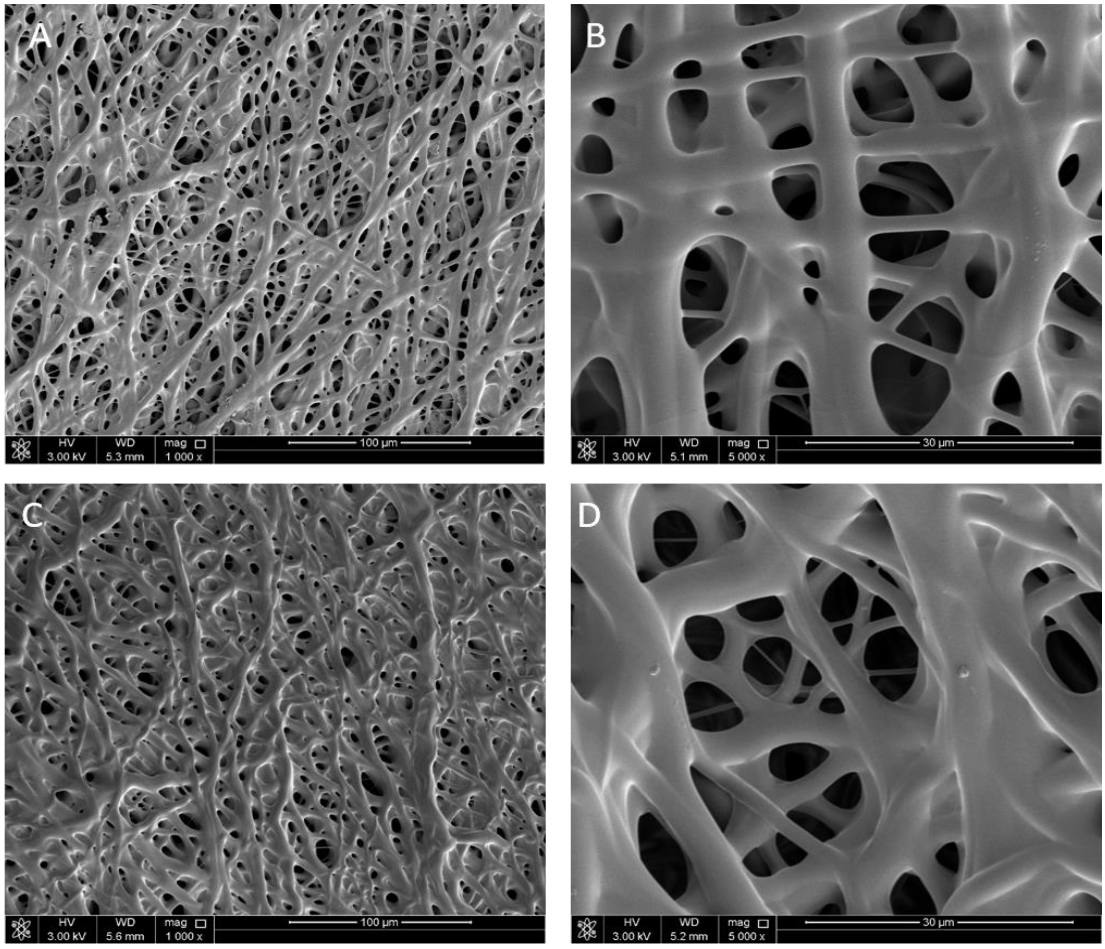

Figure 18**.** SEM micrographs of UV crosslinked electrospun scaffolds after immersion in different solvents for 24 hours. (A, B) Ethanol, (C, D) water.

This indicated the high elasticity which would enable the scaffold to withstand myocardial contraction and relaxation. In addition, the length of the scaffold before and after breakage was the same. This was due to the elastomeric behavior of our crosslinked polymer that allowed full recovery upon deformation. This was contrary to PCL, which deformed after break indicating inability to retain its original geometry (165). On the other hand, when the ESS were compared to the non-porous

photocrosslinked films reported before by our group (149), there was a decrease in both the tensile strength and young's modulus. This was attributed to the higher crosslinking degree for the ESS due to the higher energy of UV light than visible light used previously, which meant higher crosslinking efficiency. This indicates the ease of manipulation of the mechanical properties of our ESS to suit the purpose of use. This can be achieved by changing the degree of acrylation or the crosslinking degree by changing the intensity and time of exposure to UV light.

3.4 Contact angle measurement

Scaffolds used for TE applications are preferably hydrophilic to allow easy attachment of cells in a way resembling ECM. When contact angle was measured for our scaffold it was found to be $80^{o}\pm$ 5.3 which indicated the moderately hydrophilic nature of our scaffolds. It was previously reported that cells preferably attach to polymers with intermediate contact angle of around 70^{o} than lower or higher once (166). This indicated that our scaffold would be a potential candidate for TE. In addition, when the contact angle was measured at multiple time points, the contact angle was found to gradually decrease to a minimum of 30.4^{o} as shown in Appendix 3. This might be due to the porous nature of the scaffold together with its hydrophilicity, where the droplet propagates through the scaffold decreasing the contact angle. This was a strong evidence of the hydrophilic nature of our scaffolds.

3.5 In vitro cell viability and cell/scaffold interactions

3.5.1 Cell viability study using H9C2 cardiomyoblasts

The main aim for producing the scaffolds was to utilize their characteristics to be used for cardiac tissue engineering applications. We used our three types of scaffolds to perform a series of tests to detect any indirect (i.e. Scaffolds are not in contact with the cells) cytotoxicity due to traces of toxic chemicals used in the original reaction (i.e. Acryloyl chloride, Triethyl amine…etc.) or any potentially toxic degradation products. H9C2 cardiomyoblasts were used to explore any indirect cytotoxicity from our scaffolds towards cells of cardiac origin.

It was reported that H9C2 cells differentiated into cardiomyocytes by lowering the serum levels in the culture media. Hence, it can be utilized for cardiac tissue engineering applications (168). Both the average number of cells per field and percent of viable cells relative to control were analyzed. However, the percent viability was more accurate since the values were normalized to the control. This was the main reason behind reporting it here, while the average per field data are reported in the Appendix 5 and 6.

When cell viability was assessed as in Figure 19, the percentage of viable cells for ES and TRE was 86.2 %± 11.01 and 85.7 % ± 8.8 percent viability relative to the polystyrene untreated control after 24 hours of incubation. As for NA scaffolds, the cell viability was 80.4% ± 13.7 compared to the control, which was the lowest among the three scaffolds.

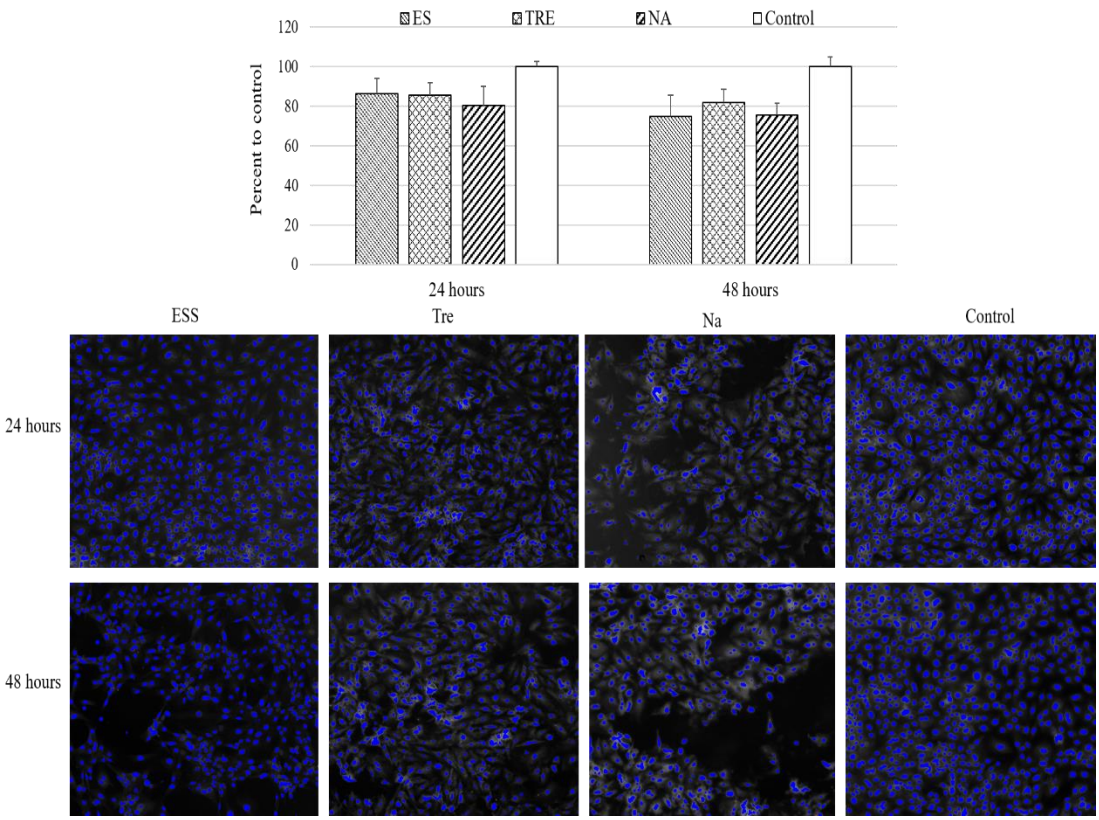

Figure 19**.** H9C2 cell viability in presence of ES, TRE and NA scaffolds at 24 and 48 hours. (Lower) Images show the DAPI stained nuclei and (Upper) the number of nuclei of viable cells represented as percentages to untreated control. Cell number was assessed by automated quantitation of DAPI positive nuclei using ArrayScan XTI (Target activation module). Data presented as Mean ± SEM. n=6 *Statistical significance: *P<0.05 compared to the control.

After 48 hours, the percent viability of the ES, TRE, NA was 74.9 ± 15.2, 81.8± 9.5, 75.67 ± 8.3 respectively. There were no significant differences between the three scaffolds relative to their controls at both time points. There were also no significant differences in cell viability between all scaffolds at a given time point.

3.5.2 Cell viability studies using adipocyte derived mesenchymal stem cells

The effect of the scaffolds on adipose derived MSCs was also explored to examine the possibility of stimulating cell differentiation into cardiomyocytes directly on seeded scaffolds. This was aimed at widening the range of applications of our scaffolds to several other cell types for TE. Those cells composed mainly of MSCs as shown in Appendix 2 where MSCs markers were the triple positive cells at 80% (105, 166, and 73). As shown in Figure 20, the percentage of viable cells after 24 hours was 75.2± 7.5 and 64 ± 11.4 for ES and NA respectively, with no significant difference to the corresponding control. Interestingly, cell viability with TRE was the highest among all scaffolds as well as the corresponding control, which was significantly different when compared to ESS (*P* value=0.001) and NA (*P* value=0.0001). After 48 hours, values for ESS and NA scaffolds were significantly lower than the control at 65.96 ± 6.5 and 66.2 ± 4.9 (P values were 0.039 and 0.041) respectively. Similarly, cell viability with TRE was significantly higher than cell viability with both ESS (*P* value=0.003) and NA (*P* value= 0.004).

One of the main limitation for this cytocompatibility study is the different seeding density for each biological replicate for MSCs. This was due to their slow growth compared to H9C2 cells. This could be overcome future studies by incubating the cells for longer time to grow until reaching a higher degree of confluence. Another solution would be to increase the number of biological and technical replicates to avoid any

possible errors. The comparison between the cell viability for the two types of cells used revealed some interesting findings.

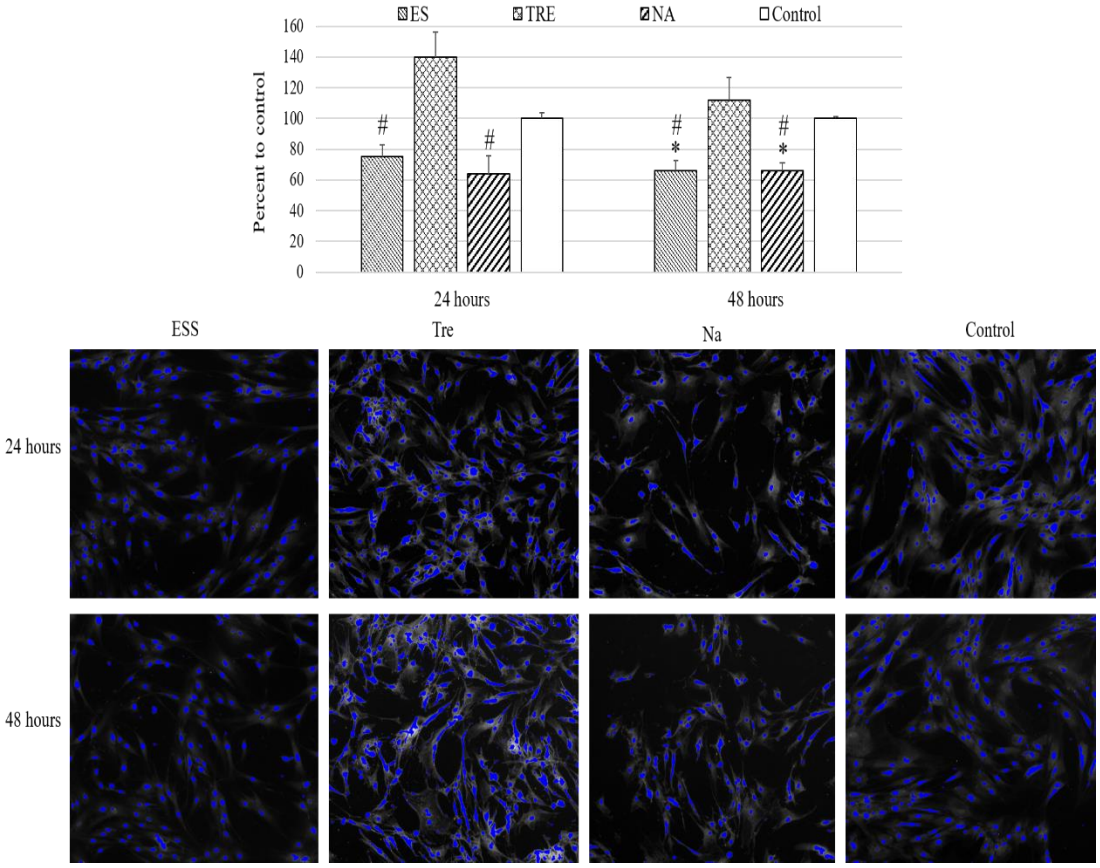

Figure 20. Mesenchymal stem cells viability in presence of ES, TRE and NA scaffolds at 24 and 48 hours. (Lower) Images show the DAPI stained nuclei (Upper) the number of nuclei of viable cells represented as percentages to untreated control. Cell number was assessed by automated quantitation of DAPI positive nuclei using ArrayScan XTI (Target activation module). Data presented as mean ± SEM. n=3. Statistical significance: *P<0.05 compared to control and #P<0.05 compared with TRE.

ES and TRE scaffolds had similar effects on H9C2 cells while it was different with MSCs. This signified the difference in cellular response to different scaffold

degradation products as well as chemical traces, where for one type, the cells survived while in the other, results varied. This opened the door for future studies to examine the effect of our ESS on different cell lines to be used for other TE applications.

These results also showed that cell viability was slightly higher for TRE than ESS with H9C2, and significantly higher in case of MSCs. This may be due to the possible existence of traces of TH. Trehalose is a disaccharide, which was reported recently to enhance cell viability and proliferation even during dehydrated conditions. It was also reported to increase the cell signaling proteins, the stress resistance proteins and other types of proteins that play a major role in cell proliferation (169). In another report, trehalose played a role in the preservation of stem cells upon freezing even when introduced intracellularly by the aid of liposomes (170). However, other reports mentioned that trehalose by itself lacks the ability to penetrate the cells due to its large size (171).

The choice of porogen concentration and particle size for TRE and NA was based on a qualitative cytocompatibility testing using live/dead assay on scaffolds with NaCl as a porogen of variable particle size and concentration (Appendix 7 and 8). The results showed that scaffolds produced with the largest particle size and concentration had the highest number of living cells. In addition to the theoretically high porosity and adjustability of pore size distribution, these were the reasons of choosing the specific particle size and concentration for the quantitative cell viability studies.

The culture media are generally replaced every other day to supply the cells with the needed nutrients and remove any waste. For that reason, it was expected that 48hours time point would have the highest concentration of any toxic traces or degradation products released from the scaffold, if any existed. We based our choice of the time points on the fact that this was the maximum period with no media change and hence, highest cell death would occur. However, due to the special degradation behavior of our polymer reported previously (149), a study that correlates the concentration of degradation products versus cell viability would be a promising future study to detect the more significant cause of decreased cell viability. It is worth mentioning that constant media change would be the closest to the *in vivo* conditions. It is closely related to what exists in the human body where a homeostatic dynamic environment created by the blood circulation creates a constant supply of oxygen and nutrients with constant sink condition. Consequently, waste materials would be removed.

3.5.3 Cell / scaffold interaction assessment

The three types of unmodified scaffolds were seeded with H9C2 cardiomyoblasts and were incubated for 14 days in non-tissue culture treated well plate. At the end of the 14 days, Calcein-AM staining was used to visualize the living cells. As shown in Figure 21, H9C2 cardiomyoblasts successfully attached to both ES and TRE scaffolds while there was no attachment appearing on the NA scaffolds. Cells were observed to grow on different planes of view in both scaffolds, signifying the penetration of cells through the 3D structure of the scaffolds. However, the number of living cells was larger with an even distributed in case of the ESS while in case of TRE cells were more

concentrated on the peripheries. There are several reasons that could have caused this: First, the mesh structure of the scaffolds which facilitated protein pre-adsorption from serum more than the other scaffolds and hence allowed more cell attachment as reported earlier (165). Second, media change that removes any toxic traces, degradation products and dead cells allowing the living cells to grow more on the scaffold. Third, when normal tissue culture treated plates were used, cells preferentially attach to the plate rather than the scaffolds due to higher affinity. However, when non treated plates were used, cells attached easily and penetrated through the scaffold. Fourth, it was reported before that different cell types have different optimum pore sizes for maximum growth, proliferation and differentiation (162,172,173,174). Consequently, a higher degree of cell attachment in case of ES was attributed to an optimum pore size, pore size distribution and fiber diameter than other scaffolds. Moreover, a previous study done using adipose derived human mesenchymal stem cells showed similar findings. Cells were seeded and incubated on electrospun scaffolds for 14 days and were analyzed by the live/dead assay, SEM imaging as well as DNA quantification. The results showed a significant increase in the number of viable cells only at day 14. In addition, findings demonstrated the role of the fiber diameter and pore size in influencing orientation and infiltration of the cells into the scaffold (175). In this context, a future study using our ESS over prolonged period would be promising to assess the use of our scaffolds for other TE applications. It was also reported that induced pluripotent stem cells differentiated into cardiomyocytes by adjusting the morphology of gelatin coated PCL scaffolds (176). Hence, a future study relating pore

size, pore size distribution and fiber diameter to cell growth and proliferation of both H9C2 and MSCs on our scaffolds at different time points is expected to generate useful findings. It is worth mentioning that cells attached and grew on the scaffolds without any chemical modification to increase cell affinity towards the scaffolds as reported earlier (165,176,177).

Our fiber collection method provided a certain degree of fiber alignment that lead the cells to arrange themselves along the fibers as shown in figure 22. In a study by Kai *et al.*, it was reported that scaffolds with aligned structures offered the required anisotropic effect well matched for cardiac tissue engineering applications. That effect rendered those aligned scaffolds superior in terms of cardiomyocyte cell attachment and orientation compared to random oriented electrospun scaffolds (178). Another promising future study would be to stimulate the differentiation of the attached cells into cadiomyocytes and examining their behavior. We wanted to demonstrate the possibility of tissue development which was reported before to be done by depriving the media from serum that suppressed cell differentiation (168). This issue could be addressed in depth in a future study to have a higher degree of alignment across the scaffolds by using rotating open cage collector (155). However, one limitation of this study would be the qualitative nature of the calcein-AM staining which gives primary results only that are inconclusive. Therefore, further tests are recommended to further analyze the cell scaffold interaction and cell penetration as SEM imaging of the critical point dried scaffolds with fixed cells and DNA quantification.

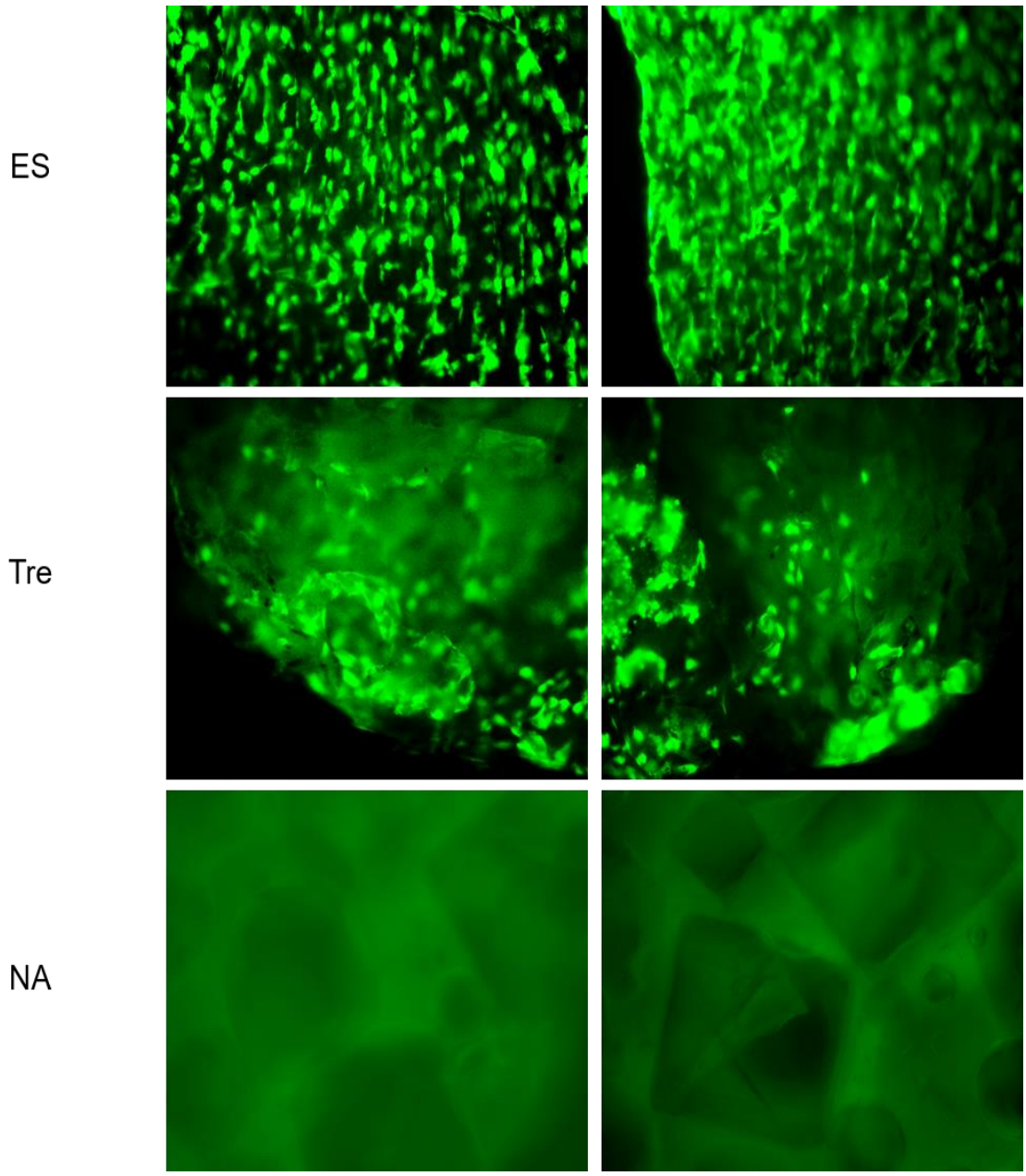

Figure 21**.** Qualitative images of Calcein-AM staining of H9C2 cells on different scaffolds show cell attachment to the scaffolds after 14 days of incubation in non-tissue culture treated well plates. Live cells appear as fluorescent green color.

Our scaffolds were known the give red fluorescence when exposed to ethidium-homodimer-1 (EthD-1) that stained the dead cells in red. In order to exclude any interference from the scaffold with the results, we performed the same test using Calcein-AM with tissue culture treated plates. This was to examine cell viability after the same time interval (i.e. 14 days). As expected in Figure 22, cells preferred to attach to the plate than the scaffold due to higher affinity as we mentioned earlier. In addition, the number of live cells under the scaffolds appeared to be in that order: TRE>ES>NA, where NA showed the least number of living cells while TRE and ES were closer to the control. In addition, it was observed that cells were taking the shape of the scaffold when they were growing in case of ESS. This might signify a growth enhancing effect from our scaffold towards cells in closer proximity to the scaffold over extended period. However, further quantitative investigation is needed to confirm such findings.

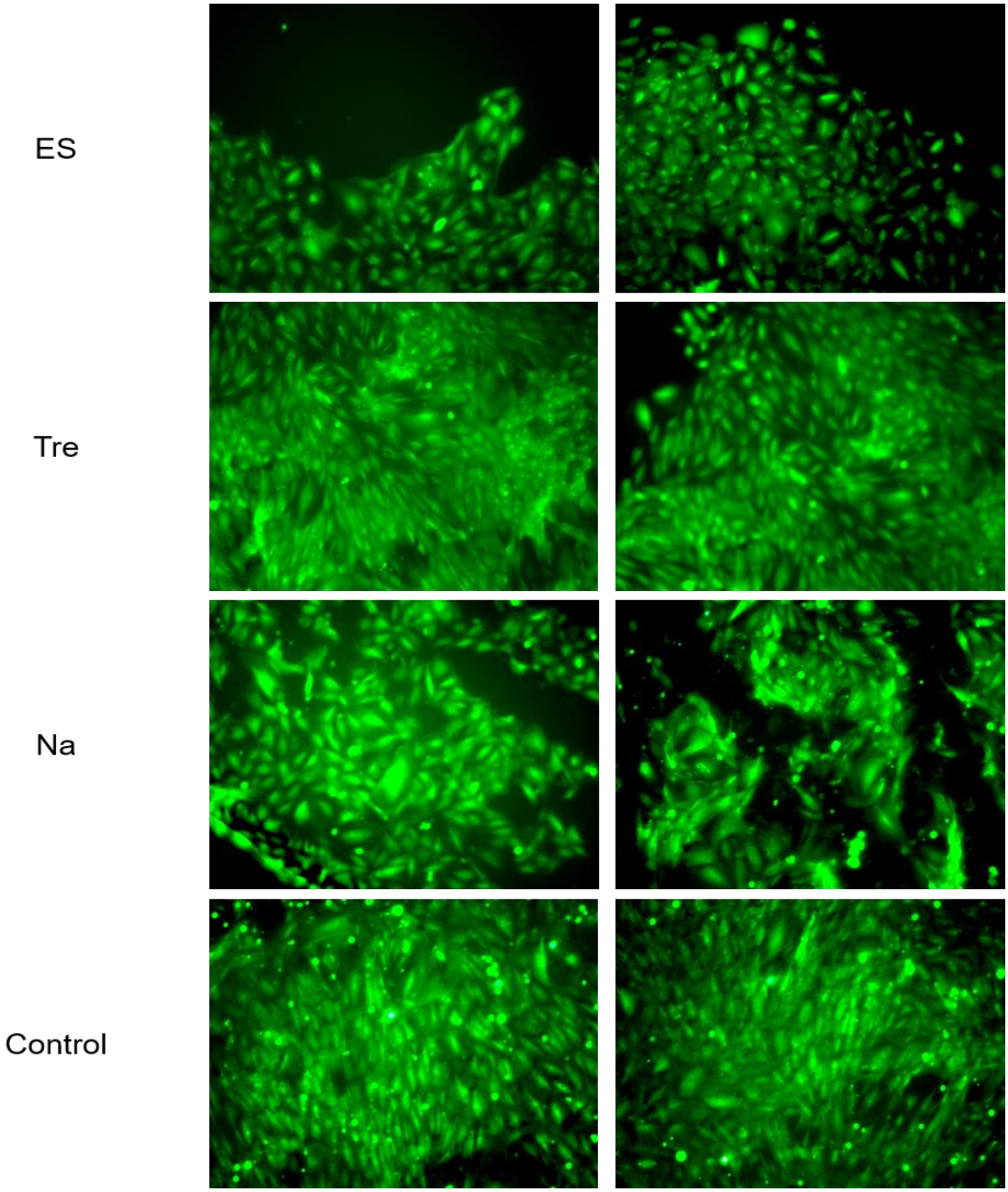

Figure 22**.** Qualitative images of Calcein-AM staining of H9C2 cells after 14 days of incubation with the three types of scaffolds in tissue culture treated plates. Live cells appear as fluorescent green color.

Conclusion

The design of the ideal porous, biocompatible, biodegradable, mechanically controllable scaffold with the highest resemblance to extracellular matrix was investigated in various studies. This was done using a wide array of techniques for tissue engineering and regenerative medicine purposes. In our study, we successfully synthesized the APDT polymer with high molecular weight. Afterwards, we successfully produced ECM resembling porous scaffolds using the promising photoreactive electrospinning technique. In addition, we produced porous scaffolds using our polymer using particulate leaching technique using two porogens: the conventional sodium chloride and the newly introduced trehalose dihydrate.

Full chemical, thermal, morphological and mechanical was performed for all scaffolds. Morphological analysis demonstrated three-dimensional structure with high porosity and a variable pore size range. In addition, mechanical testing of the electrospun scaffolds demonstrated high elasticity that was suitable for cardiac tissue engineering purposes. The high crosslinking density of the produced scaffold offered another aspect of the highly tunable mechanical properties of our polymer during synthesis or fabrication. Electrospun scaffolds were resistant to different solvents with preserving its fibrous structure. The produced scaffolds were of amorphous nature with a Tg lower than the core body temperature as represented by thermal analysis. This would ensure the existence of the scaffold in the rubbery elastic state at all times which is required to withstand the continuous cardiac contraction and relaxation.

In vitro quantitative cell viability on cardiomyoblasts showed a non-significant effect of both ESS and TRE scaffolds. However, ESS demonstrated superior cell attachment and growth capability over TRE when cell scaffold interaction was investigated. Interestingly, when cell viability was investigated using adipose derived mesenchymal stem cells, TRE scaffolds showed a growth enhancement effect.

Based on the above data, we have successfully demonstrated that ESS was a promising candidate for cardiac TE applications. In addition, future investigation of long-term cell scaffold interaction between the electrospun scaffold and MSCs is recommended. Finally, Further investigation on TRE scaffold is a recommended for further investigation for other tissue engineering applications.

Funding

This project was made possible by NPRP grant # NPRP 09-969-3-251 from Qatar National Research Foundation (a member of Qatar Foundation) through its National Priorities Research Program granted to Dr. H. Younes. The statement made herein are solely the responsibility of the authors.

References

(1) The Effects of Tissue Plasminogen Activator, Streptokinase, or Both on Coronary-Artery Patency, Ventricular Function, and Survival after Acute Myocardial Infarction. N Engl J Med 1993 Nov 25;329(22):1615-22.

(2) Ripa RS, Jorgensen E, Wang Y, Thune JJ, Nilsson JC, Sondergaard L, et al. Stem Cell Mobilization Induced by Subcutaneous Granulocyte-Colony Stimulating Factor to Improve Cardiac Regeneration After Acute ST-Elevation Myocardial Infarction: Result of the Double-Blind, Randomized, Placebo-Controlled Stem Cells in Myocardial Infarction (STEMMI) Trial. Circulation 2006 Apr 25;113(16):1983-92.

(3) Cheng Y, Yi G, Conditt GB, Sheehy A, Kolodgie FD, Tellez A, et al. Catheter-Based Endomyocardial Delivery of Mesenchymal Precursor Cells Using 3D Echo Guidance Improves Cardiac Function in a Chronic Myocardial Injury Ovine Model. Cell Transplantation 2013 Dec 23;22(12):2299-309.

(4) Kular JK, Basu S, Sharma RI. The extracellular matrix: Structure, composition, age-related differences, tools for analysis and applications for tissue engineering. J Tissue Eng 2014 Jan 1;5.

(5) Naderi H, Matin MM, Bahrami AR. Review paper: Critical Issues in Tissue Engineering: Biomaterials, Cell Sources, Angiogenesis, and Drug Delivery Systems. J Biomater Appl 2011 Nov 1;26(4):383-417.

(6) Choi JH, Gimble JM, Lee K, Marra KG, Rubin JP, Yoo JJ, et al. Adipose Tissue Engineering for Soft Tissue Regeneration. Tissue Eng Part B Rev 2010 Aug 18;16(4):413-26.

(7) Oh SH, Kang SG, Kim ES, Cho SH, Lee JH. Fabrication and characterization of hydrophilic poly(lactic-co-glycolic acid)/poly(vinyl alcohol) blend cell scaffolds by melt-molding particulate-leaching method. Biomaterials 2003 Oct;24(22):4011-21.

(8) Williams DF. On the mechanisms of biocompatibility. Biomaterials 2008 Jul;29(20):2941-53.

(9) Chiquet M, Renedo AS, Huber F, Flück M. How do fibroblasts translate mechanical signals into changes in extracellular matrix production? Matrix Biol 2003 Mar;22(1):73-80.

(10) Sahoo S, Ang LT, Goh JC-H, Toh SL. Growth factor delivery through electrospun nanofibers in scaffolds for tissue engineering applications. J Biomed Mater Res 2010 Jun 15;93A(4):1539-50.

(11) Cai X, Tong H, Shen X, Chen W, Yan J, Hu J. Preparation and characterization of homogeneous chitosan-copolylactic acid/hydroxyapatite nanocomposite for bone tissue engineering and evaluation of its mechanical properties. Acta Biomater 2009 Sep;5(7):2693-703.

(12) Kane RJ, Roeder RK. Effects of hydroxyapatite reinforcement on the architecture and mechanical properties of freeze-dried collagen scaffolds. J Mech Behav Biomed Mater 2012 Mar;7(0):41-9.

(13) Amensag S, McFetridge PS. Tuning scaffold mechanics by laminating native extracellular matrix membranes and effects on early cellular remodeling. J Biomed Mater Res A 2014 May 11;102(5):1325-33.

(14) Poursamar SA, Azami M, Mozafari M. Controllable synthesis and characterization of porous polyvinyl alcohol/hydroxyapatite nanocomposite scaffolds via an in situ colloidal technique. Colloids Surf , B 2011 Jun 1;84(2):310-6.

(15) Ma L, Jiang W, Li W. Solvent-free Fabrication of Tissue Engineering Scaffolds with Immiscible Polymer Blends. Int J Polym Mater 2014 Mar 13;63(10):510-7.

(16) Deitzel JM, Kleinmeyer J, Harris D, Beck Tan NC. The effect of processing variables on the morphology of electrospun nanofibers and textiles. Polymer 2001 Jan;42(1):261-72.

(17) Ilagan BG, Amsden BG. Macroporous photocrosslinked elastomer scaffolds containing microposity: Preparation and in vitro degradation properties. J Biomed Mater Res 2010 Apr 1;93A(1):211-8.

(18) Li J, Chen Y, Mak AF, Tuan RS, Li L, Li Y. A one-step method to fabricate PLLA scaffolds with deposition of bioactive hydroxyapatite and collagen using ice-based microporogens. Acta Biomater 2010 Jun;6(6):2013-9.

(19) Lin W, Li Q, Zhu T. Study of solvent casting/particulate leaching technique membranes in pervaporation for dehydration of caprolactam. J Ind Eng Chem 2012 May 25;18(3):941-7.

(20) Suntornnond R, An J, Yeong WY, Chua CK. Biodegradable Polymeric Films and Membranes Processing and Forming for Tissue Engineering. Macromol Mater Eng 2015 Apr 1.

(21) Nitschke M, Schmack G, Janke A, Simon F, Pleul D, Werner C. Low pressure plasma treatment of poly(3-hydroxybutyrate): Toward tailored polymer surfaces for tissue engineering scaffolds. J Biomed Mater Res 2002 Mar 15;59(4):632-8.

(22) Mou ZL, Duan LM, Qi XN, Zhang ZQ. Preparation of silk fibroin/collagen/hydroxyapatite composite scaffold by particulate leaching method. Materials Letters 2013 Aug 15;105(0):189-91.

(23) Uchida T, Ikeda S, Oura H, Tada M, Nakano T, Fukuda T, et al. Development of biodegradable scaffolds based on patient-specific arterial configuration. Journal of Biotechnology 2008 Jan 20;133(2):213-8.

(24) Ko J, Kan D, Jun MBG. Combining melt electrospinning and particulate leaching for fabrication of porous microfibers. Manufacturing Letters 2015 Jan;3:5-8.

(25) Phull M, Eydmann T, Roxburgh J, Sharpe J, Lawrence-Watt D, Phillips G, et al. Novel macro-microporous gelatin scaffold fabricated by particulate leaching for soft tissue reconstruction with adipose-derived stem cells. J Mater Sci: Mater Med 2013;24(2):461-7.

(26) Liao CJ, Chen CF, Chen JH, Chiang SF, Lin YJ, Chang KY. Fabrication of porous biodegradable polymer scaffolds using a solvent merging/particulate leaching method. Journal of Biomedical Materials Research 2002 Mar 15;59(4):676-81.

(27) Hu C, Tercero C, Ikeda S, Nakajima M, Tajima H, Shen Y, et al. Biodegradable porous sheet-like scaffolds for soft-tissue engineering using a combined particulate leaching of salt particles and magnetic sugar particles. Journal of Bioscience and Bioengineering 2013 Jul;116(1):126-31.

(28) Niu Y, Guo L, Liu J, Shen H, Su J, An X, et al. Bioactive and degradable scaffolds of the mesoporous bioglass and poly(l-lactide) composite for bone tissue regeneration. J Mater Chem B 2015;3(15):2962-70.

(29) Koupaei N, Karkhaneh A, Daliri Joupari M. Preparation and characterization of (PCL-crosslinked-PEG)/Hydroxyapatite as bone tissue engineering scaffolds. J Biomed Mater Res 2015 May 1.

(30) Minton J, Janney C, Akbarzadeh R, Focke C, Subramanian A, Smith T, et al. Solvent-free polymer/bioceramic scaffolds for bone tissue engineering: fabrication, analysis, and cell growth. Journal of Biomaterials Science, Polymer Edition 2014 Sep 2;25(16):1856-74.

(31) Gong Y, Ma Z, Zhou Q, Li J, Gao C, Shen J. Poly(lactic acid) scaffold fabricated by gelatin particle leaching has good biocompatibility for chondrogenesis. J Biomater Sci Polym Ed 2008;19(2):207-21.

(32) Cho YS, Kim BS, You HK, Cho YS. A novel technique for scaffold fabrication: SLUP (salt leaching using powder). Current Applied Physics 2014 Mar;14(3):371-7.

(33) Reignier J, Huneault MA. Preparation of interconnected poly(epsilon-caprolactone) porous scaffolds by a combination of polymer and salt particulate leaching. Polymer 2006;47(13):4703-17.

(34) Thadavirul N, Pavasant P, Supaphol P. Development of polycaprolactone porous scaffolds by combining solvent casting, particulate leaching, and polymer leaching techniques for bone tissue engineering. J Biomed Mater Res 2014 Oct 1;102(10):3379-92.

(35) Baheiraei N, Yeganeh H, Ai J, Gharibi R, Ebrahimi-Barough S, Azami M, et al. Preparation of a porous conductive scaffold from aniline pentamer-modified polyurethane/PCL blend for cardiac tissue engineering. J Biomed Mater Res 2015 Mar 1.

(36) Yim JH, Jeong HD, Sun Pu L. The preparation of nanoporous siloxane films using saccharide derivatives as new porogen. Thin Solid Films 2005 Apr 1;476(1):46-50.

(37) Kumbar and SG. Electrospun nanofiber scaffolds: engineering soft tissues. Biomedical Materials 2008;3(3):034002.

(38) Rogina A. Electrospinning process: Versatile preparation method for biodegradable and natural polymers and biocomposite systems applied in tissue engineering and drug delivery. Appl Surf Sci 2014 Mar 30;296(0):221-30.

(39) Gao Q, Luo J, Wang X, Gao C, Ge M. Novel hollow alpha-Fe2O3 nanofibers via electrospinning for dye adsorption. Nanoscale Res Lett 2015;10(1):176.

(40) Formhals A, inventor; Process and apparatus for preparing artificial threads. USA patent US 1975504 A. 1934 Oct 2.

(41) Formhals A, inventor; Method and apparatus for spinning. USA patent US2160962 A. 1939 Jun 6.

(42) Formhals A, inventor; Artificial Thread and method of producing SME.US2187306 A. 1940 Jan 16.

(43) Taylor G. Electrically Driven Jets. Proceedings of the Royal Society of London A: Mathematical, Physical and Engineering Sciences 1969 Dec 2;313(1515):453-75.

(44) Baumgarten PK. Electrostatic spinning of acrylic microfibers. Journal of Colloid and Interface Science 1971 May;36(1):71-9.

(45) Annis D, Bornat A, Edwards RO. An elastomeric vascular prosthesis. 1978;VOL.24:209-14.

(46) Fisher AC, De Cossart L, How TV, Annis D. Long term in-vivo performance of an electrostatically-spun small bore arterial prosthesis: the contribution of mechanical compliance and anti-platelet therapy. 1985;3 Suppl 1:462-5.

(47) Han T, Reneker DH, Yarin AL. Buckling of jets in electrospinning. Polymer 2007 Sep 21;48(20):6064-76.

(48) Wendorff JH, Agarwal S, Greiner A. Electrospinning- Some Technical Aspects. Electrospinning. Wiley-VCH Verlag GmbH & Co. KGaA; 2012. p. 127-42.

(49) Okutan N, Terzi P, Altay F. Affecting parameters on electrospinning process and characterization of electrospun gelatin nanofibers. Food Hydrocolloids 2014 Aug;39(0):19-26.

(50) Chen SH, Chang Y, Lee KR, Lai JY. A three-dimensional dual-layer nano/microfibrous structure of electrospun chitosan/poly(d,l-lactide) membrane for the improvement of cytocompatibility. J Membr Sci 2014 Jan 15;450(0):224-34.

(51) Lee KH, Kim HY, Bang HJ, Jung YH, Lee SG. The change of bead morphology formed on electrospun polystyrene fibers. Polymer 2003 Jun;44(14):4029-34.

(52) Gudkova V, Krumme A, Märtson T, Rikko M, Tarassova E, Viirsalu M. The impact of 1-butyl-3-methylimidazolium chloride on electrospinning process of SAN polymer solutions and electrospun fiber morphology. Journal of Electrostatics 2014 Dec;72(6):433-6.

(53) Ki CS, Baek DH, Gang KD, Lee KH, Um IC, Park YH. Characterization of gelatin nanofiber prepared from gelatin-formic acid solution. 2005;46(14):5094-102.

(54) Hua CC, Yang CY. Entanglement loss in fast-flowing entangled polymer: Numerical simulation of the short-chain behavior and interpretation of phenomenology. 2002;9(2):79-90.

(55) Rothstein JP, McKinley GH. A comparison of the stress and birefringence growth of dilute, semi-dilute and concentrated polymer solutions in uniaxial extensional flows. 2002;108(1-3):275-90.

(56) Shenoy SL, Bates WD, Frisch HL, Wnek GE. Role of chain entanglements on fiber formation during electrospinning of polymer solutions: good solvent, non-specific polymer-polymer interaction limit. Polymer 2005 Apr 25;46(10):3372-84.

(57) Fernandes JG, Correia DM, Botelho G, Padrão j, Dourado F, Ribeiro C, et al. PHB-PEO electrospun fiber membranes containing chlorhexidine for drug delivery applications. Polymer Testing 2014 Apr;34(0):64-71.

(58) Cheng F, Gao J, Wang L, Hu X. Composite chitosan/poly(ethylene oxide) electrospun nanofibrous mats as novel wound dressing matrixes for the controlled release of drugs. J Appl Polym Sci 2015 Jun 20;132(24).

(59) Reddy N, Yang Y. Electrospun Fibers from Polysaccharides. Innovative Biofibers from Renewable Resources. Springer Berlin Heidelberg; 2015. p. 259-86.

(60) Xu X, Zhang JF, Fan Y. Fabrication of Cross-Linked Polyethyleneimine Microfibers by Reactive Electrospinning with In Situ Photo-Cross-Linking by UV Radiation. Biomacromolecules 2010 Sep 13;11(9):2283-9.

(61) Nasouri K, Shoushtari AM, Kaflou A. Investigation of polyacrylonitrile electrospun nanofibres morphology as a function of polymer concentration, viscosity and berry number. Micro & Nano Letters, IET 2012 May;7(5):423-6.

(62) Nasouri K, Shoushtari AM, Mojtahedi MRM. Thermodynamic Studies on Polyvinylpyrrolidone Solution Systems Used for Fabrication of Electrospun Nanostructures: Effects of the Solvent. Adv Polym Technol 2015 Jan 1;34(3).

(63) Schuermann J, Huber T, LeCorre D, Mortha G+, Sellier M, Duchemin Bt, et al. Surface tension of concentrated cellulose solutions in 1-ethyl-3-methylimidazolium acetate. Cellulose 2016;23(2):1043-50.

(64) Nartetamrongsutt K, Chase GG. The influence of salt and solvent concentrations on electrospun polyvinylpyrrolidone fiber diameters and bead formation. Polymer 2013 Apr 3;54(8):2166-73.

(65) Uyar T, Besenbacher F. Electrospinning of uniform polystyrene fibers: The effect of solvent conductivity. Polymer 2008 Nov 10;49(24):5336-43.

(66) Shi Q, Zhou C, Yue Y, Guo W, Wu Y, Wu Q. Mechanical properties and in vitro degradation of electrospun bio-nanocomposite mats from PLA and cellulose nanocrystals. Carbohydrate Polymers 2012 Sep 1;90(1):301-8.

(67) Angammana CJ, Jayaram SH. Analysis of the Effects of Solution Conductivity on Electrospinning Process and Fiber Morphology. Industry Applications, IEEE Transactions on 2011 May;47(3):1109-17.

(68) Chen MC, Sun YC, Chen YH. Electrically conductive nanofibers with highly oriented structures and their potential application in skeletal muscle tissue engineering. Acta Biomaterialia 2013 Mar;9(3):5562-72.

(69) Meng L, Klinkajon W, hasuwan Pr, Harkin S, Supaphol P, Wnek GE. Electrospun crosslinked poly(acrylic acid) fiber constructs: towards a synthetic model of the cortical layer of nerve. Polym Int 2015 Jan 1;64(1):42-8.

(70) Rnjak-Kovacina J, Wise SG, Li Z, Maitz PKM, Young CJ, Wang Y, et al. Tailoring the porosity and pore size of electrospun synthetic human elastin scaffolds for dermal tissue engineering. Biomaterials 2011 Oct;32(28):6729-36.

(71) Megelski S, Stephens JS, Bruce Chase D, Rabolt JF. Micro- and nanostructured surface morphology on electrospun polymer fibers. 2002;35(22):8456-66.

(72) Mazoochi T, Hamadanian M, Ahmadi M, Jabbari V. Investigation on the morphological characteristics of nanofiberous membrane as electrospun in the different processing parameters. Int J Ind Chem 2012;3(1):1-8.

(73) Okutan N, Terzi P, Altay F. Affecting parameters on electrospinning process and characterization of electrospun gelatin nanofibers. Food Hydrocolloids 2014 Aug;39(0):19-26.

(74) Vaquette C, Cooper-White JJ. Increasing electrospun scaffold pore size with tailored collectors for improved cell penetration. Acta Biomaterialia 2011 Jun;7(6):2544-57.

(75) Fashandi H, Karimi M. Pore formation in polystyrene fiber by superimposing temperature and relative humidity of electrospinning atmosphere. Polymer 2012 Nov 30;53(25):5832-49.

(76) Casper CL, Stephens JS, Tassi NG, Chase DB, Rabolt JF. Controlling Surface Morphology of Electrospun Polystyrene Fibers:GÇë Effect of Humidity and Molecular Weight in the Electrospinning Process. Macromolecules 2004 Jan 1;37(2):573-8.

(77) Mit-uppatham C, Nithitanakul M, Supaphol P. Ultrafine Electrospun Polyamide-6 Fibers: Effect of Solution Conditions on Morphology and Average Fiber Diameter. Macromol Chem Phys 2004 Nov 26;205(17):2327-38.

(78) Laurencin CT, Nair LS. Nanotechnology and Regenerative Engineering: The Scaffold, Second Edition. Taylor & Francis; 2014.

(79) Zhang Y, Huang ZM, Xu X, Lim CT, Ramakrishna S. Preparation of Core-Shell Structured PCL-r-Gelatin Bi-Component Nanofibers by Coaxial Electrospinning. Chem Mater 2004 Sep 1;16(18):3406-9.

(80) He M, Xue J, Geng H, Gu H, Chen D, Shi R, et al. Fibrous guided tissue regeneration membrane loaded with anti-inflammatory agent prepared by coaxial electrospinning for the purpose of controlled release. Applied Surface Science 2015 Apr 30;335:121-9.

(81) Jiang H, Wang L, Zhu K. Coaxial electrospinning for encapsulation and controlled release of fragile water-soluble bioactive agents. J Controlled Release 2014 Nov 10;193:296-303.

(82) Meng W, Xing ZC, Jung KH, Kim SY, Yuan J, Kang IK, et al. Synthesis of gelatin-containing PHBV nanofiber mats for biomedical application. J Mater Sci: Mater Med 2008;19(8):2799-807.

(83) Duan B, Wu L, Yuan X, Hu Z, Li X, Zhang Y, et al. Hybrid nanofibrous membranes of PLGA/chitosan fabricated via an electrospinning array. J Biomed Mater Res 2007 Dec 1;83A(3):868-78.

(84) Brown TD, Edin F, Detta N, Skelton AD, Hutmacher DW, Dalton PD. Melt electrospinning of poly(e-caprolactone) scaffolds: Phenomenological observations associated with collection and direct writing. Mater Sci Eng , C 2014 Dec 1;45:698-708.

(85) Ko J, Mohtaram NK, Ahmed F, Montgomery A, Carlson M, Lee PCD, et al. Fabrication of poly (e-caprolactone) microfiber scaffolds with varying topography and mechanical properties for stem cell-based tissue engineering applications. Journal of Biomaterials Science, Polymer Edition 2013 Sep 2;25(1):1-17.

(86) Wang C, Wang M. Dual-source dual-power electrospinning and characteristics of multifunctional scaffolds for bone tissue engineering. J Mater Sci: Mater Med 2012;23(10):2381-97.

(87) Xu X, inventor; Process of fabricating nanofibers by reactive electrospinning.US 8066932 B2. 2004 Nov 29.

(88) Molnar K, Juriga D, Nagy PM, Sinko K, Jedlovszky-Hajdu A, Zrinyi M. Electrospun poly(aspartic acid) gel scaffolds for artificial extracellular matrix. Polym Int 2014 Sep 1;63(9):1608-15.

(89) Dong RH, Qin CC, Qiu X, Yan X, Yu M, Cui L, et al. In situ precision electrospinning as an effective delivery technique for cyanoacrylate medical glue with high efficiency and low toxicity. Nanoscale 2015;7(46):19468-75.

(90) Ji Y, Ghosh K, Li B, Sokolov JC, Clark RAF, Rafailovich MH. Dual-Syringe Reactive Electrospinning of Cross-Linked Hyaluronic Acid Hydrogel Nanofibers for Tissue Engineering Applications. Macromol Biosci 2006 Oct 20;6(10):811-7.

(91) Touny AH, Bhaduri SB. A reactive electrospinning approach for nanoporous PLA/monetite nanocomposite fibers. Mater Sci Eng , C 2010 Oct 12;30(8):1304-12.

(92) Schreiber M, Vivekanandhan S, Cooke P, Mohanty A, Misra M. Electrospun green fibres from lignin and chitosan: a novel polycomplexation process for the production of lignin-based fibres. J Mater Sci 2014;49(23):7949-58.

(93) Niu H, Wang H, Zhou H, Lin T. Ultrafine PDMS fibers: preparation from in situ curing-electrospinning and mechanical characterization. RSC Adv 2014;4(23):11782-7.

(94) Kong L, Ziegler GR. Fabrication of pure starch fibers by electrospinning. Food Hydrocolloids 2014 May;36:20-5.

(95) Kim HS, Ham HO, Son YJ, Messersmith PB, Yoo HS. Electrospun catechol-modified poly(ethyleneglycol) nanofibrous mesh for anti-fouling properties. J Mater Chem B 2013;1(32):3940-9.

(96) Meng L, Arnoult O, Smith M, Wnek GE. Electrospinning of in situ crosslinked collagen nanofibers. J Mater Chem 2012;22(37):19412-7.

(97) Yuan J, Mo H, Wang M, Li L, Zhang J, Shen J. Reactive electrospinning of poly(vinyl alcohol) nanofibers. J Appl Polym Sci 2012 Apr 15;124(2):1067-73.

(98) Zhang YZ, Venugopal J, Huang ZM, Lim CT, Ramakrishna S. Crosslinking of the electrospun gelatin nanofibers. Polymer 2006 Apr 5;47(8):2911-7.

(99) Yao L, Haas TW, Guiseppi-Elie A, Bowlin GL, Simpson D, Wnek GE. Electrospinning and Stabilization of Fully Hydrolyzed Poly(Vinyl Alcohol) Fibers. Chem Mater 2003 May 1;15(9):1860-4.

(100) Tian M, Hu Q, Wu H, Zhang L, Fong H, Zhang L. Formation and morphological stability of polybutadiene rubber fibers prepared through combination of electrospinning and in-situ photo-crosslinking. Mater Lett 2011 Oct;65(19-20):3076-9.

(101) Theron JP, Knoetze JH, Sanderson RD, Hunter R, Mequanint K, Franz T, et al. Modification, crosslinking and reactive electrospinning of a thermoplastic medical polyurethane for vascular graft applications. Acta Biomater 2010 Jul;6(7):2434-47.

(102) Burcu Oktay and Nilhan Kayaman-Apohan and Serap Erdem-Kuruca. Fabrication of nanofiber mats from electrospinning of functionalized polymers. IOP Conference Series: Materials Science and Engineering 2014;64(1):012011.

(103) Ruizhi Wu and Jian-Feng Zhang and Yuwei Fan and Diana Stoute and Thomas Lallier and Xiaoming Xu. Reactive electrospinning and biodegradation of cross-linked methacrylated polycarbonate nanofibers. Biomedical Materials 2011;6(3):035004.

(104) Kim SH, Kim SH, Nair S, Moore E. Reactive Electrospinning of Cross-Linked Poly(2-hydroxyethyl methacrylate) Nanofibers and Elastic Properties of Individual Hydrogel Nanofibers in Aqueous Solutions. Macromolecules 2005 May 1;38(9):3719-23.

(105) Gupta P, Trenor SR, Long TE, Wilkes GL. In Situ Photo-Cross-Linking of Cinnamate Functionalized Poly(methyl methacrylate-co-2-hydroxyethyl acrylate) Fibers during Electrospinning. Macromolecules 2004 Nov 1;37(24):9211-8.

(106) Wei-Han Lin and Wei-Bor Tsai. In situ UV-crosslinking gelatin electrospun fibers for tissue engineering applications. Biofabrication 2013;5(3):035008.

(107) Duygu Yüksel D, Kahraman MV, Kuruca SE. UV-reactive electrospinning of keratin/4-vinyl benzene boronic acid-hydroxyapatite/poly(vinyl alcohol) composite nanofibers. Polym Compos 2015 Jul 1.

(108) Wang H, Feng Y, An B, Zhang W, Sun M, Fang Z, et al. Fabrication of PU/PEGMA crosslinked hybrid scaffolds by in situ UV photopolymerization favoring human endothelial cells growth for vascular tissue engineering. J Mater Sci: Mater Med 2012;23(6):1499-510.

(109) Wang H, Feng Y, Yuan W, Zhao H, Fang Z, Khan M, et al. Fabrication and characterization of electrospun biocompatible PU/PEGMA hybrid nanofibers by in-situ UV photopolymerization. Sci China Phys Mech Astron 2012;55(7):1189-93.

(110) Dargaville BL, Vaquette C, Rasoul F, Cooper-White JJ, Campbell JH, Whittaker AK. Electrospinning and crosslinking of low-molecular-weight poly(trimethylene carbonate-co-l-lactide) as an elastomeric scaffold for vascular engineering. Acta Biomaterialia 2013 Jun;9(6):6885-97.

(111) Kang HK, Shin HK, Jeun JP, Kim HB, Kang PH. Fabrication and characterization of electrospun polyamide 66 fibers crosslinked by gamma irradiation. Macromol Res 2011;19(4):364-9.

(112) Bosworth LA, Gibb A, Downes S. Gamma irradiation of electrospun poly(e-caprolactone) fibers affects material properties but not cell response. J Polym Sci B Polym Phys 2012 Jun 15;50(12):870-6.

(113) Tang C, Saquing CD, Harding JR, Khan SA. In Situ Cross-Linking of Electrospun Poly(vinyl alcohol) Nanofibers. Macromolecules 2010 Jan 26;43(2):630-7.

(114) Prádný M, Martinová L, Michálek j, Fenclov+í T, n, Krumbholcov+í E. Electrospinning of the hydrophilic poly (2-hydroxyethyl methacrylate) and its copolymers with 2-ethoxyethyl methacrylate. cent eur j chem 2007;5(3):779-92.

(115) Schiffman JD, Schauer CL. One-Step Electrospinning of Cross-Linked Chitosan Fibers. Biomacromolecules 2007 Sep 1;8(9):2665-7.

(116) Masutani K, Lee CW, Kanki R, Yamane H, Kimura Y. Reactive Electrospinning of Stereoblock Polylactides Prepared via Spontaneous Diels-Alder Coupling of Bis Maleimide-terminated Poly-L-lactide and Bis Furan-terminated Poly-D-lactide. Sen'i Gakkaishi 2012;68(3):64-72.

(117) Bastürk E, Oktay B, Kahraman M. Dual-crosslinked thiol-ene/sol gel hybrid electrospun nanowires: preparation and characterization. J Polym Res 2015;22(7):1-7.

(118) çakmak E, Güngör A, Kayaman-Apohan N, Kuruca SE, çetin MB, Dar KA. Cell Growth on In Situ Photo-Cross-Linked Electrospun Acrylated Cellulose Acetate Butyrate. Journal of Biomaterials Science, Polymer Edition 2012 Jan 1;23(7):887-99.

(119) Wei-Han Lin and Wei-Bor Tsai. In situ UV-crosslinking gelatin electrospun fibers for tissue engineering applications. Biofabrication 2013;5(3):035008.

(120) Deniz DY, Kahraman MV, Kuruca SE. UV-reactive electrospinning of keratin/4-vinyl benzene boronic acid-hydroxyapatite/poly(vinyl alcohol) composite nanofibers. Polym Compos 2015 Jul 1.

(121) Greiner A, Wendorff J. Electrospinning: A Fascinating Method for the Preparation of Ultrathin Fibers. Angewandte Chemie International Edition 2007 Jul 23;46(30):5670-703.

(122) Sill TJ, von Recum HA. Electrospinning: Applications in drug delivery and tissue engineering. Biomaterials 2008 May;29(13):1989-2006.

(123) Sell SA, Wolfe PS, Garg K, McCool JM, Rodriguez IA, Bowlin GL. The use of natural polymers in tissue engineering: A focus on electrospun extracellular matrix analogues. 2010;2(4):522-53.

(124) Joy J, Gupta P, Ray AR, Gupta A, Sharma A, Sharma D, et al. Fabrication of Smooth Electrospun Nanofibrous Gelatin Mat for Potential Application in

Tissue Engineering. Int J Polym Mater Polym Biomater 2015 Feb 2;64(10):509-18.

(125) Matthews JA, Wnek GE, Simpson DG, Bowlin GL. Electrospinning of Collagen Nanofibers. Biomacromolecules 2002 Mar 1;3(2):232-8.

(126) Rho KS, Jeong L, Lee G, Seo BM, Park YJ, Hong SD, et al. Electrospinning of collagen nanofibers: Effects on the behavior of normal human keratinocytes and early-stage wound healing. Biomaterials 2006 Mar;27(8):1452-61.

(127) Zhong S, Teo WE, Zhu X, Beuerman RW, Ramakrishna S, Yung LYL. An aligned nanofibrous collagen scaffold by electrospinning and its effects on in vitro fibroblast culture. J Biomed Mater Res 2006 Dec 1;79A(3):456-63.

(128) Punnoose AM, Elamparithi A, Kuruvilla S. Electrospun Type 1 Collagen Matrices Using a Novel Benign Solvent for Cardiac Tissue Engineering. J Cell Physiol 2015 May 1;n/a.

(129) Nada AA, James R, Shelke NB, Harmon MD, Awad HM, Nagarale RK, et al. A smart methodology to fabricate electrospun chitosan nanofiber matrices for regenerative engineering applications. Polym Adv Technol 2014 May 1;25(5):507-15.

(130) Rajzer I, Menaszek E, Kwiatkowski R, Planell JA, Castano O. Electrospun gelatin/poly(e-caprolactone) fibrous scaffold modified with calcium phosphate for bone tissue engineering. Mater Sci Eng C 2014 Nov 1;44:183-90.

(131) Chahal S, Jahir Hussain FS, Kumar A, Yusoff MM, Bahari Abdull Rasad MS. Electrospun hydroxyethyl cellulose nanofibers functionalized with calcium phosphate coating for bone tissue engineering. RSC Adv 2015;5(37):29497-504.

(132) Unnithan AR, Gnanasekaran G, Sathishkumar Y, Lee YS, Kim CS. Electrospun antibacterial polyurethane-cellulose acetate-zein composite mats for wound dressing. Carbohydr Polym 2014 Feb 15;102:884-92.

(133) Munj HR, Nelson MT, Karandikar PS, Lannutti JJ, Tomasko DL. Biocompatible electrospun polymer blends for biomedical applications. Journal of Biomedical Materials Research Part B: Applied Biomaterials 2014 Oct 1;102(7):1517-27.

(134) McClure MJ, Sell SA, Simpson DG, Walpoth BH, Bowlin GL. Tri-layered Electrospinning to Mimic Native Arterial Architecture using Polycaprolactone, Elastin, and Collagen: A Preliminary Study. J Vis Exp 2011 Jan 4;(47):2084.

(135) McClure MJ, Simpson DG, Bowlin GL. Tri-layered vascular grafts composed of polycaprolactone, elastin, collagen, and silk: Optimization of graft properties. Journal of the Mechanical Behavior of Biomedical Materials 2012 Jun;10:48-61.

(136) Pathan SG, Fitzgerald LM, Ali SM, Damrauer SM, Bide MJ, Nelson DW, et al. Cytotoxicity associated with electrospun polyvinyl alcohol. Journal of Biomedical Materials Research Part B: Applied Biomaterials 2015 Jan 1;n/a.

(137) Punnakitikashem P, Truong D, Menon JU, Nguyen KT, Hong Y. Electrospun biodegradable elastic polyurethane scaffolds with dipyridamole release for small diameter vascular grafts. Acta Biomaterialia 2014 Nov;10(11):4618-28.

(138) Nangrejo M, Bragman F, Ahmad Z, Stride E, Edirisinghe M. Hot electrospinning of polyurethane fibres. Materials Letters 2012 Feb 1;68:482-5.

(139) Ying Y, Zhidong J, Qiang L, Zhicheng G. Experimental investigation of the governing parameters in the electrospinning of polyethylene oxide solution. Dielectrics and Electrical Insulation, IEEE Transactions on 2006 Jun;13(3):580-5.

(140) Wutticharoenmongkol P, Sanchavanakit N, Pavasant P, Supaphol P. Preparation and Characterization of Novel Bone Scaffolds Based on

Electrospun Polycaprolactone Fibers Filled with Nanoparticles. Macromol Biosci 2006 Jan 5;6(1):70-7.

(141) Boland ED, Wnek GE, Simpson DG, Pawlowski KJ, Bowlin GL. Tailoring tissue engineering scaffolds using electrostatic processing techniques: A study of poly(glycolic acid) electrospinning. 2001;38 A(12):1231-43.

(142) Shalumon KT, Chennazhi KP, Tamura H, Kawahara K, Nair SV, Jayakumar R. Fabrication of three-dimensional nano, micro and micro/nano scaffolds of porous poly(lactic acid) by electrospinning and comparison of cell infiltration by Z-stacking/three-dimensional projection technique. Nanobiotechnology, IET 2012 Mar;6(1):16-25.

(143) Casasola R, Thomas NL, Trybala A, Georgiadou S. Electrospun poly lactic acid (PLA) fibres: Effect of different solvent systems on fibre morphology and diameter. Polymer 2014 Sep 2;55(18):4728-37.

(144) Kim S, Jeong L, Lee S, Cho D, Park W. Fabrication and surface modification of melt-electrospun poly(D,L-lactic-co-glycolic acid) microfibers. Fibers Polym 2013;14(9):1491-6.

(145) Paskiabi FA, Mirzaei E, Amani A, Shokrgozar MA, Saber R, Faridi-Majidi R. Optimizing parameters on alignment of PCL/PGA nanofibrous scaffold: An artificial neural networks approach. Int J Biol Macromol 2015 Nov 1.

(146) Spearman SS, Rivero IV, Abidi N. Influence of polycaprolactone/polyglycolide blended electrospun fibers on the morphology and mechanical properties of polycaprolactone. J Appl Polym Sci 2014 May 5;131(9).

(147) Selcan Gungor-Ozkerim P, Balkan T, Kose GT, Sezai Sarac A, Kok FN. Incorporation of growth factor loaded microspheres into polymeric electrospun nanofibers for tissue engineering applications. J Biomed Mater Res 2014 Jun 1;102(6):1897-908.

(148) Younes HM, inventor; Biodegradable elastomers prepared by the condensation of an organic di-, tri- or tetra-carboxylic acid and an organic diol. USA patent US 20130237625 A1. 2013 Sep 12.

(149) Shaker MA, Doré JJE, Younes HM. Synthesis, Characterization and Cytocompatibility of a Poly(diol-tricarballylate) Visible Light Photo-Cross-Linked Biodegradable Elastomer. J Biomater Sci , Polym Ed 2010 Mar 15;21(4):507-28.

(150) Shaker MA, Daneshtalab N, Doré JJE, Younes HM. Biocompatibility and biodegradability of implantable drug delivery matrices based on novel poly(decane-co-tricarballylate) photocured elastomers. J Bioact Compat Polym 2012 Jan 1;27(1):78-94.

(151) Shaker MA, Younes HM. Osmotic-driven release of papaverine hydrochloride from novel poly(decane-co-tricarballylate) elastomeric matrices. Ther Delivery 2010 Jun 25;1(1):37-50.

(152) Connors KA, Albert KS. Determination of hydroxy compounds by 4-dimethylaminopyridine-catalyzed acetylation. J Pharm Sci 1973 May 1;62(5):845-6.

(153) Bunnell BA, Estes BT, Guilak F, Gimble JM. Differentiation of Adipose Stem Cells. In: Yang K, editor. Adipose Tissue Protocols.Totowa, NJ: Humana Press; 2008. p. 155-71.

(154) Chuangchote S, Sagawa T, Yoshikawa S. Electrospinning of poly(vinyl pyrrolidone): Effects of solvents on electrospinnability for the fabrication of poly(p-phenylene vinylene) and TiO2 nanofibers. J Appl Polym Sci 2009 Dec 1;114(5):2777-91.

(155) Sun T, Norton D, McKean RJ, Haycock JW, Ryan AJ, MacNeil S. Development of a 3D cell culture system for investigating cell interactions with electrospun fibers. Biotechnol Bioeng 2007 Aug 1;97(5):1318-28.

(156) Zamani M, Morshed M, Varshosaz J, Jannesari M. Controlled release of metronidazole benzoate from poly +¦-caprolactone electrospun nanofibers for periodontal diseases. Eur J Pharm Biopharm 2010 Jun;75(2):179-85.

(157) Shenoy SL, Bates WD, Frisch HL, Wnek GE. Role of chain entanglements on fiber formation during electrospinning of polymer solutions: good solvent, non-specific polymer-polymer interaction limit. Polymer 2005 Apr 25;46(10):3372-84.

(158) Barakat NAM, Kanjwal MA, Sheikh FA, Kim HY. Spider-net within the N6, PVA and PU electrospun nanofiber mats using salt addition: Novel strategy in the electrospinning process. Polymer 2009 Aug 26;50(18):4389-96.

(159) Yarin AL, Kataphinan W, Reneker DH. Branching in electrospinning of nanofibers. J Appl Phys 2005 Sep 15;98(6):064501.

(160) Tan S, Huang X, Wu B. Some fascinating phenomena in electrospinning processes and applications of electrospun nanofibers. Polym Int 2007 Nov 1;56(11):1330-9.

(161) Chen-Ming H, Shivkumar S. Nano-sized beads and porous fiber constructs of Poly(E-caprolactone) produced by electrospinning. J Mater Sci 2004 May;39(9):3003-13.

(162) Karageorgiou V, Kaplan D. Porosity of 3D biomaterial scaffolds and osteogenesis. Biomaterials 2005 Sep;26(27):5474-91.

(163) Heydarkhan-Hagvall S, Schenke-Layland K, Dhanasopon AP, Rofail F, Smith H, Wu BM, et al. Three-dimensional electrospun ECM-based hybrid

scaffolds for cardiovascular tissue engineering. Biomaterials 2008 Jul;29(19):2907-14.

(164) Tulloch NL, Muskheli V, Razumova MV, Korte FS, Regnier M, Hauch KD, et al. Growth of Engineered Human Myocardium With Mechanical Loading and Vascular Coculture. Circ Res 2011 Jun 24;109(1):47-59.

(165) Ifkovits JL, Devlin JJ, Eng G, Martens TP, Vunjak-Novakovic G, Burdick JA. Biodegradable Fibrous Scaffolds with Tunable Properties Formed from Photocrosslinkable Poly(glycerol sebacate). ACS Appl Mater Interfaces 2009 Sep 30;1(9):1878-92.

(166) Tamada Y, Ikada Y. Effect of Preadsorbed Proteins on Cell Adhesion to Polymer Surfaces. J Colloid Interface Sci 1993 Feb;155(2):334-9.

(167) Engelmayr GC, Cheng M, Bettinger CJ, Borenstein JT, Langer R, Freed LE. Accordion-Like Honeycombs for Tissue Engineering of Cardiac Anisotropy. Nat Mater 2008 Dec 2;7(12):1003-10.

(168) Pagano M, Naviglio S, Spina A, Chiosi E, Castoria G, Romano M, et al. Differentiation of H9c2 cardiomyoblasts: The role of adenylate cyclase system. J Cell Physiol 2004 Mar 1;198(3):408-16.

(169) Lee Kyung Eun, Moon Doo Hwan, Kang Sang Gu. Trehalose improves cell proliferation and dehydration tolerance of human HaCaT cells. Archives of Biological Sciences 2015;67(3):849-60.

(170) Motta JPR, Paraguass+¦-Braga FH, Bouzas LF, Porto LsCv. Evaluation of intracellular and extracellular trehalose as a cryoprotectant of stem cells obtained from umbilical cord blood. Cryobiology 2014 Jun;68(3):343-8.

(171) Crowe JH, Carpenter JF, Crowe LM. THE ROLE OF VITRIFICATION IN ANHYDROBIOSIS. Annu Rev Physiol 1998 Oct 1;60(1):73-103.

(172) Lien SM, Ko LY, Huang TJ. Effect of pore size on ECM secretion and cell growth in gelatin scaffold for articular cartilage tissue engineering. Acta Biomaterialia 2009 Feb;5(2):670-9.

(173) Sicchieri LG, Crippa GE, de Oliveira PT, Beloti MM, Rosa AL. Pore size regulates cell and tissue interactions with PLGAGÇôCaP scaffolds used for bone engineering. J Tissue Eng Regen Med 2012 Feb 1;6(2):155-62.

(174) Phipps MC, Clem WC, Grunda JM, Clines GA, Bellis SL. Increasing the pore sizes of bone-mimetic electrospun scaffolds comprised of polycaprolactone, collagen I and hydroxyapatite to enhance cell infiltration. Biomaterials 2012 Jan;33(2):524-34.

(175) McCullen SD, Stevens DR, Roberts WA, Clarke LI, Bernacki SH, Gorga RE, et al. Characterization of electrospun nanocomposite scaffolds and biocompatibility with adipose-derived human mesenchymal stem cells. Int J Nanomedicine 2007 Jun;2(2):253-63.

(176) Chen Y, Zeng D, Ding L, Li XL, Liu XT, Li WJ, et al. Three-dimensional poly-(e-caprolactone) nanofibrous scaffolds directly promote the cardiomyocyte differentiation of murine-induced pluripotent stem cells through Wnt/B-catenin signaling. BMC Cell Biol 2015;16(1):1-13.

(177) Jahani H, Jalilian FA, Wu CY, Kaviani S, Soleimani M, Abassi N, et al. Controlled surface morphology and hydrophilicity of polycaprolactone toward selective differentiation of mesenchymal stem cells to neural like cells. J Biomed Mater Res 2015 May 1;103(5):1875-81.

(178) Kai D, Prabhakaran MP, Jin G, Ramakrishna S. Guided orientation of cardiomyocytes on electrospun aligned nanofibers for cardiac tissue engineering. J Biomed Mater Res , Part B 2011 Aug 1;98B(2):379-86.

Appendix A

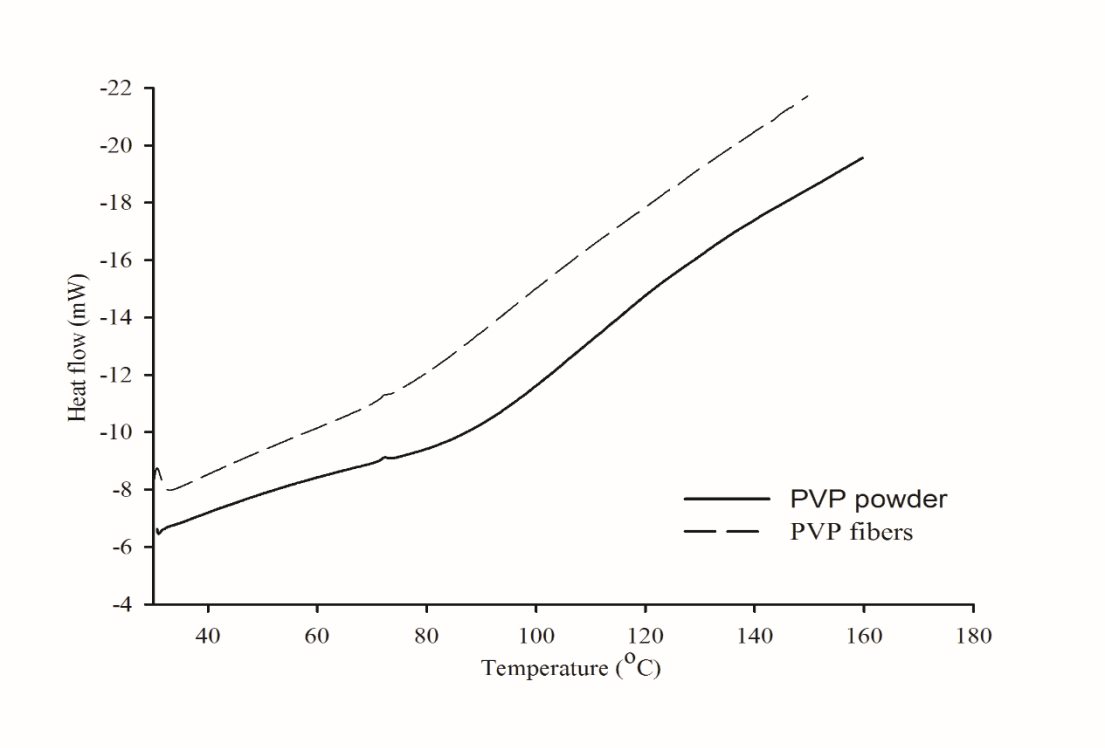

Appendix A. DSC thermograms of PVP powder and PVP fibers.

Appendix B

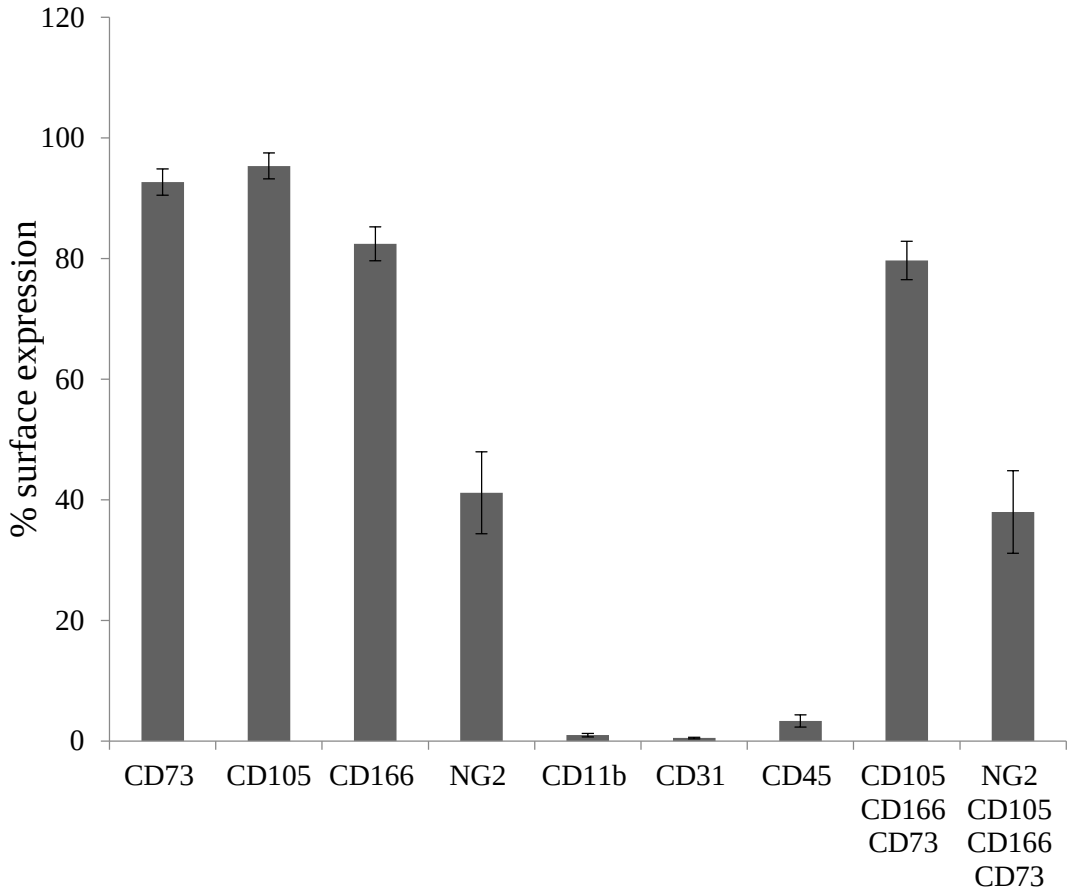

Appendix B. Flow cytometry analysis of surface markers in subcutaneous adipose tissue-derived preadipocytes (n=9). Data are presented as mean±SEM.

Appendix C

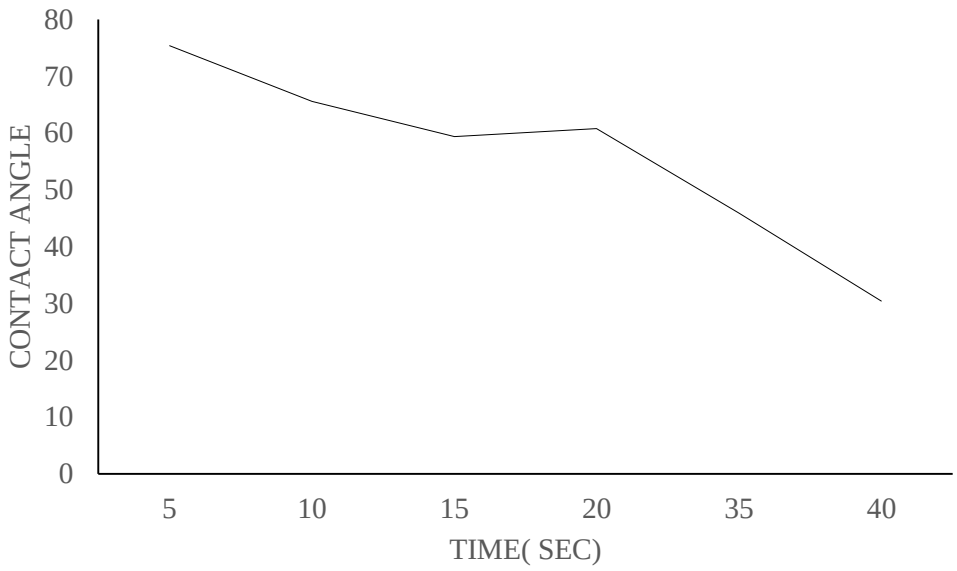

Appendix C. Contact angle measurement over extended period for ESS.

Appendix D

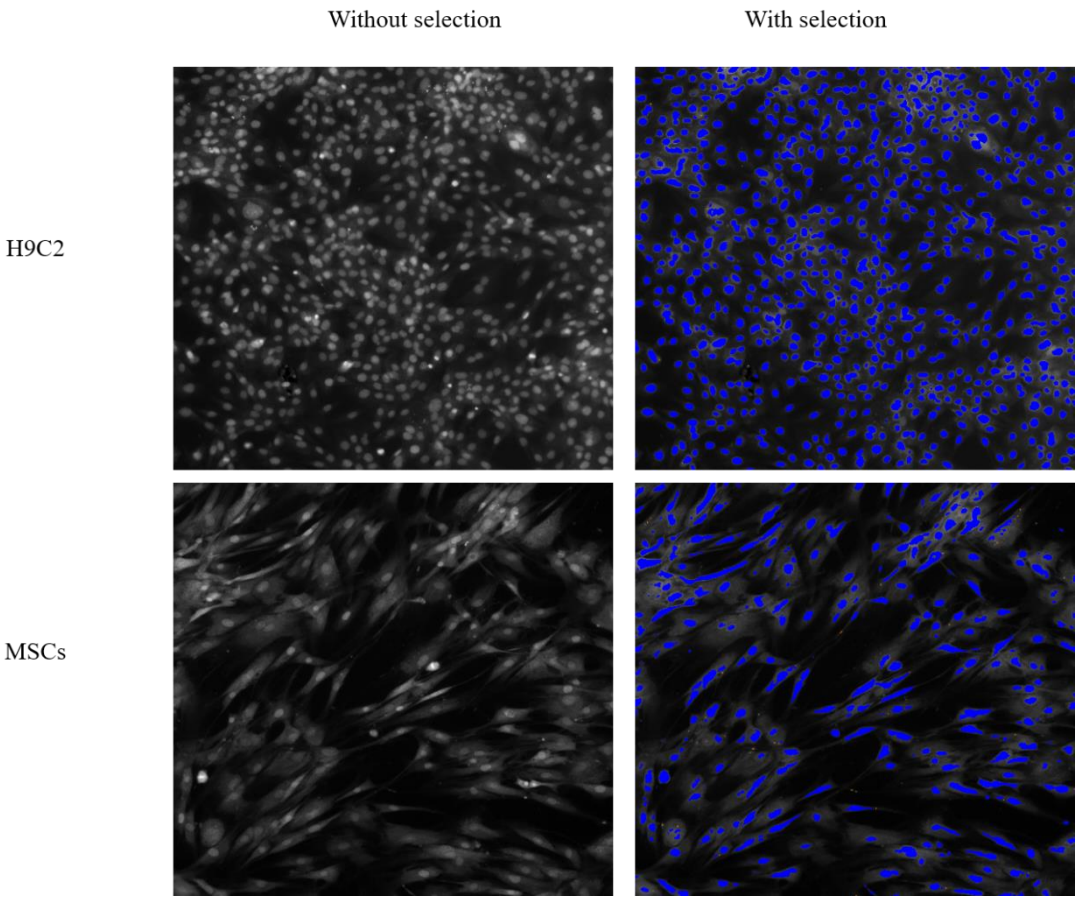

Appendix D. Images of H9C2 cells and MSCs with and without the selection of DAPI positive Nuclei counted by target activation module (Array scan XTI)

Appendix E

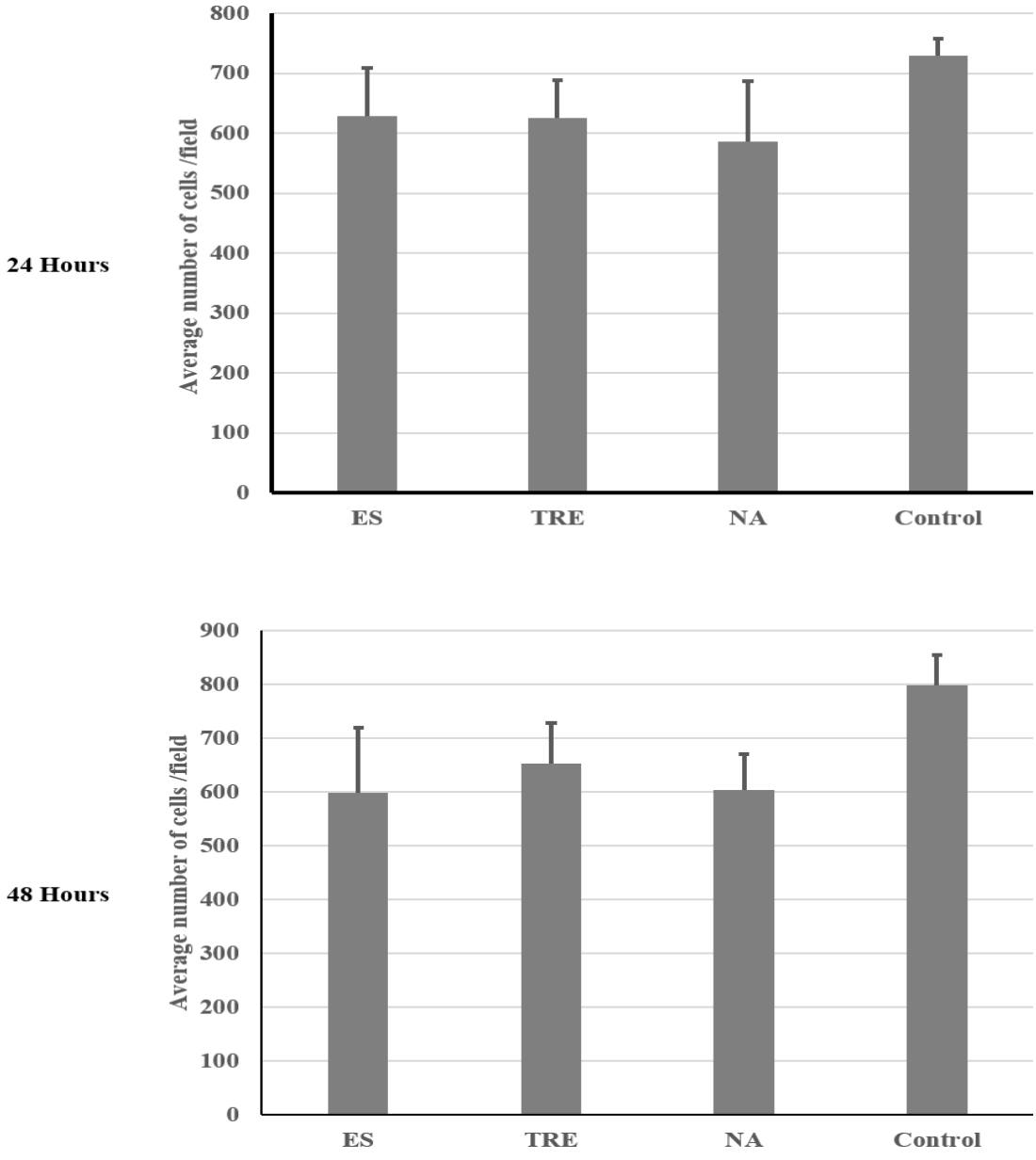

Appendix E. H9C2 cell viability in presence of ES, TRE and NA scaffolds at 24 and 48 hours represented as the average number of nuclei of viable cells per field. Data are presented as Mean ± SEM (n=6)

Appendix F

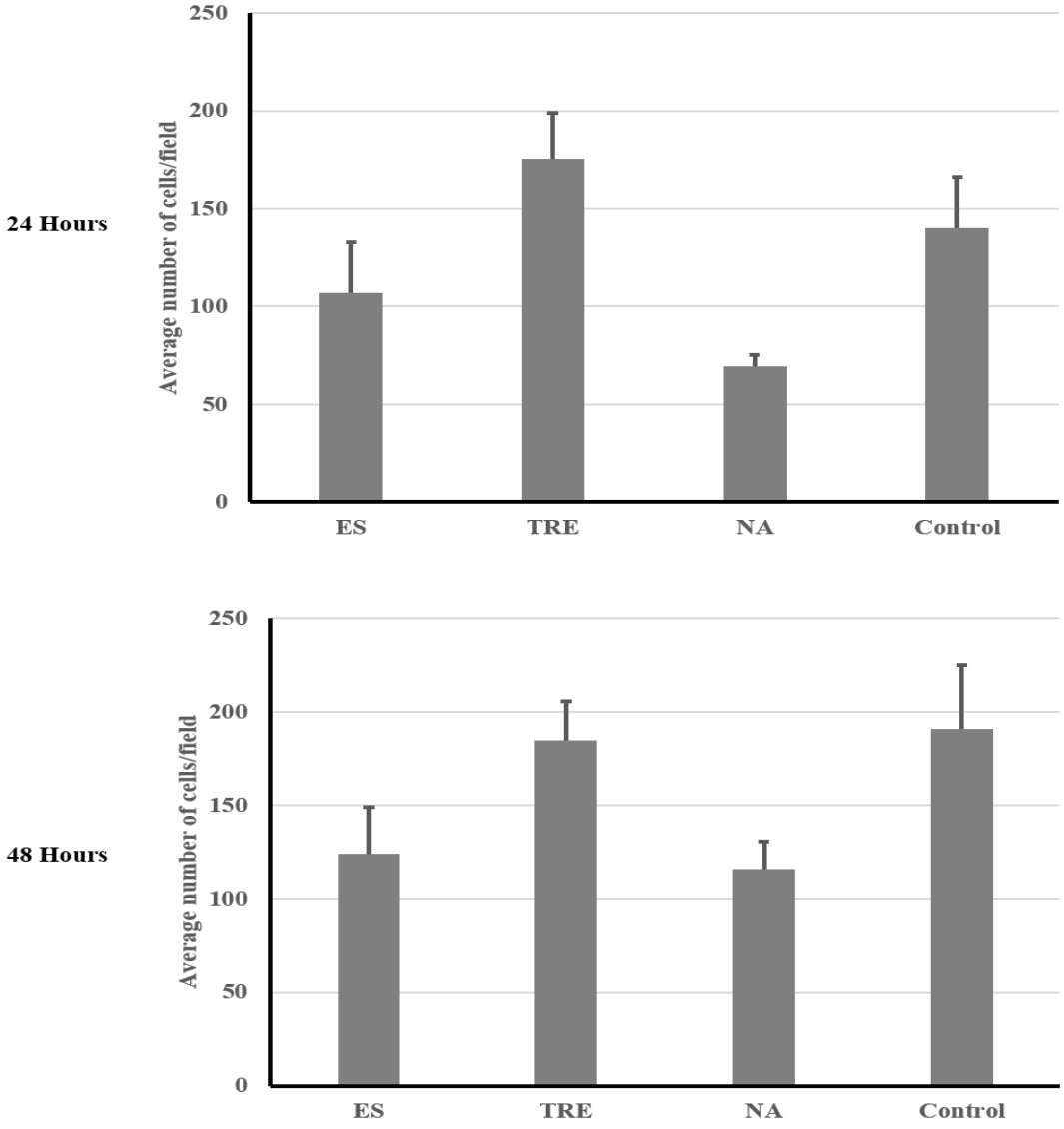

Appendix F. MSCs cell viability in presence of ES, TRE and NA scaffolds at 24 and 48 hours represented as the average number of nuclei of viable cells per field Data are presented as Mean ± SEM (n=3).

Appendix G

Appendix G**.** Table showing different pore sizes and concentrations of porogens used for qualitative cytocompatibility testing to determine the optimum combination for cell viability.

Preparation name	**PDT (Weight)**	**NaCl concentration (Wt. %)**	**NaCl particle size (µm)**	**UV exposure time**
A	0.2gm	70%	250	10 min
B	0.2gm	0% (Blank)	N/A	10 min
C	0.2gm	50%	125	10 min
D	0.2gm	70%	125	10 min
E	0.2 gm	50%	250	10 min

Appendix H

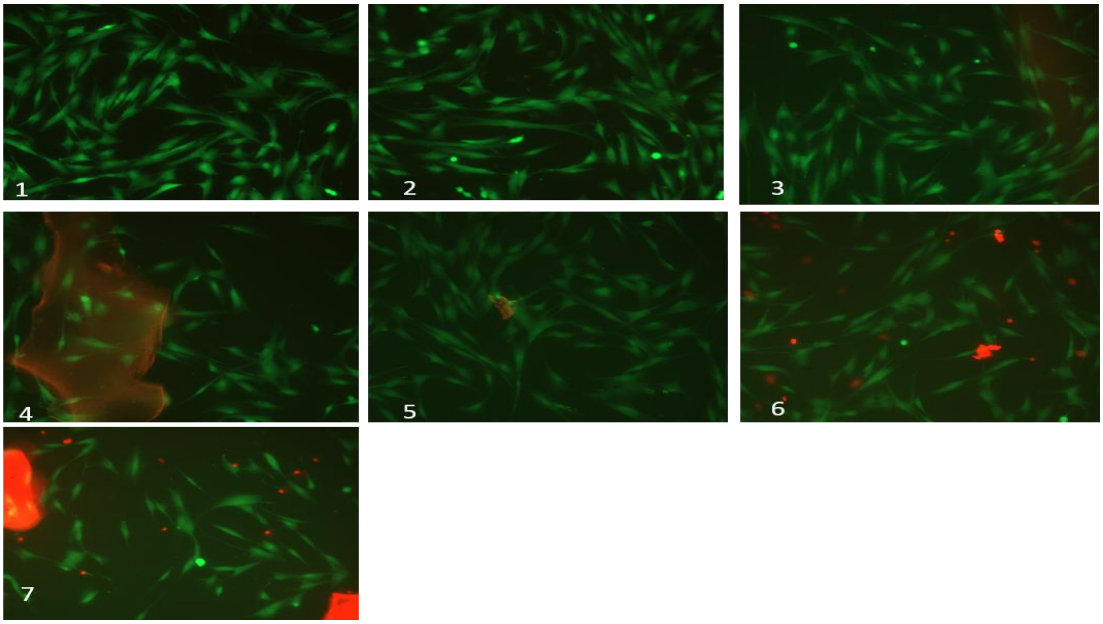

Fluorescent images of the cells in 48 well plates after 24 hours incubation. 1: Control 2: Positive Control 3: Blank scaffold (group B), 4: Group A, 5: Group C, 6: Group D, 7: Group E

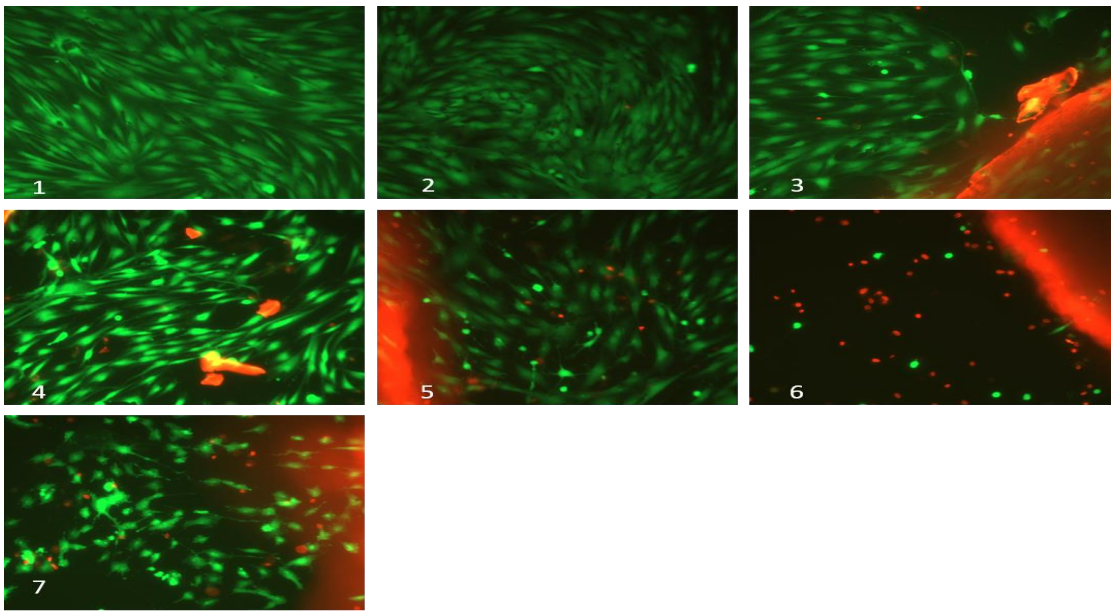

Fluorescent Images of the cells in 48 well plates after 48 hours incubation. 1: Control 2: Positive Control 3: Blank scaffold (group B), 4: Group A, 5: Group C, 6: Group D, 7: Group E